



HOLOGRAPHIC RECORDING OF
OPTICAL SPACE VARIANT SYSTEMS

A Thesis

submitted by

Robert J. Marks II

In partial fulfillment
of the requirements for the degree
Master of Science

Rose-Hulman Institute of Technology

August, 1973

ABSTRACT

The primary objective of this thesis is investigation of the holographic recording of a linear optical system in such manner that the resulting hologram displays the same input-output relationship as the recorded system. This proposition is defined herein through application and derivation of necessary theory. Needed approximations are cited and corresponding consequences explored.

A basic review of the optical properties of the thin lens and the concepts of planar holography are offered. Transition is then made to a more rigorous treatment of the topology and diffraction efficiency of the volume hologram, whose multiple wavefront storage capacity offers a possible solution to optical system recording.

Linear system theory is then revisited. Practicality is shown to dictate compromise, necessitating the formulation of the piecewise isoplanatic approximation, a method by which desired output functions may be synthesized.

The linear system and volume holography discussions merge under recording theory. Schemes are advanced for physically recording the response of a system, and limited implementation results are presented. A generalization of necessary system recording criteria is also offered.

ACKNOWLEDGMENTS

The author wishes to thank Mr. Thomas Engle for his instruction in the Rose-Hulman Optics Lab concerning the arts of holography and photography, Mrs. Mildred Smith for her secretarial assistance, and primarily Dr. Thomas F. Krile of the Electrical Engineering Department of Rose-Hulman for his initial suggestion of the thesis topic and for his advice and encouragement throughout the thesis formulation.

CONTENTS

	Page
Abstract	i
Acknowledgments	ii
Contents	iii
List of Figures	vi
I) The Thin Lens	1
A) Classical Ray Tracing	1
1) The Ray	2
2) Ray Tracing Laws	4
B) Magnification	6
C) Fourier Transforming Properties ..	10
II) Holography	16
A) A General View of Holography ...	16
B) Volume Holography	20
1) The Grating	20
a) The Three Dimensional Grating	20
b) The Two Dimensional Grating	24
c) The Reflection Analogy ..	26
2) Diffraction Efficiency	28
a) Derivation	28
b) The Bragg Condition	33
c) The Extinction Angle ...	35
d) Effects of Refraction ..	39
III) Linear System Theory	42
A) Linear Systems	42
1) Superposition Integral	43
2) Invariance and Convolution.	45
3) Fourier Relationships	46

B)	Linear Optical Systems	47
1)	Isoplanicity	48
2)	Measurement of Spatial Variance	50
C)	The Piecewise Isoplanatic Approximation	56
1)	The System Model	56
2)	Consequences	60
3)	Isoplanatic Linear Systems.	67
4)	Generalizations and Reflections	71
IV)	Recording Theory and Implementation	74
A)	Generating Spread and Transfer Functions	74
1)	The Dirac Delta and Spread Function	74
2)	The Transfer Function	76
3)	Holographically Recording the Transfer Function	78
a)	Availability of Form ...	78
b)	Desired Fourier Plane Expressions	81
c)	Limitations on Record- able Waveforms	81
B)	System Recording Employing the Extinction Angle	82
1)	Angular Intervals of Wave- forms	83
2)	The Angular Bandpass	85
3)	Recording and Reconstruction	87
4)	Implementation of a Holo- graphic Recording of a Non-inverting Magnifier ..	92
5)	Macroscopically Thick Holo- gram System Recording	94
C)	Generalization of System Record- ing Criteria	97
1)	Fly's Eye Implementation of the Magnifier	99
V)	Conclusions	102
VI)	Appendix	
A)	Distortion	104
B)	Fortran Generation of Extinction Angle Data	105

C)	Fortran Generation of the P.I.A. of the Fourier Trans- form of a Pulse	105
D)	Photographic Development of Holograms	105
VII)	References	106

LIST OF FIGURES

<u>Number</u>	<u>Description</u>
1	Formation of the double convex thin lens and the lens axis.
2	Rays describing equiphase surfaces.
3	Ray representation of a point source.
4	Illustration of ray tracing laws for the double convex thin lens.
5	Illustration of the Huygens-Fresnel principle.
6	Application of the Huygens-Fresnel principle for normal plane wave illumination of a transmittance.
7	Ray tracing geometry describing magnification employing the double convex thin lens.
8	Collimation of a point source.
9	Collimation of a point source in three dimensions.
10	General hologram recording.
11	Ray representations of conjugate plane waves.
12	Wavefront reconstruction of the hologram recorded in Fig. 10.
13	Period vector describing grating separation in an elementary volume hologram.
14	Side view of the gratings formed in an elementary volume hologram.
15	Direction cosine relationship in two dimensions.
16	Geometry of the reflection analogy.
17	Geometry describing the two-dimensional Fresnel-Kirchhoff diffraction integral.
18	The extinction angle as a function of reconstruction angular incidence.
19	Illustration of Snell's Law.

- 20 The extinction angle as a function of external recording parameters.
- 21 The limitation placed on direction cosines by refractive index.
- 22 The general system model.
- 23 The general optical system.
- 24 Extraction of an isoplanatic region from an arbitrary function.
- 25 The piecewise isoplanatic approximation (P.I.A.) output of the magnifier with a pulse input.
- 26 The P.I.A. of a magnifier with a general input.
- 27 The P.I.A. of a Fourier transformer with a pulse input.
- 28 The P.I.A. of an integrator and a differentiator with a pulse input.
- 29 Optical generation of the Dirac Delta.
- 30 Optical generation of the point spread function.
- 31 Optical generation of transfer function expressions.
- 32 Methods of reconstructing a recorded transfer function.
- 33 The angular interval of a transformed isoplanatic patch.
- 34 Angular bandpasses from the reconstruction of recordings in Fig. 32.
- 35 Desired reconstruction for extinction angle system recording.
- 36 Desired transfer function generation for extinction angle recording.
- 37 Extinction angle system recording for the Fourier transformer.
- 38 Extinction angle system recording for the magnifier.
- 39 Recording and corresponding diffraction efficiency from recording two patches of a magnifier.

- 40 Reconstruction geometry and corresponding output of the system recorded in Fig. 39.
- 41 Recording and reconstruction employing a macroscopically thick hologram.
- 42 Comparison of the piecewise isoplanatic approximation and macroscopically thick hologram outputs of various systems.
- 43 Block diagram of the extinction angle recording scheme.
- 44 Mapping of block orthogonal patches to block orthogonal angular intervals.
- 45 Block diagram of an alternate system recording scheme.
- 46 The fly's eye lens.
- 47 Implementation of P.I.A. of the simple magnifier employing fly's eye techniques.
- 48 Illustration of hologram distortion.

I) The Thin Lens

With applications ranging from simple magnification to Fourier transformation, the thin lens is distinguished as the most basic instrument in optical processing. Due primarily to the extensive use of Fourier transforms in linear system theory, and secondly, to lens' appearance in many optical systems of interest, a basic review of the properties of the thin lens is in order.

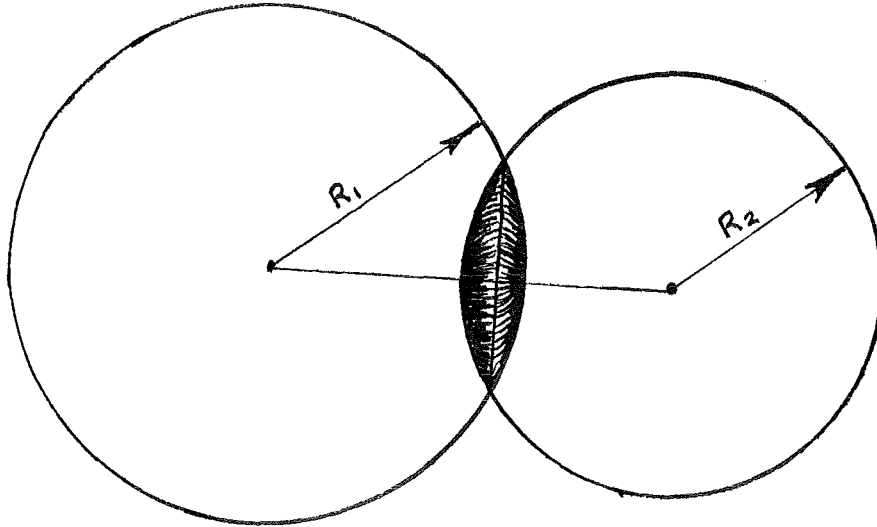
In general terms, a lens may be defined as a non-attenuating optical element which alters the phase of incident waveforms in a non-random manner. A lens is said to be thin if a ray incident on the lens at coordinates (x,y) emerges at the same coordinates. Properties of the thin lens may be derived from either wave optics or from geometrical tracing. For purely illustrative purposes, a combination of these models is employed here to describe thin lens operations with attention restricted to the double convex thin lens.

A) Classical Ray Tracing

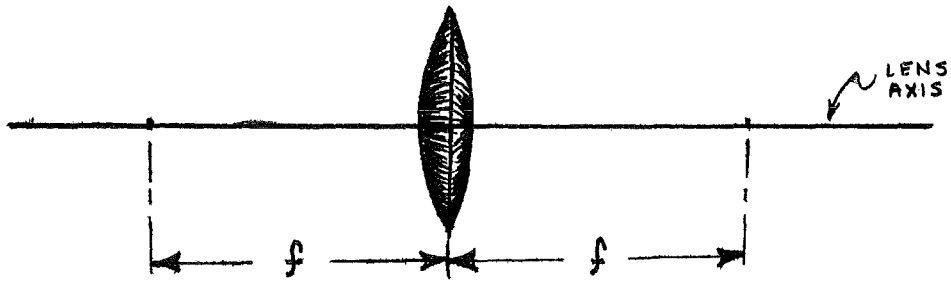
By far the most important lens parameter is the focal length. For the double convex lens, comprised of two adjoined sphere slices (Fig. 1a), the focal length is defined as ⁽¹⁾

$$f = \frac{1}{(n-1)\left(\frac{1}{R_1} + \frac{1}{R_2}\right)} \quad (1-1)$$

where n is the homogeneous index of refraction of the lens media, and R_1 and R_2 are the spheres' radii, which are positive.



- a) Formation from two adjoining sphere slices.
The spheres have radii R_1 and R_2 .



- b) Location of the focal points and lens axis.

Fig. 1 : Defining parameters of the double convex lens.

The lens axis is the line defined by joining the 'spheres' centers.

The properties of the thin lens may be illustrated through ray tracing techniques.

1) The Ray

In order to determine the lens' effect on incident waveforms we now introduce and discuss the concept of the optical ray. The electromagnetic theory presented by Maxwell predicts the presence of electric and magnetic vector fields in light waves. In 1890, Weiner experimentally confirmed the electric field's nearly complete dominance over the magnetic field in the formation of photographs. This hierarchy holds true not only for photographic emulsion, but for all photosensitive media in which holograms have been formed⁽²⁾. In diffraction analysis, the electric and magnetic fields may also be treated separately under the condition that the diffracting aperture is large in comparison to the wavelength of the illuminating light. Under these conditions, attention may be restricted to the electric field component of the electromagnetic wave.

Maxwell's equations relate the space and time derivatives of the electric field $\vec{v}(x,y,z,t)$ for propagation in free space⁽³⁾

$$\nabla^2 \vec{v}(x,y,z,t) = \frac{1}{c^2} \frac{\delta^2 \vec{v}(x,y,z,t)}{\delta t^2} \quad (1-2)$$

where $c = 3 \times 10^8 \frac{M}{Sec}$ is the speed of light in free space and ∇^2 , the Lapacian operator, is given as

$$\nabla^2 = \frac{\delta^2}{\delta x^2} + \frac{\delta^2}{\delta y^2} + \frac{\delta^2}{\delta z^2} \quad (1-3)$$

A scalar solution to (1-2) for the case of monochromatic (single-wavelength) light is⁽⁴⁾

$$V(x, y, z, t) = A(x, y, z) e^{j2\pi ct/\lambda} \quad (1-4)$$

where λ is the light's wavelength, and $A(x, y, z)$ is the complex amplitude or phasor describing both the phase and amplitude of the wave. Since the phase term in (1-4) is contained in most mathematical manipulations in the study of monochromatic wavefronts, we focus attention on

$$A(x, y, z) = a(x, y, z) e^{-j\phi(x, y, z)} \quad (1-5)$$

where $a(x, y, z)$ and $\phi(x, y, z)$ are respectively the magnitude and phase of $A(x, y, z)$.

A wavefront, or equiphase surface, is defined as the closed three-dimensional surface at time t_0 for which

$$\phi(x, y, z) = \phi_0 \quad (1-6)$$

where ϕ_0 is constant⁽⁵⁾. After passage of a short time δt , the same equiphase surface may be described by

$$\phi(x, y, z) = \phi_0 + \delta\phi \quad (1-7)$$

The point to point correlation of these wavefronts is established by "rays" as illustrated in Fig. 2. The ray also gives the direction of energy flow in the electric field.

In homogeneous isotropic materials, such as glass and air, rays are perpendicular to the described equiphase surfaces and may be thought of as incremental planar wavefronts. Consider, for example, Fig. 3a, in which a point source gives rise to spherical wavefronts at times t_0 and $t_0 + \delta t$. The correspond-

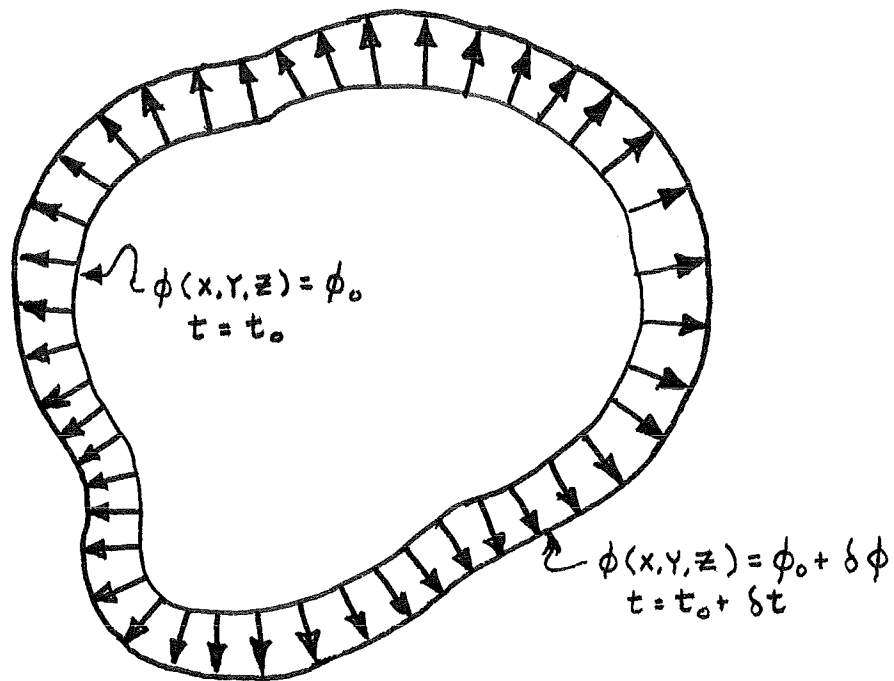


Fig. 2 : Equiphase surfaces or wave fronts,
 $\phi(x, y, z)$ at times t_0 and $t_0 + \delta t$
 The point by point mapping of the
 inner to outer surface is established
 by the rays.

ing ray representation given in Fig. 3b, consists of a family of rays diverging from the point source. Each ray is obviously normal to all of the spherical wavefronts generated by the point source.

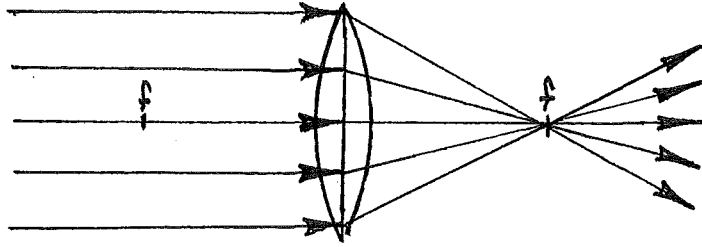
The optical ray proves to be an intuitively gratifying tool in analysis of electromagnetic propagation in homogeneous isotropic media, and is particularly useful in analysis of optical properties of the thin lens.

2) Ray Tracing Laws⁽⁶⁾

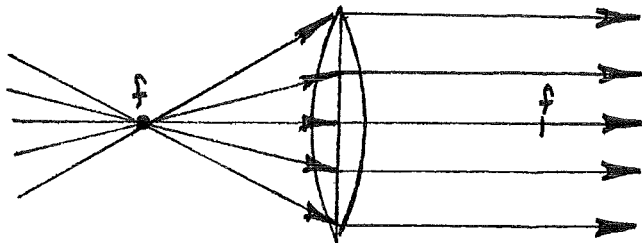
Classical ray tracing is a familiar topic in elementary optics for the case of the thin lens. With reference to Fig. 4, the ray tracing laws for the double convex thin lens are as follows:

- a) rays propagating parallel to the lens axis are bent by the lens to pass through the back focal point,
- b) rays passing through the front focal point emerge parallel to the lens axis,
- c) rays incident on the lens at the lens axis remain unbent.

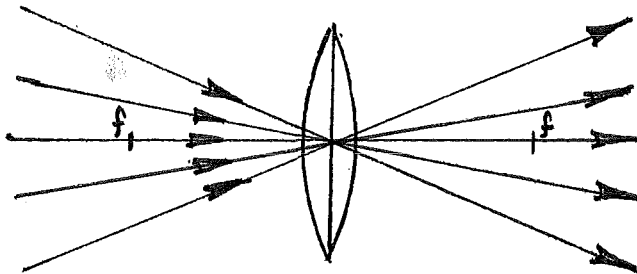
We now venture to illustrate the magnification and Fourier transformation properties of the thin lens employing these ray tracing laws.



- a) All rays parallel to the lens axis pass through the back focal point.



- b) All rays passing through the front focal point emerge parallel to lens axis.



- c) All rays passing through the lens at the lens axis remain unbent.

Fig. 4 : Ray tracing laws for the double convex thin lens.

B) Magnification

Prior to the advent of the laser, the lens was used primarily for magnification. A foundation for magnification theory is now offered followed by analysis of a simple one lens magnifier.

In the 17th century, Christian Huygens formulated what is presently called the Huygens-Fresnel Principle⁽⁷⁾. Huygens reasoned that each element of a wavefront can be considered as a secondary source and that the wavefront at any later instant can be found by the superposition of the resulting spherical wavelets, (Fig. 5). Although not rigorous in concept, application of the Huygens-Fresnel Principle has predicted results that agree amazingly well with experiment.

Consider then Fig. 6 in which a two dimensional transmittance function $g(x,y)$ is illuminated by a normal unit amplitude plane wave (i.e., a wavefront consisting of planar equiphase surfaces propagating perpendicular to the x-y plane.) The Huygens-Fresnel Principle dictates that each point on the transmittance acts as a secondary point source. That is

$$g(x,y) = \int_{-\infty}^{\infty} g(\xi,\eta) \delta(x-\xi, y-\eta) d\xi d\eta \quad (1-8)$$

where $\delta(x,y)$, the Dirac Delta, represents a point source and may be defined* as

$$\delta(x,y) = \lim_{N \rightarrow \infty} N^2 e^{-N^2 \pi (x^2 + y^2)} \quad (1-9)$$

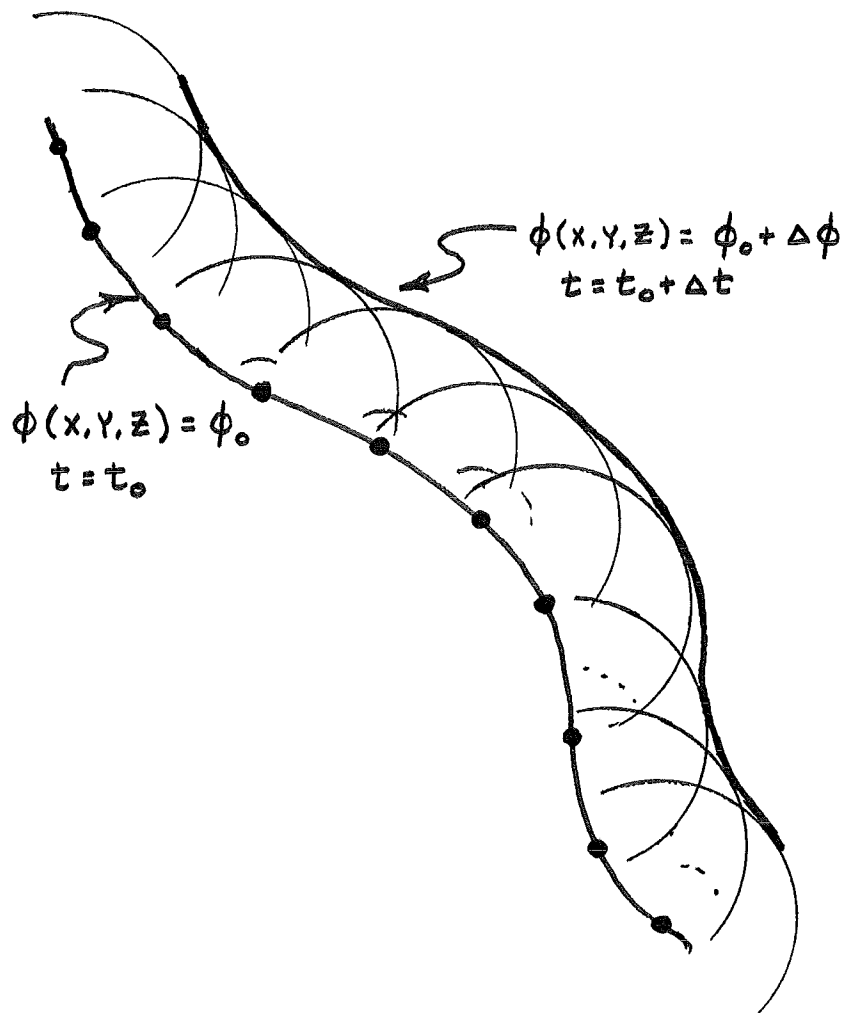


Fig. 5 : Illustration of the Huygens - Fresnel Principle. A wavefront at time t_0 , ($\phi(x, y, z) = \phi_0$) may be modeled as a continuum of secondary sources. The envelope of the resulting spherical wavelets after time Δt gives the position of the wavefront at time $t_0 + \Delta t$, ($\phi(x, y, z) = \phi_0 + \Delta\phi$).

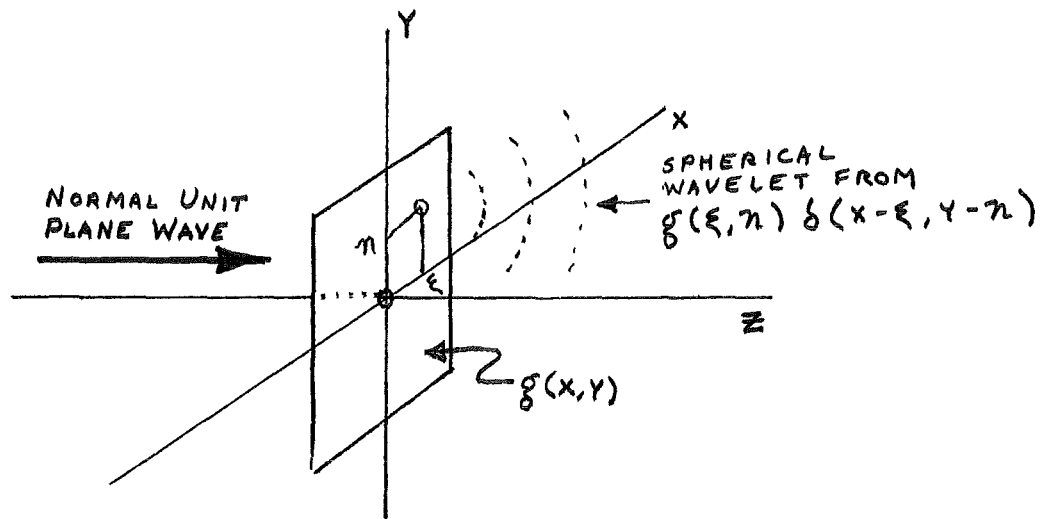


Fig. 6 : Application of the Huygens - Fresnel Principle to a transmittance, each point on $g(x, y)$ acts as a secondary source.

Equation (1-8), termed the sifting property of the Dirac Delta, is the mathematical statement of the Huygens-Fresnel Principle for the case at hand. The transmittance is expressed as a superposition of secondary point sources located at coordinates (ξ, η) and weighted by $g(\xi, \eta)$.

Suppose the configuration in Fig. 6 is placed a distance d_0 in front of a thin lens. Without loss of generality, attention is restricted to one dimension.

Consider first, the case where $d_0 > f$ as illustrated in Fig. 7a. The point at $x = \xi$ on the transmittance may be thought of as a secondary point source given as

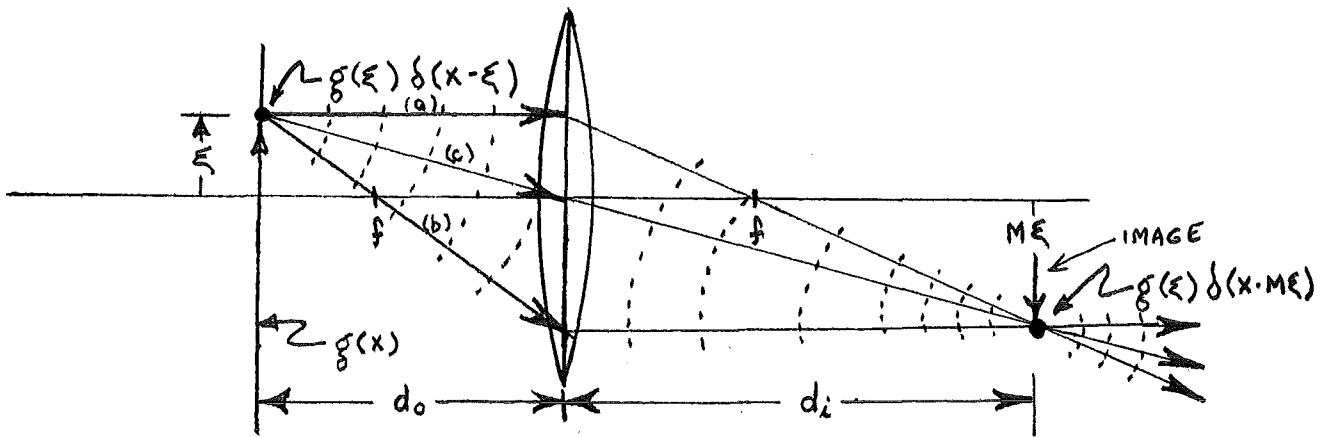
$$g(\xi) \delta(x - \xi) \quad (1-10)$$

From the resulting spherical wavelet, rays are chosen which apply directly to the ray tracing laws. With reference to Fig. 7a:

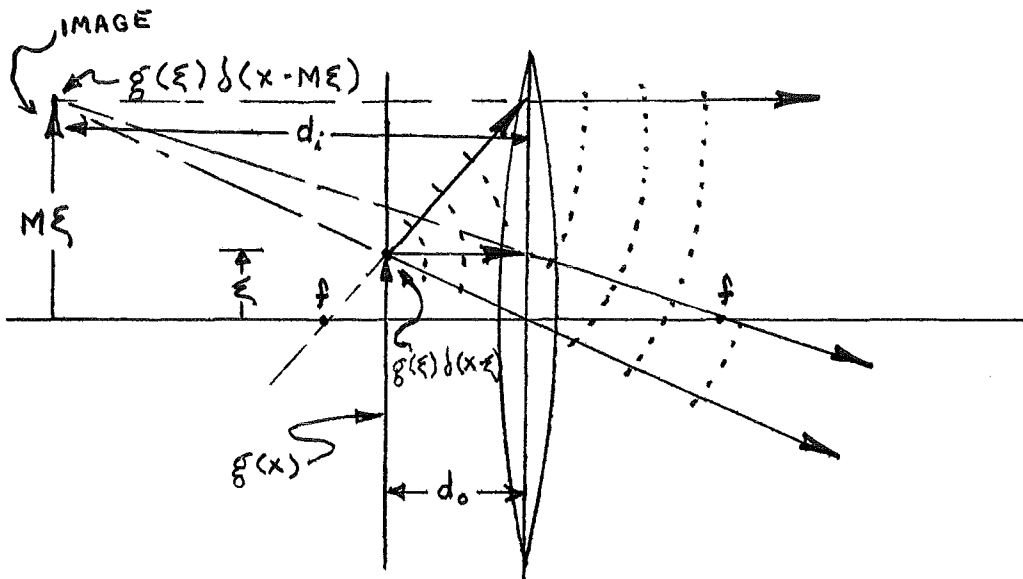
- a) The ray component propagating parallel to the lens axis is bent to pass through the back focal point.
- b) The ray passing through the front focal point emerges from the lens parallel to the lens axis.
- c) The ray incident on the lens at the lens axis remains unbent.

From the resulting geometry, each of these rays is seen to intersect at a distance d_i to the right of the lens and distance $M\xi$ below the lens axis, where M , the magnification, is the ratio of the displacement from the lens axis of these intersecting rays and the displacement from the lens axis to the secondary source on the transmittance. If the intersecting rays are extended

* For a wealth of limit definitions of the Dirac Delta, see Goodman⁽⁸⁾.



a) Magnifier when $d_o > f$. The image is inverted ($M < 0$) and real.



b) Magnification when $f < d_o$. The image is erect ($M > 0$) and virtual.

Fig. 7 : Employment of the thin lens as a simple magnifier. Dashed curves represent equiphase surfaces of spherical wavelets.

beyond their point of intersection, they will appear to be diverging from a common point, constituting the ray representation of a point source (Fig. 3). For this reason, the ray intersection point may be interpreted as a secondary point source given as

$$g(\xi) \delta(x - M\xi) \quad (1-11)$$

Magnification may thus be viewed as a mapping of secondary sources. From (1-10) and (1-11) we write

$$g(\xi) \delta(x - \xi) \longrightarrow g(\xi) \delta(x - M\xi)$$

where (\longrightarrow) denotes the mapping operation. To determine the effects of the entire transmittance we need to merely sum the effects of all the secondary sources on the transmittance. That is

$$\int_{-\infty}^{\infty} g(\xi) \delta(x - \xi) d\xi \longrightarrow \int_{-\infty}^{\infty} g(\xi) \delta(x - M\xi) d\xi \quad (1-12)$$

From a one dimensional equivalent of the Dirac Delta sifting property given in (1-8) it follows that

$$g(x) \longrightarrow g_0(x) = \int_{-\infty}^{\infty} g(\xi) \delta(x - M\xi) d\xi \quad (1-13)$$

where $g_0(x)$ represents the secondary source distribution resulting from the mapping. To evaluate the integral in (1-13), we must first recognize two identities of the Dirac Delta:

$$\delta(Mx) = \frac{1}{|M|} \delta(x) \quad (1-14)$$

and

$$\delta(x - \xi) = \delta(\xi - x) \quad (1-15)$$

Thus

$$g_o(x) = \frac{1}{|M|} \int_{-\infty}^{\infty} g(\xi) \delta(\xi - \frac{x}{M}) d\xi \quad (1-16)$$

or equivalently, from (1-8)

$$g_o(x) = \frac{1}{|M|} g(x/M) \quad (1-17)$$

The final mapping relationship is then expressed as

$$g(x) \longrightarrow \frac{1}{|M|} g(x/M) \quad (1-18)$$

This expression is the mathematical statement of the operation of magnification. The input function, $g(x)$, is "squashed down" in amplitude and "spread out" in space by a factor of M .

The above considerations are for $d_o > f$. Nearly identical results come from a similar analysis of the case where $d_o < f$ with the following differences: (compare Figs. 7a and 7b)

- 1) For $d_o < f$, the extended rays intersect behind the lens, constituting a virtual image. For $d_o > f$, the image is real and may be actually imaged on a screen.
- 2) For $d_o < f$, the image is erect. The magnification, M , is thus positive. The inverted image resulting when $d_o > f$ yields a negative value for M .

From the geometry of both Figs. 7a and 7b, one may derive the following general system parameter relationships:

$$M = -d_i / d_o \quad (1-19)$$

and

$$\frac{1}{f} = \frac{1}{d_i} + \frac{1}{d_o} \quad (1-20)$$

where d_o , the object distance, is always positive when located to the left of the lens and

$$\begin{aligned} d_i > 0 & \quad \text{if} \quad d_o > f \\ d_i < 0 & \quad \text{if} \quad d_o < f \end{aligned} \quad (1-21)$$

These expressions may be employed to find the orientation, magnitude, magnification, and location of an image given only the focal length and object distance of the magnifier.

The ray tracing analysis of the simple one lens magnifier predicts image formation for all $d \neq f$. We now illustrate, through similar ray tracing techniques, the effect of equating the object distance and focal length.

C) Fourier Transforming Properties of the Lens

When a transmittance, $\mathcal{G}(x,y)$ is placed in the front focal plane* of a double convex thin lens and illuminated with a normal monochromatic plane wave, the distribution on the lens' back focal plane* under certain conditions, is proportional to the Fourier transform of $\mathcal{G}(x,y)$. This operation may be illustrated through ray tracing techniques.

Consider the geometry presented in Fig. 8, where a point source is placed at $(x,z) = (\xi, -f)$ on the front focal plane of a double convex thin lens. Application of the ray tracing laws states that the ray propagating parallel to the lens axis is bent to pass through $(x,z) = (0,f)$ and the ray traveling through the

* The front and back focal planes are defined respectively as the planes perpendicular to the lens axis at a focal distance in front of and behind a lens.

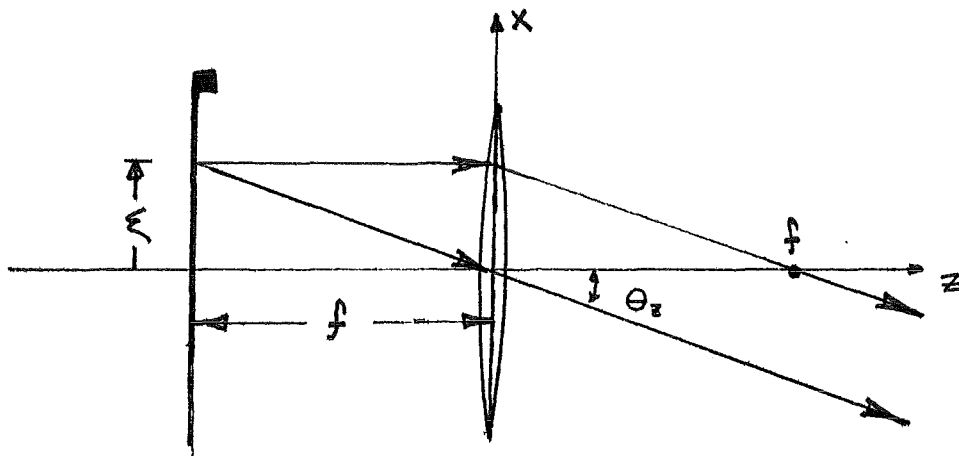


Fig. 8 : A point source on the front focal plane is collimated by the double convex thin lens to a plane wave.

lens at the lens axis remains unbent. Both of these rays lie at an angle

$$\theta_z = \text{atan}(-\xi/f) \quad (1-22)$$

with respect to the z axis. Thus these rays are parallel. Note that the third ray of possible interest is propagating in the negative x direction, and consequently never incident on the lens. It is true, however, that each ray incident on the lens emerges at an angle of θ_z with respect to the lens axis. The result is then a plane wave.

Consider Fig. 9 in which the above argument is extended into three dimensions. A point source at $(x,y,z) = (\xi, \eta, -f)$ is collimated into a plane wave, whose propagation direction is uniquely specified by direction cosines

$$\begin{aligned} \alpha &= \cos \theta_x = -\xi/r \\ \beta &= \cos \theta_y = -\eta/r \\ \gamma &= \cos \theta_z = f/r \end{aligned} \quad (1-23)$$

where

$$r = \sqrt{\xi^2 + \eta^2 + f^2} \quad (1-24)$$

and θ_x , θ_y , and θ_z are, respectively, the angles made by the ray with the x , y , and z axes. Note, that by definition,

$$\alpha^2 + \beta^2 + \gamma^2 = 1 \quad (1-25)$$

The expression for a unit amplitude monochromatic plane wave propagating with direction cosines α , β , and γ is given by

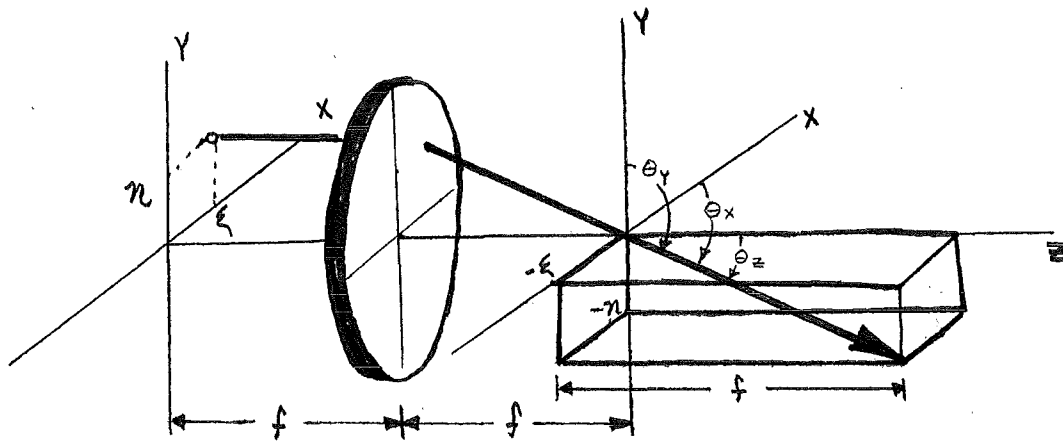


Fig. 9 : Collimation of a point source located in the front focal plane of a double convex thin lens three dimensions. The resulting propagation direction of the plane wave is defined by θ_x , θ_y and θ_z .

$$A(x, y, z) = e^{j\frac{2\pi}{\lambda}(\alpha x + \beta y + \gamma z)} \quad (1-26)$$

where λ represents wavelength. The validity of the interpretation of (1-26) is obvious when one equates the phase exponent to a constant ϕ_0 . The resulting expression is

$$\alpha x + \beta y + \gamma z = \lambda \phi_0 / 2\pi \quad (1-27)$$

This relationship describes a family of parallel equiphase planar wavefronts in space. From the previous discussion of equiphase surfaces, equation (1-26) is thus seen to be representative of a plane wave and is furthermore a solution to the wave equation [(1-2), (1-4)]⁽¹⁰⁾.

Substitution of the direction cosine relationships [(1-23)] into the plane wave expression [(1-26)] gives

$$A(x, y, z) = e^{-j\frac{2\pi}{\lambda f}(\xi x + \eta y - f z)} \quad (1-28)$$

Attention is now restricted to the case where

$$\xi \ll f \quad ; \quad \eta \ll f \quad (1-29)$$

so that

$$r \approx f \quad (1-30)$$

Equation (1-28) then becomes

$$A(x, y, z) \approx e^{j2\pi z/\lambda} * e^{-j\frac{2\pi}{\lambda f}(\xi x + \eta y)} \quad (1-31)$$

The consequences of this approximation are to be discussed shortly.

If attention is further restricted to the back focal plane of the lens, we have

$$\begin{aligned} U(x, y) &= A(x, y, f) \\ &\approx A_0 e^{-j \frac{2\pi}{\lambda f} (\xi x + \eta y)} \end{aligned} \quad (1-32)$$

where

$$A_0 = e^{-j 2\pi f / \lambda} \quad (1-33)$$

is a constant phase term.

Equation (1-32) gives the field distribution on the back focal plane of a double convex thin lens resulting from a point source, $\delta(x-\xi, y-\eta)$, located on the front focal plane. As with the magnifier, we have a mapping:

$$\delta(x-\xi, y-\eta) \rightarrow A_0 e^{-j \frac{2\pi}{\lambda f} (\xi x + \eta y)} \quad (1-34)$$

This relationship may be generalized employing the Huygens-Fresnel Principle of modeling a transmittance as a continuum of secondary sources when illuminated by a normal plane wave [(1-8)]. It follows that when the transmittance, $g(x, y)$, is placed on the front focal plane, the mapping becomes

$$\begin{aligned} g(x, y) &= \int_{-\infty}^{\infty} \int_{-\infty}^{\infty} g(\xi, \eta) \delta(x-\xi, y-\eta) d\xi d\eta \\ \rightarrow G_0(x, y) &= \int_{-\infty}^{\infty} \int_{-\infty}^{\infty} A_0 g(\xi, \eta) \\ &\quad \times e^{-j \frac{2\pi}{\lambda f} (\xi x + \eta y)} d\xi d\eta \end{aligned} \quad (1-35)$$

The interpretation of $G_0(x, y)$ becomes more apparent with the variable substitutions

$$f_x = \frac{x}{\lambda f} \quad ; \quad f_y = \frac{y}{\lambda f} \quad (1-36)$$

so that

$$\begin{aligned} G_1(f_x, f_y) &= G_0(x, y) \\ &= A_0 \int_{-\infty}^{\infty} \int_{-\infty}^{\infty} g(\xi, \eta) e^{-j2\pi(\xi f_x + \eta f_y)} d\xi d\eta \end{aligned} \quad (1-37)$$

Outside of the proportionality constant, A_0 , this expression is recognized as the Fourier transform of $g(x, y)$:

$$G(f_x, f_y) = \int_{-\infty}^{\infty} \int_{-\infty}^{\infty} g(x, y) e^{-j2\pi(f_x x + f_y y)} dx dy \quad (1-38)$$

In the more familiar one dimensional case, the Fourier transform of $g(t)$ is given as

$$G(f) = \int_{-\infty}^{\infty} g(t) e^{-j2\pi f t} dt \quad (1-39)$$

Optically, the Fourier transform, $G(f_x, f_y)$, appearing in the back focal plane of a double convex thin lens, is seen to be a superposition of planar wavelets, each originating from a secondary point source on the transmittance $g(x, y)$ placed at the front focal plane. One of the most remarkable and useful properties of a converging lens is its inherent ability to perform two-dimensional Fourier transformations.

In derivation of this lens operation, the equating of r and the focal length [(1-30)] is a rather radical approximation due to the large value of r which is on the order of 10^6 reciprocal meters for the case of visible light. The approximation error, multiplied by this large number, results in possible errors in excess of 2 radians. The final Fourier transform relationship, however, is in excellent agreement with the more rigorous wave optics derivation offered by Goodman⁽⁹⁾.

The field as viewed perpendicular to the z axis in Fig. 6 at a distance far exceeding the dimensional extent of the transmittance is termed the far field. The far field may also be shown to be proportional to the Fourier transform of the transmittance under a condition titled the Fraunhofer approximation⁽¹¹⁾. Though not directly analogous to (1-30), this approximation also deals with an alternate expression for r and consequently yields similar error.

The importance of this section is illustration of the remarkable capacity of the thin lens to perform Fourier transformations. This operation has proved a useful tool in optics and holds prominent status in this thesis.

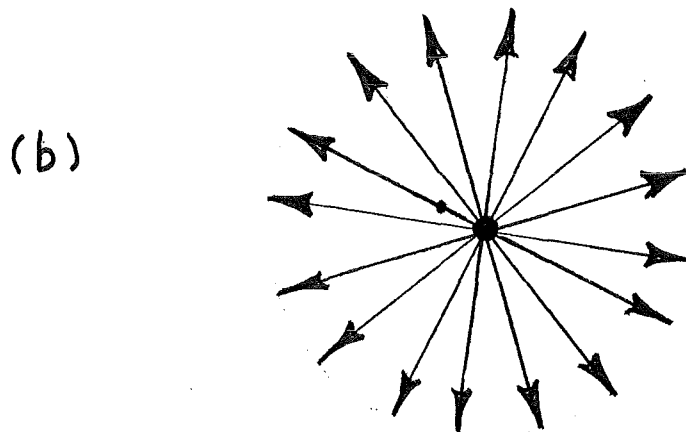
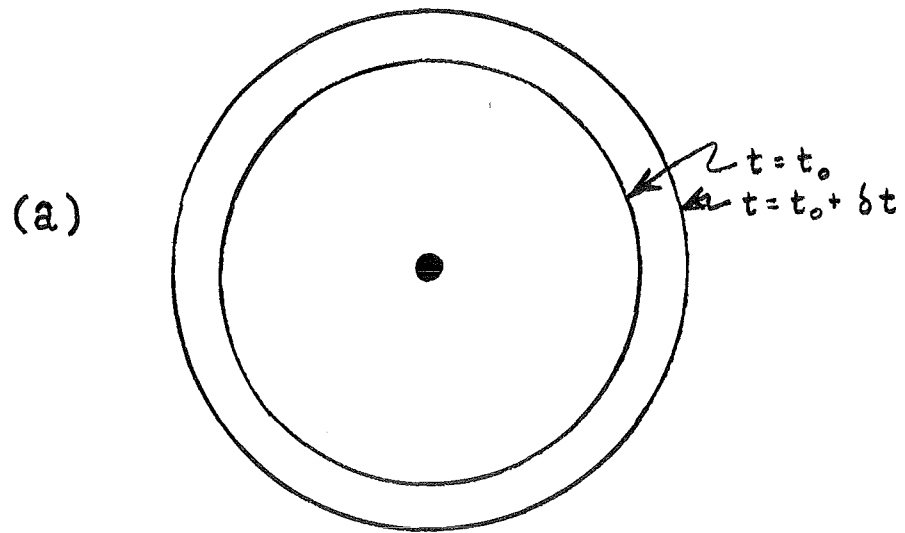


Fig. 3 : Spherical waves from a point source.

a) Spherical wavefronts at t_0 and $t_0 + \delta t$

b) Ray representation of the same point source.

II) Holography

In order to faithfully mimic a system's response, input-output amplitude and phase relationships of the system need to be known. Holography, or wavefront reconstruction, lends itself nicely to fulfilling these needs.

A) A General View of Holography⁽¹²⁾.

The wavefront reconstruction process consists of a recording and a reconstruction operation. First to be examined is the recording process.

Consider two wavefronts incident on a photosensitive medium (Fig. 10). The wave $U_o(x,y)$ is here referred to as the object wave and is allowed to be arbitrary in nature. The wave $U_r(x,y)$ is the reference beam. Both waves are monochromatic and may be expressed in terms of phase and magnitude as

$$\begin{aligned} U_o(x,y) &= V_o(x,y) e^{-j\phi_o(x,y)} \\ U_r(x,y) &= V_r(x,y) e^{-j\phi_r(x,y)} \end{aligned} \quad (2-1)$$

The film ideally records a transmittance proportional to the resulting intensity of incident waveforms. If a wave

$$U(x,y) = V(x,y) e^{-j\phi(x,y)} \quad (2-2)$$

is incident, the film records

$$\begin{aligned} I(x,y) &\propto |U(x,y)|^2 \\ &= U(x,y) U^*(x,y) \\ &= V^2(x,y) \end{aligned} \quad (2-3)$$

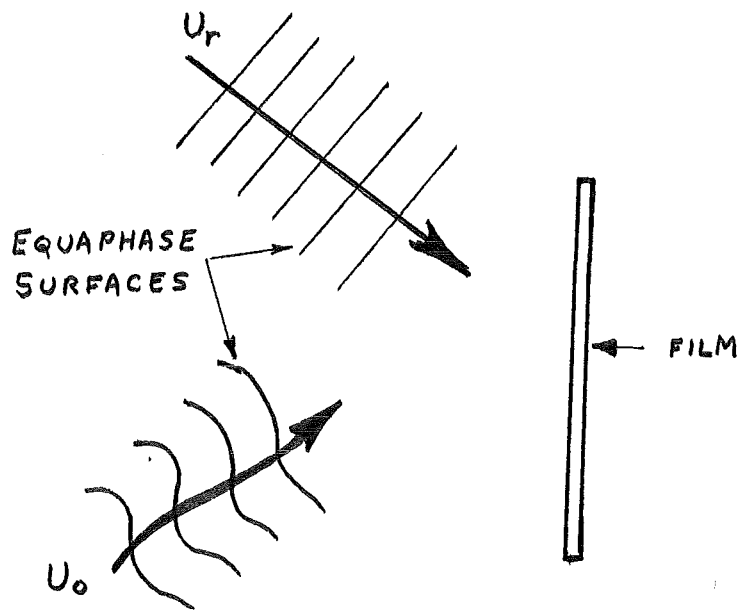


Fig. 10 : Holographic recording results from two beating waves. The reference wave (U_r) chosen here as planar, is recorded simultaneously with an object wave, (U_o) depicted here by wave equiphase surfaces to illustrate its more arbitrary nature.

where (\propto) is read "is proportional to" and (*) denotes complex conjugate. Here, and henceforth, the convenient proportionality constant of unity is adopted, so that (2-3) becomes

$$I(x, y) = |U(x, y)|^2 \quad (2-4)$$

Returning now to the object and reference beams, we have incident on the film

$$U(x, y) = U_o(x, y) + U_r(x, y) \quad (2-5)$$

so that the resulting intensity is given as

$$\begin{aligned} I(x, y) &= |U_o(x, y) + U_r(x, y)|^2 \\ &= [U_o(x, y) + U_r(x, y)][U_o^*(x, y) + U_r^*(x, y)] \end{aligned} \quad (2-6)$$

Substitution of the phase-amplitude relationships [(2-1)] gives

$$I = V_o^2 + V_r^2 + V_o V_r e^{-j(\phi_o - \phi_r)} + V_o V_r e^{j(\phi_o - \phi_r)} \quad (2-7)$$

or equivalently, from Euler's identity

$$I = V_o^2 + V_r^2 + 2 V_o V_r \cos(\phi_o - \phi_r) \quad (2-8)$$

Both phase and amplitude information are then contained in the final intensity distribution. Such a recording is dubbed a hologram, meaning a "total recording".

Before proceeding, an examination of the interpretation of a wave's conjugate expression is needed. In that a wavefront may be modeled by a number of rays, attention may be restricted to the plane wave with generalization to follow.

The conjugate of the plane wave expression given in (1-26) is

$$\begin{aligned} A^*(x, y, z) &= e^{-j\frac{2\pi}{\lambda}(\alpha x + \beta y + \gamma z)} \\ &= e^{j\frac{2\pi}{\lambda}[(-\alpha)x + (-\beta)y + (-\gamma)z]} \end{aligned} \quad (2-9)$$

The signs of the direction cosines are seen to be negated. The corresponding rays describing the plane wave and its conjugate, illustrated in Fig. 11a, have the same magnitude but opposite propagation directions. Generalization suggests this same relationship holds for any wavefront.

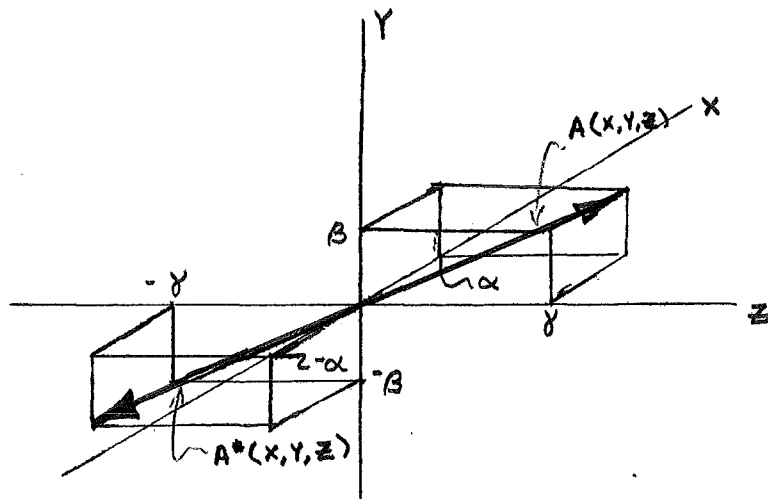
When one is concerned with distributions on planar surfaces, an additional wavefront may be considered as conjugate. For the plane wave case, we have from Fig. 11b

$$\bar{A}(x, y, z) = e^{j\frac{2\pi}{\lambda}[(-\alpha)x + (-\beta)y + \gamma z]} \quad (2-10)$$

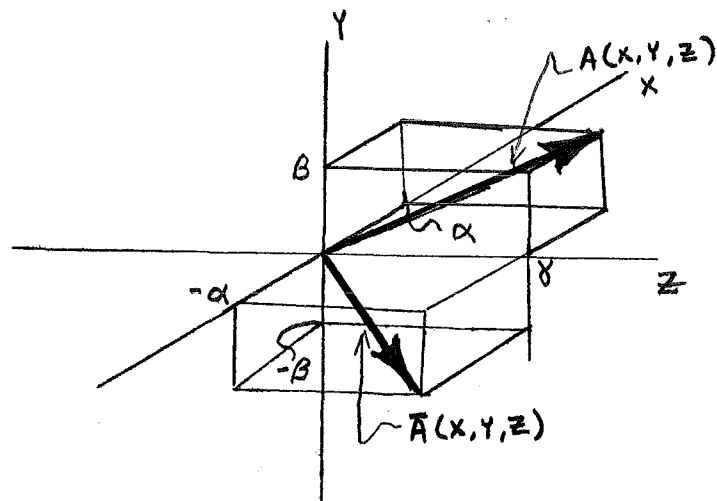
Obviously

$$\bar{A}(x, y, 0) = A^*(x, y, 0) \quad (2-11)$$

Thus, both distributions on the x-y plane are conjugate expressions of the distribution resulting from $A(x, y, 0)$. Generalization to more arbitrary wavefronts may be accomplished by a mapping of describing rays in this manner. With a feeling for conjugate waveforms, we turn now to reconstruction analysis.



a) The true conjugate ray.



b) The alternate conjugate ray for the case where one is concerned solely with the distribution on the X - Y plane. Note the equivalent X and Y components of the conjugate unit amplitude ray here and in Fig. 7a.

Fig. 11 : A unit amplitude ray and corresponding conjugate rays.

Once developed, the hologram is a complex transmittance which is described best for present purposes by (2-7). The first two terms, containing no phase information, turn out to be of little consequence and are thus presently disregarded.

Consider first, the illumination of the developed film by $U_r(x,y)$. The resulting waveform from the third term in (2-7) would be

$$U_3(x,y) = |U_r(x,y)|^2 U_o(x,y) \quad (2-12)$$

Suppose, for simplicity's sake, that a unit amplitude plane wave is chosen for the reference beam, so that

$$|U_r|^2 = \left| e^{j \frac{2\pi}{\lambda} (\alpha x + \beta y)} \right|^2 = 1 \quad (2-13)$$

Equation (2-12) then becomes

$$U_3(x,y) = U_o(x,y) \quad (2-11)$$

The original wavefront is thus reconstructed (Fig. 7a). If U_r^* is chosen for re-illumination, the fourth term in (2-7) becomes of interest and yields

$$U_4 = |U_r|^2 U_o^* = U_o^* \quad (2-12)$$

The resulting waveform of interest is seen to be the conjugate of the original object beam, which is physically represented by a mirror image of U_o off the system axis in the case for illumination as in Fig. 12.

Obviously, unit amplitude plane waves and ideal film cannot be actually used in holography, yet the resulting reconstructed wavefronts in practice are attenuated and possibly distorted versions of the original object wave.

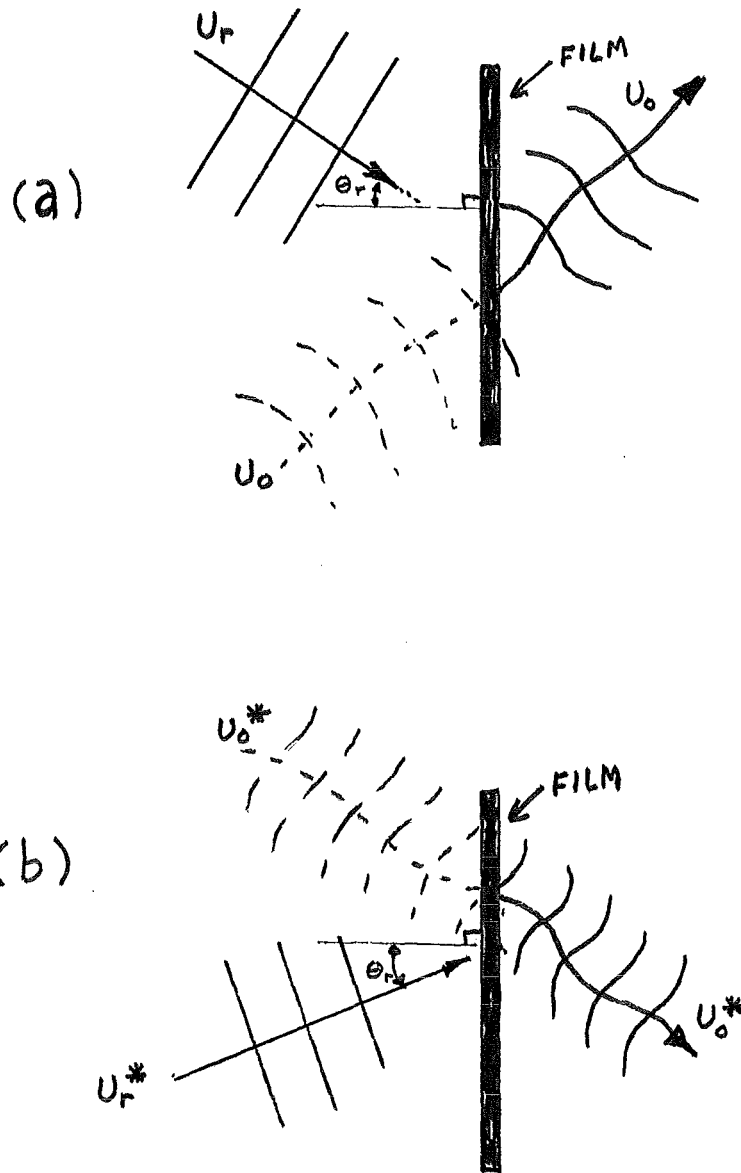


Fig. 12 : Illustration of wavefront reconstruction.
 (Compare with the recording geometry of Fig. 10)

- a) Wavefront reconstruction using the original reference beam.
- b) Conjugate wavefront reconstruction using the conjugate reference beam.

(The reconstructed wave in (a) is sometimes referred to as the virtual wavefront, and that in (b) as the real wavefront)

Upon reconstruction, terms were seemingly chosen arbitrarily from (2-7) in order to match the reconstruction wave. This is valid in implementation when the reconstructed beams are separated in space by proper choice of a reference beam, or when unwanted reconstructed waveforms may be successfully suppressed. When this is not the case, the interference of overlapping beams needs to be taken into account.

The hologram is seen to have the capacity to store both the phase and the amplitude of a wavefront in a pure amplitude recording. This operation proves useful in system recording.

B) Volume Holography

When the emulsion thickness of the film used in holography is large in comparison with the illuminating light's wavelength, the recording is termed a volume hologram. The volume hologram has the capacity to store a number of wavefronts within the emulsion of a single piece of film as opposed to the single wavefront storage capacity of the planar hologram.

The volume hologram is presently being employed in the field of optical computers⁽¹³⁾ and has been suggested as a possible model for the brain⁽¹⁴⁾.

1) The Grating

a) The three dimensional grating

To illustrate the intensity distribution within a volume hologram, the elementary case of two beating plane waves is now examined⁽¹⁵⁾. More complex distributions may then be

analyzed by Fourier techniques.

Consider two unit amplitude plane waves incident on a film with a refractive index of unity. From (1-26) we write

$$\begin{aligned} U_1(x, y, z) &= e^{jk(\alpha_1 x + \beta_1 y + \gamma_1 z)} \\ U_2(x, y, z) &= e^{jk(\alpha_2 x + \beta_2 y + \gamma_2 z)} \end{aligned} \quad (2-13)$$

where

$$k = 2\pi/\lambda \quad (2-14)$$

The emulsion of thickness t and height $2H$ records the resultant intensity of these waves. Following the three dimensional generalization of the intensity definition offered by (2-4), we write

$$I(x, y, z) = |U_1(x, y, z) + U_2(x, y, z)|^2 \left[\mu(x+H, y+H, z + \frac{t}{2}) - \mu(x-H, y-H, z - \frac{t}{2}) \right] \quad (2-15)$$

where $\mu(x, y, z)$ is the three dimensional generalization of the unit step function.

With the volume limits understood, substitution of the plane wave expressions [(2-13)] and expansion gives

$$\begin{aligned} I(x, y, z) &= 2 + e^{jk[(\alpha_1 - \alpha_2)x + (\beta_1 - \beta_2)y + (\gamma_1 - \gamma_2)z]} \\ &+ e^{-jk[(\alpha_1 - \alpha_2)x + (\beta_1 - \beta_2)y + (\gamma_1 - \gamma_2)z]} \\ &= 2[1 + \cos k\{(\alpha_1 - \alpha_2)x + (\beta_1 - \beta_2)y + (\gamma_1 - \gamma_2)z\}] \end{aligned} \quad (2-16)$$

This expression then describes the intensity distribution within the emulsion. For greater insight into this geometry, consider the locus of intensity maxima which occur when

$$\cos k [(\alpha_1 - \alpha_2)x + (\beta_1 - \beta_2)y + (\gamma_1 - \gamma_2)z] = 1 \quad (2-17)$$

or equivalently when

$$(\alpha_1 - \alpha_2)x + (\beta_1 - \beta_2)y + (\gamma_1 - \gamma_2)z = n\lambda ; \quad (2-18)$$

$$n = 0, \pm 1, \pm 2, \dots$$

On the x axis, these maxima occur when

$$(\alpha_1 - \alpha_2)x = n\lambda \quad (2-19)$$

For this reason, the x component of the spatial period and spatial frequency are defined respectively as

$$T_x = \frac{\lambda}{\alpha_1 - \alpha_2} \quad ; \quad f_x = \frac{1}{T_x} = \frac{\alpha_1 - \alpha_2}{\lambda} \quad (2-20a)$$

Similarly

$$T_y = \frac{\lambda}{\beta_1 - \beta_2} \quad ; \quad f_y = \frac{1}{T_y} = \frac{\beta_1 - \beta_2}{\lambda} \quad (2-20b)$$

$$T_z = \frac{\lambda}{\gamma_1 - \gamma_2} \quad ; \quad f_z = \frac{1}{T_z} = \frac{\gamma_1 - \gamma_2}{\lambda} \quad (2-20c)$$

It thus becomes evident that the maximum intensity loci is a family of parallel planes described best by the substitution of the above expressions into (2-18):

$$f_x x + f_y y + f_z z = n \quad (2-21)$$

The case for $n=1$ is illustrated in Fig. 13, along with the vector \vec{T} descriptive of the true plane spacing. The direction of \vec{T} coincides with the direction of the gradient of (2-21):

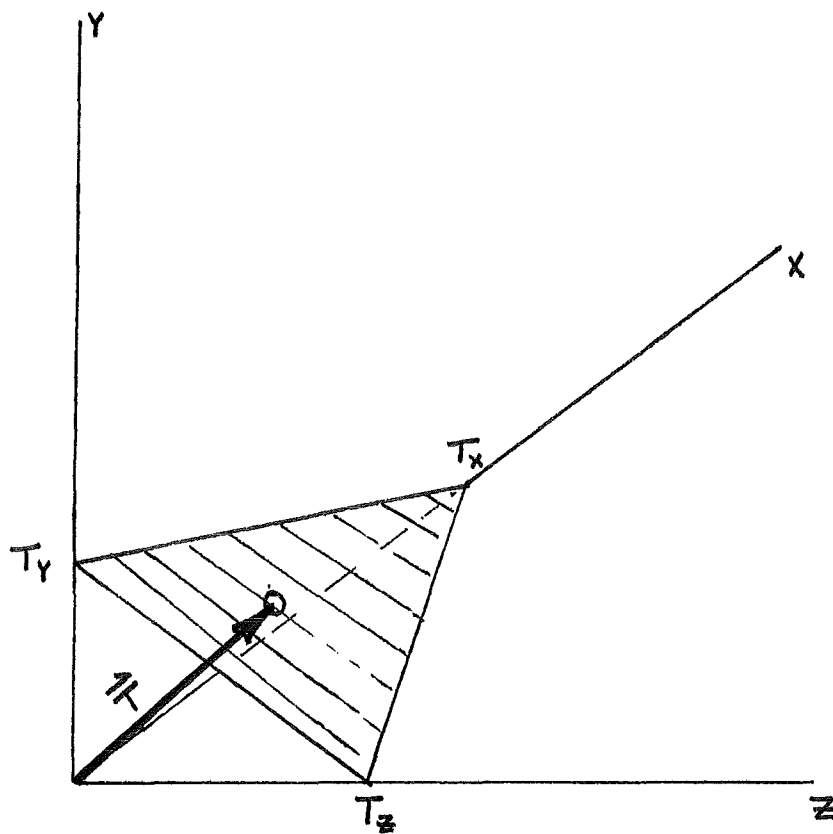


Fig. 13 : A plane of constant intensity formed by two beating plane waves. The perpendicular distance between two adjacent planes is given by the period vector \vec{T} .

$$\nabla (f_x x + f_y y + f_z z) = f_x \vec{i} + f_y \vec{j} + f_z \vec{k} \quad (2-22)$$

where \vec{i} , \vec{j} , and \vec{k} are unit vectors in the x, y, and z directions, respectively. The components of \vec{T} must also satisfy (2-21) so that

$$\vec{T} = \frac{f_x \vec{i} + f_y \vec{j} + f_z \vec{k}}{f_x^2 + f_y^2 + f_z^2} \quad (2-23)$$

Thus we may write

$$|\vec{T}| = [f_x^2 + f_y^2 + f_z^2]^{-1/2} \quad (2-24)$$

Substitution of the frequency expressions in (2-20) gives

$$|\vec{T}| = \frac{\lambda}{\sqrt{(\alpha_1 - \alpha_2)^2 + (\beta_1 - \beta_2)^2 + (\gamma_1 - \gamma_2)^2}} \quad (2-25)$$

Recalling that the sum of squares of a direction cosine set is unity [(1-25)] further simplifies this relationship to

$$|\vec{T}| = \frac{\lambda / \sqrt{2}}{\sqrt{1 - (\alpha_1 \alpha_2 + \beta_1 \beta_2 + \gamma_1 \gamma_2)}} \quad (2-26)$$

The magnitude of the spatial frequency vector, defined in the same direction as \vec{T} , is given as

$$|\vec{f}| = 1/|\vec{T}| = \frac{\sqrt{2}}{\lambda} \sqrt{1 - (\alpha_1 \alpha_2 + \beta_1 \beta_2 + \gamma_1 \gamma_2)} \quad (2-27)$$

The above relationships describe the intensity distribution within the thick emulsion. A further insight into this topology is gained through a two-dimensional analysis.

b) The two dimensional grating⁽¹⁵⁾.

Transition from three to two dimensional analysis may here be accomplished by assuming no variation with respect to Y.

We thus set

$$\beta_1 = \beta_2 = 0 \quad (2-28)$$

This assumes the plane waves which formed the grating were propagating normal to the Y axis. For this case, the maximum intensity loci are described according to (2-18) as

$$(\alpha_1 - \alpha_2)x + (\gamma_1 - \gamma_2)z = n\lambda \quad (2-29)$$

Solving for x gives

$$x = - \frac{\gamma_1 - \gamma_2}{\alpha_1 - \alpha_2} z + \frac{n\lambda}{\alpha_1 - \alpha_2} \quad (2-30)$$

This relationship suggests a family of constant intensity lines as seen from an end on view of the hologram (Fig. 14).

Two dimensional analysis allows convenient relationships between the direction cosines. From Fig. 15:

$$\gamma = \cos \Theta_z = \cos \Theta \quad (2-31)$$

$$\alpha = \cos \Theta_x = \cos \left(\frac{\pi}{2} - \Theta \right) = \sin \Theta$$

From (2-30), the constant intensity lines have slope,

$$\frac{dx}{dz} = - \frac{\gamma_1 - \gamma_2}{\alpha_1 - \alpha_2} \quad (2-32)$$

Substitution of (2-31) with appropriate subscripts yields

$$\frac{dx}{dz} = - \frac{\cos \Theta_1 - \cos \Theta_2}{\sin \Theta_1 - \sin \Theta_2} \quad (2-33)$$

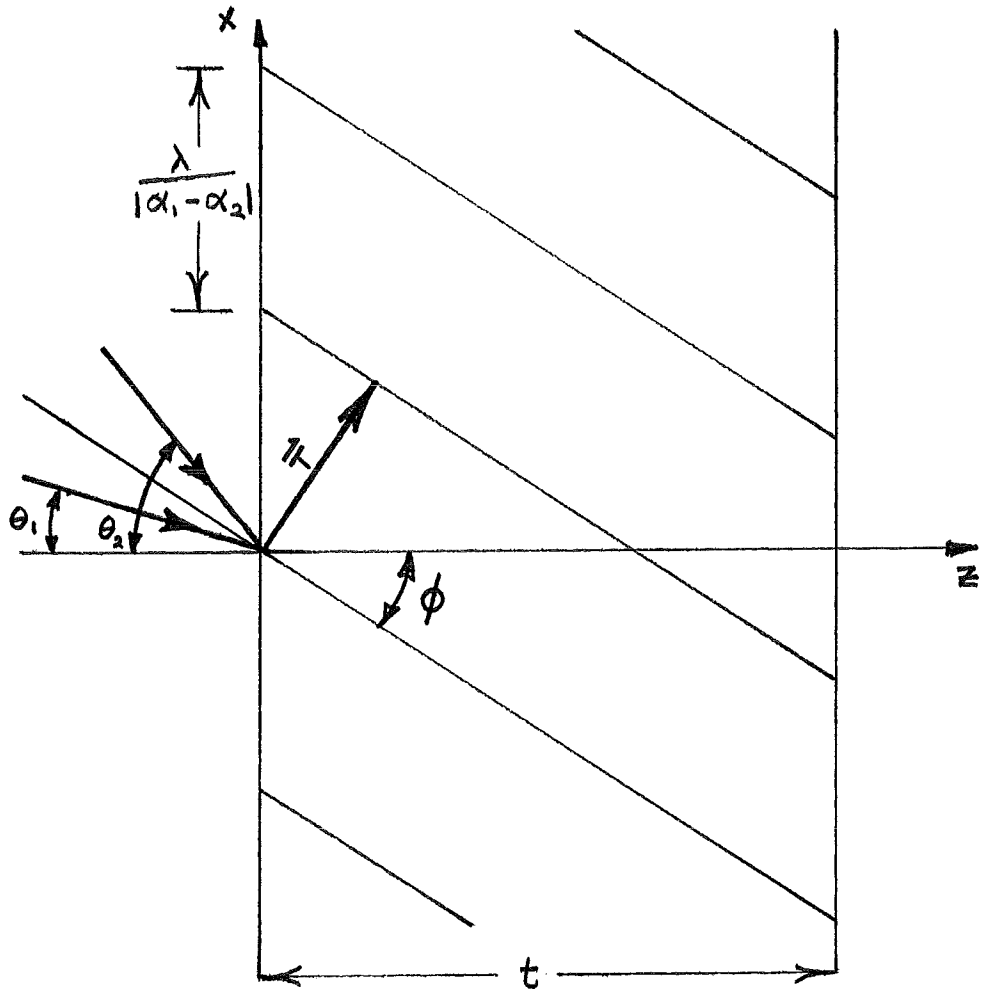


Fig. 14 : Geometry of the maximum intensity loci in a volume hologram formed by two plane waves propagating at angles θ_1 and θ_2 with respect to the hologram's normal.

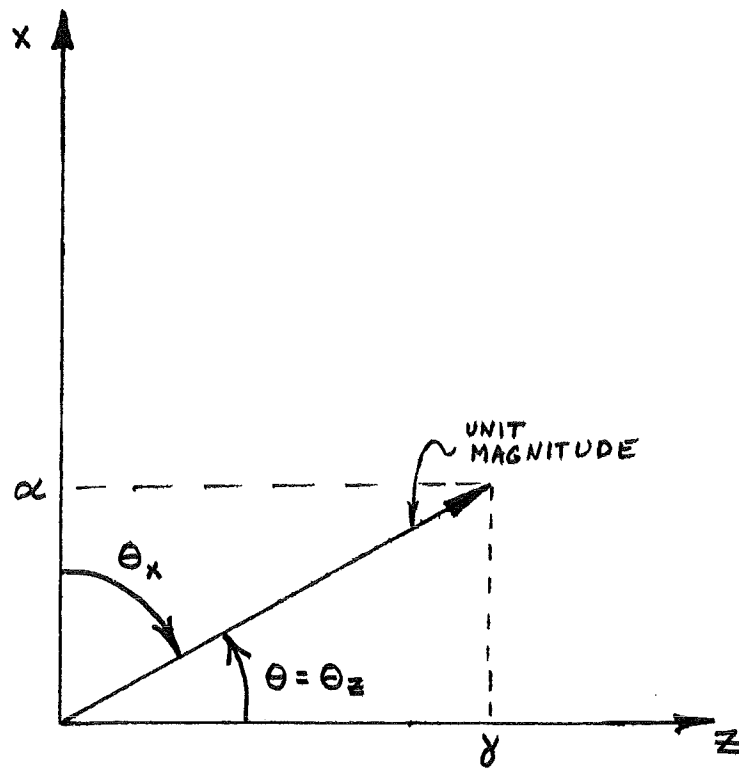


Fig. 15 : Relationship of the direction cosines (α and γ) in two dimensions.

This can be reduced via trigonometric identities to:

$$\frac{dx}{dz} = \tan \frac{\theta_1 + \theta_2}{2} \quad (2-34)$$

Defining the arithmetic mean of θ_1 and θ_2 as

$$\phi = \frac{\theta_1 + \theta_2}{2} \quad (2-35)$$

we have

$$\frac{dx}{dz} = \tan \phi \quad (2-36)$$

Thus, two waves incident on a thick photosensitive medium at angles θ_1 and θ_2 with respect to the film's normal, form a sinusoidal grating whose constant intensity loci lie at the bisected angle between θ_1 and θ_2 . (See Fig. 14).

The spatial frequency of the fringes for the two dimensional grating is given from (2-27) as

$$f = \frac{\sqrt{1 - (\alpha_1 \alpha_2 + \delta_1 \delta_2)}}{\lambda / \sqrt{2}} \quad (2-37)$$

Substitution of the sinusoidal assignments [(2-31)] followed by trigonometric simplification gives

$$f = \frac{\sqrt{1 - \cos(\theta_1 - \theta_2)}}{\lambda / \sqrt{2}} \quad (2-38)$$

Further simplification follows.

$$\begin{aligned} f &= \frac{2}{\lambda} \sin\left(\frac{\theta_1 - \theta_2}{2}\right) \\ &= \frac{\sin \theta_1 - \sin \theta_2}{\lambda \cos\left(\frac{\theta_1 + \theta_2}{2}\right)} \\ &= \frac{\sin \theta_1 - \sin \theta_2}{\lambda \cos \phi} \end{aligned} \quad (2-39)$$

This final relationship will later prove useful in diffraction efficiency analysis of volume holograms.

c) The reflection analogy⁽¹⁴⁾.

As in planar holography, one would expect illumination of the developed transmittance with one of the recording plane waves to yield a diffracted plane wave propagating in the same direction as the second recorded plane waves.

Consider, then, the geometry of Figure 16a where the grating formed by two plane waves propagating at angles θ_1 and θ_2 is recorded. The volume transmittance is illuminated with a plane wave propagating at an angle θ_1 . Thinking of the constant intensity fringe as a mirror, one sees that the equivalent angle of incidence is

$$\psi = \phi - \theta_1 \quad (2-40)$$

The beam then is reflected at an angle of

$$\theta_r = \phi + \psi \quad (2-41)$$

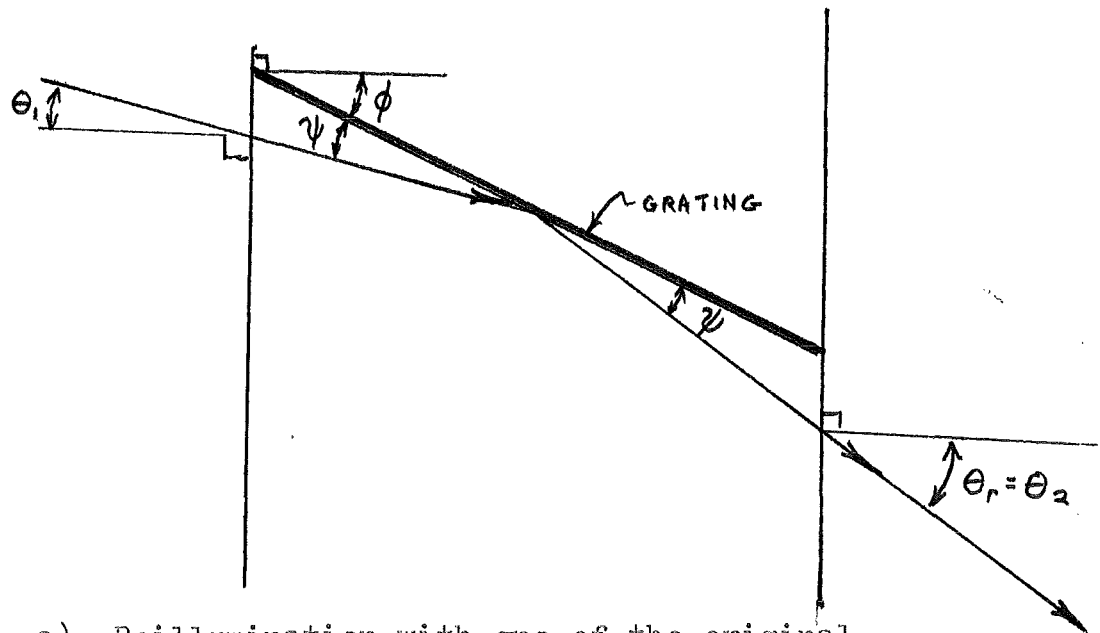
or equivalently

$$\theta_r = 2\phi - \theta_1 \quad (2-42)$$

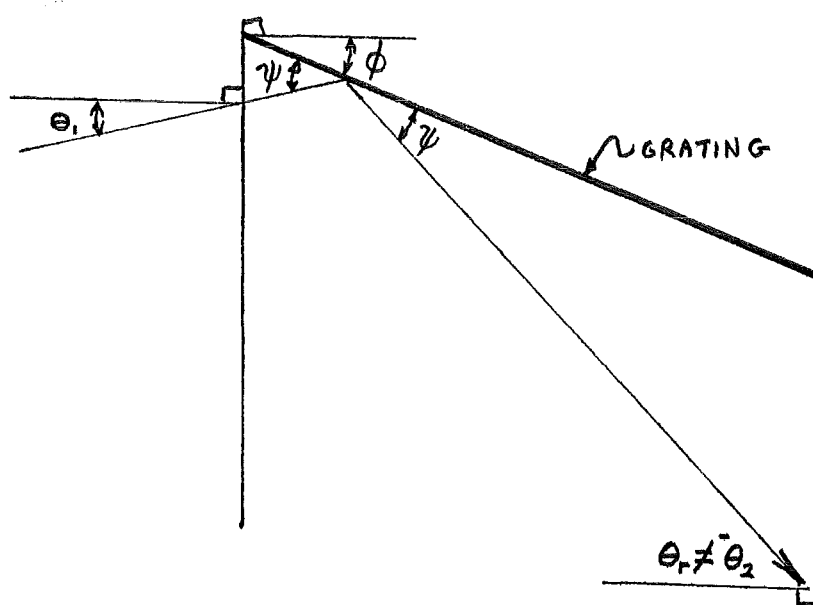
and finally from (2-35)

$$\theta_r = \theta_2 \quad (2-43)$$

A similar analysis gives θ_1 as the reflected propagation direction when the hologram is re-illuminated with a ray propagating at an angle θ_2 . These results are in harmony with the arguments presented by (2-11) and Fig. 12a (in the case of planar holography) and prove to be useful tools in intuitive analysis of gratings.



- a) Reillumination with one of the original recording beams yields a diffracted wave in the direction of the other recorded beam, supporting the reflection analogy.



- b) Reillumination with the conjugate of one of the recording beams gives a reflected beam not propagating in the direction of the second recording beam. The reflection analogy thus fails for conjugate reconstruction.

Fig. 16 : Geometry describing the reflection analogy. The constant intensity grating at angle ϕ in the hologram is modeled as a mirror, and was formed by two beating plane waves. (See Fig. 13)

What, then, of the conjugate case? As previously stated, the conjugate of a wavefront may be thought of as a reflection of the original wavefront on the system axis. Thus, the conjugate of the plane wave represented by θ_1 would be a plane wave propagating at an angle of $-\theta_1$ with respect to the hologram normal. As witnessed by the geometry of Fig. 16b, the reflection analogy does not hold for conjugate illumination as the following analysis reveals.

The angle of incidence to the mirror modeled grating in Fig. 16b is

$$\psi = \phi + \theta_1 \quad (2-44)$$

and is thus reflected at an angle of

$$\theta_r = \phi + \psi \quad (2-45)$$

Combining and substituting (2-35) gives:

$$\begin{aligned} \theta_r &= 2\phi + \theta_1 \\ &= 2\theta_1 + \theta_2 \end{aligned} \quad (2-46)$$

If the reflection analogy did hold we would expect

$$\theta_r = -\theta_2 \quad (2-47)$$

A similarly distasteful result evolves when considering illumination by $-\theta_2$.

The reflection analogy is thus seen to be valid only for illumination with original wavefronts and not for the conjugate case. Due to this limitation, care must be taken in its application.

2) Diffraction efficiency.

In order to efficiently store a number of wavefronts in a volume hologram, an a priori knowledge of diffraction efficiency is needed. Diffraction efficiency is the ratio of power in the reconstruction and reconstructed waveforms. We are here primarily concerned with diffraction efficiency as a function of the angle of incidence of the reconstruction beam.

The scalar derivation to follow is taken closely from Smith⁽¹⁶⁾. A more rigorous derivation yielding diffraction efficiency amplitudes and similar angular orientation sensitivity is derived using coupled wave theory by Collier, Burchart, and Lin⁽¹⁷⁾.

a) Derivation

Analysis of diffraction efficiency begins with a two-dimensional approximation of the Fresnel-Kirchhoff diffraction integral described by the geometry of Fig. 17 which is given by Smith⁽¹⁶⁾ as

$$U(P_i) = A \cos \phi \sqrt{\frac{-i}{\lambda}} \int_{\Sigma} \frac{e^{ik(s+r)}}{\sqrt{rs}} dx \quad (2-48)$$

where integration is over the aperture Σ . As depicted in Fig. 17, P_c is a line source with amplitude "A" at a unit distance, and ϕ is the angle between the object and image lines with respect to the z axis. If point P_c lies at coordinates (x_c, z_c) , and P_i at (x_i, z_i) , then

$$r_c^2 = x_c^2 + z_c^2 \quad (2-49a)$$

$$s_i^2 = x_i^2 + z_i^2 \quad (2-49b)$$

The magnitude of r is similarly given as

$$r = \sqrt{(x - x_c)^2 + z_c^2} \quad (2-50)$$

Expanding the quadratic and noting (2-49a) gives

$$r = \sqrt{x^2 - 2xx_c + r_o^2} \quad (2-51)$$

or equivalently

$$r = r_o \sqrt{1 - \frac{2x_c x - x^2}{r_o^2}} \quad (2-52)$$

The paraxial approximation states

$$\sqrt{1 - a^2} \approx 1 - a^2/2 \quad \text{IF} \quad a \ll 1 \quad (2-53)$$

Thus, if attention is restricted such that

$$(2x_c x - x^2)/r_o^2 \ll 1 \quad (2-54)$$

The relationship in (2-52) becomes

$$\begin{aligned} r &= r_o \left[1 - \frac{2x_c x - x^2}{2r_o^2} \right] \\ &= r_o - \frac{x_c x}{r_o} + \frac{x^2}{2r_o} \end{aligned} \quad (2-55)$$

Through similar analysis

$$s \approx s_o - \frac{x_i x}{s_o} + \frac{x^2}{2s_o} \quad (2-56)$$

Another approximation which may be made under the cited assumptions is

$$\sqrt{rs} \approx \sqrt{r_o s_o} \quad (2-57)$$

Substitution of the above three expressions into the Fresnel-Kirchhoff integral [(2-48)] gives

$$U(P_i) = A \sqrt{\frac{-j}{\lambda s_0 r_0}} e^{jk(r_0 + s_0)} \cos \phi \quad (2-58)$$

$$\times \int_{\Sigma} e^{-jk \left[\frac{xx_c}{r_0} - \frac{x^2}{2r_0} + \frac{xx_i}{s_0} - \frac{x^2}{2s_0} \right]} dx$$

Direction cosines are now assigned the rays in Fig. 14

$$\begin{aligned} l_c &= \cos \theta_c & l_i &= \cos \theta_i \\ m_c &= \sin \theta_c & m_i &= \sin \theta_i \end{aligned} \quad (2-59)$$

or equivalent

$$\begin{aligned} l_c &= -z_c/r_0 & l_i &= z_i/s_0 \\ m_c &= -x_c/r_0 & m_i &= x_i/s_0 \end{aligned} \quad (2-60)$$

The c subscripts denote the incident ray $\vec{P}_c Q$ and i the diffracted ray $\vec{Q} P_i$. Substituting into (2-58) gives

$$U(P_i) = A \cos \phi \sqrt{\frac{-j}{\lambda s_0 r_0}} e^{jk(r_0 + s_0)} \quad (2-61)$$

$$\times \int_{\Sigma} e^{-jk \left[x(m_i - m_c) - \frac{x^2}{2r_0} - \frac{x^2}{2s_0} \right]} dx$$

We now take the limit as s_0 and r_0 approach infinity so that the quadratic terms in the exponential under the integral vanish. It is also assumed that the source strength A may be made arbitrarily large, so that

$$\lim_{\substack{r_0 \rightarrow \infty \\ s_0 \rightarrow \infty \\ A \rightarrow \infty}} A \cos \phi \sqrt{\frac{-j}{\lambda s_0 r_0}} e^{jk(r_0 + s_0)} = c' \quad (2-62)$$

where c' is a complex constant. Under these assumptions,

(2-61) becomes

$$U(m_i) = c' \int_{\Sigma} e^{-jk(m_i - m_c)x} dx \quad (2-63)$$

This expression governs Fraunhofer's diffraction from a thin aperture in terms of direction cosines. One is tempted to generalize (2-63) to govern diffraction from a volume hologram by writing

$$U(l_i, m_i) = c'' \int_{\Sigma} \int e^{-j k [(m_i - m_c)x + (l_i - l_c)z]} dx dz \quad (2-64)$$

This expression, though, assumes each wave incident on each slice of dz thickness is equivalent, and thus holds only as a first order approximation for weak diffraction. For stronger diffraction from a spatial transmittance, a summation of all elementary diffractions must be made. The following diffraction integral results:

$$U(l_i, m_i) = c \int_{-H}^H \int_{-t/2}^{t/2} G(x, z) e^{-j k [(m_i - m_c)x + (l_i - l_c)z]} dx dz \quad (2-65)$$

The integral limits are here defined via the step function in (2-15).

The function $G(x, z)$ in (2-65) is the pupil function, and is representative of the spatial transmittance variation within the aperture. For the case of two beating plane waves, $G(x, z)$ may be determined from (2-16) under the conditions of (2-28):

$$G(x, z) = 2 [1 + \cos k \{(\alpha_1 - \alpha_2)x + (\gamma_1 - \gamma_2)z\}] \quad (2-66)$$

or equivalently,

$$G(x, z) = 2 [1 + \cos k (\alpha_1 - \alpha_2) \left(x + \frac{\gamma_1 - \gamma_2}{\alpha_1 - \alpha_2} z \right)] \quad (2-67)$$

For a more representative expression of the pupil function, direction cosines are assigned the fringes in Fig. 14:

$$\begin{aligned} \ell &= \cos \phi \\ m &= \sin \phi \end{aligned} \quad (2-68)$$

From (2-32) and (2-36) the slope of these fringes may then be expressed as

$$\tan \phi = \frac{m}{\ell} = \frac{\gamma_2 - \gamma_1}{\alpha_1 - \alpha_2} \quad (2-69)$$

Substituting into the pupil function [(2-67)] gives

$$G(x, z) = 2 \left[1 + \cos k (\alpha_1 - \alpha_2) \left(x - \frac{m}{\ell} z \right) \right] \quad (2-70)$$

or equivalently

$$G(x, z) = 2 \left[1 + \cos \frac{k}{\ell} (\alpha_1 - \alpha_2) (\ell x - m z) \right] \quad (2-71)$$

As promised, we now recall equation (2-39). Employing (2-31) and (2-68) we write

$$f_0 = \frac{\alpha_1 - \alpha_2}{\lambda \ell} \quad (2-72)$$

which may be expressed in angular terms as

$$\omega_0 = 2\pi f_0 = \frac{k (\alpha_1 - \alpha_2)}{\ell} \quad (2-73)$$

Substitution into (2-71) produces the desired expression for the pupil function formed by two beating plane waves:

$$G(x, z) = 2 \left[1 + \cos \omega_0 (\ell x - m z) \right] \quad (2-74)$$

This relationship is now employed to give a measure of the volume hologram's diffraction efficiency as a function of angular incidence of the reconstruction beam.

b) Bragg condition

Expanding the sinusoidal term of the pupil function via Euler's identity, and substituting into equation (2-65) yields

$$U(l_i, m_i) = c \int_{-H}^H \int_{-t/2}^{t/2} \left[2 + e^{j\omega_0(lx - mz)} + e^{-j\omega_0(lx - mz)} \right] \times e^{-jkx(m_i - m_c)} e^{-jkz(l_i - l_c)} dz dx \quad (2-75)$$

This expression divides into three integrals

$$\begin{aligned} U(l_i, m_i) = & 2c \int_{-H}^H \int_{-t/2}^{t/2} e^{-jkx(m_i - m_c)} e^{-jkz(l_i - l_c)} dz dx \\ & + c \int_{-H}^H \int_{-t/2}^{t/2} e^{-j[km_i - km_c - \omega_0 l]x} e^{-j[kl_i - kl_c + \omega_0 m]z} dz dx \\ & + c \int_{-H}^H \int_{-t/2}^{t/2} e^{-j[km_i - km_c + \omega_0 l]x} e^{-j[kl_i - kl_c - \omega_0 m]z} dz dx \end{aligned} \quad (2-76)$$

Since

$$\int_{-A}^A e^{-jB\xi} d\xi = 2A \operatorname{sinc}(BA) \quad (2-77)$$

where

$$\operatorname{sinc}(x) = \frac{\sin(x)}{x} \quad (2-78)$$

the diffraction expression becomes:

$$\begin{aligned}
 U(l_i, m_i) = & 4CHt \sin x \left[\frac{t}{2} (kl_i - kl_c) \right] \\
 & \times \sin x [H(km_i - km_c)] \\
 & + 2CHt \sin x \left[\frac{t}{2} (kl_i - kl_c + \omega_0 m) \right] \\
 & \times \sin x [H(km_i - km_c - \omega_0 l)] \\
 & + 2CHt \sin x \left[\frac{t}{2} (kl_i - kl_c - \omega_0 m) \right] \\
 & \times \sin x [H(km_i - km_c + \omega_0 l)]
 \end{aligned} \tag{2-79}$$

This diffraction expression has strict analogy to the complex transmittance of a planar hologram offered in (2-7). The first two terms in (2-7) correspond to the first term in (2-79) which yields the zeroth order diffracted beam that contains no information, and is disregarded when possible. The second and third terms correspond respectively to the primary and conjugate reconstructed object beams.

Equation (2-79) also contains information pertaining to diffraction efficiency as a function of angular orientation. As will be shown, the volume grating may be thought of as an angular bandpass filter, attenuating all diffracted waves which are not propagating in the direction of the recording beam or in the direction of the recording beam's conjugate. This property is analogous to Bragg's law of constructive and destructive interference and is appropriately called the Bragg condition.

c) Extinction Angle

Since one is usually concerned with the primary diffracted beam, and not the conjugate, attention is now restricted to the second term in (2-79):

$$U_2(l_i, m_i) = 2CHt \sin x \left[\frac{t}{2} (kl_i - kl_c + \omega_0 m) \right] \times \sin x [H(km_i - km_c - \omega_0 l)] \quad (2-80)$$

The Bragg condition is satisfied when (2-80) is maximum, which occurs when the arguments of the $\sin x$ function are zero.

$$l_i = l_c - \frac{\omega_0 m}{K} \quad ; \quad m_i = m_c + \frac{\omega_0 l}{K} \quad (2-81)$$

Substitution of (2-69) and (2-73) and simplification gives the following equivalent expressions

$$l_i = l_c + \gamma_1 - \gamma_2 \quad ; \quad m_i = m_c + \alpha_1 - \alpha_2 \quad (2-82)$$

Substitution of the sinusoids assigned to each of these variables yields the not-too-surprising conclusion that the Bragg condition is satisfied when

$$\theta_i = \theta_1 \quad ; \quad \theta_c = \theta_2 \quad (2-83)$$

That is, the reconstruction beam is identical to a recording beam and the diffracted beam is identical to the second recording beam.

We now define the extinction angle as the angular deviation from maximum diffraction efficiency necessary to extinguish the diffracted waveform. This occurs when the $\sin x$ functions in (2-80) become zero. The first does so when

$$\frac{t}{2} [k(l_i + \Delta l_i) - k(l_c + \Delta l_c) - \omega_0 m] = \pi \quad (2-84)$$

where l_i and l_c are chosen to meet the Bragg condition. Substitution of (2-69) and (2-73) into (2-84) followed by simplification, gives

$$l_i + \Delta l_i - l_c - \Delta l_c + \delta_2 - \delta_1 = \lambda/t \quad (2-85)$$

Since the Bragg condition specified by (2-82a) is met, we may write:

$$\Delta l_i - \Delta l_c = \lambda/t \quad (2-86)$$

Similarly, analysis for the second $\sin x$ function yields

$$\Delta m_c - \Delta m_i = \lambda/2H \quad (2-87)$$

In the case where

$$H \gg \lambda \quad (2-88)$$

we may safely restate (2-87) as

$$\Delta m_c - \Delta m_i = 0 \quad (2-89)$$

If attention is restricted to small angular deviations, the direction cosines may be estimated from the differentials of equations (2-59)

$$\Delta l_c = -\sin \theta_c \Delta \theta_c = -m_c \Delta \theta_c \quad (2-90a)$$

$$\Delta l_i = -\sin \theta_i \Delta \theta_i = -m_i \Delta \theta_i \quad (2-90b)$$

$$\Delta m_c = \cos \theta_c \Delta \theta_c = l_c \Delta \theta_c \quad (2-90c)$$

$$\Delta m_i = \cos \theta_i \Delta \theta_i = l_i \Delta \theta_i \quad (2-90d)$$

Note that $\Delta \theta_c$ is, by the previously given definition, the extinction angle, which now needs to be solved in terms of non-incremented values. From (2-89), (2-90c) and (2-90d)

$$\Delta \theta_i = \frac{l_c}{l_i} \Delta \theta_c \quad (2-91)$$

Substituting into (2-90b)

$$\Delta l_i = -m_i \frac{l_c}{l_i} \Delta \theta_c \quad (2-92)$$

Subtracting (2-90a) from (2-92) and noting (2-86), we write

$$\Delta l_i - \Delta l_c = \left(m_c - m_i \frac{l_c}{l_i} \right) \Delta \theta_c = \lambda/t \quad (2-93)$$

Solving for the extinction angle then gives

$$\Delta \theta_c = \frac{\lambda}{t} \left[\frac{l_i}{m_c l_i - m_i l_c} \right] \quad (2-94)$$

Note that because of (2-83)

$$(l_i, m_i) = (\gamma_1, \alpha_1) \quad (2-95a)$$

and

$$(l_c, m_c) = (\gamma_2, \alpha_2) \quad (2-95b)$$

As a function of recording parameters, the extinction angle is then

$$\Delta \theta_c = \frac{\lambda}{t} \frac{\gamma_o}{\alpha_r \gamma_o - \alpha_o \gamma_r} \quad (2-96)$$

where for clarity the r subscript denoting the reference beam has replaced the 1 subscript and 0 denoting the object beam has replaced the 2 subscript.

Substituting the trigonometric assignments to the direction cosines [(2-31)] into the extinction angle relationship, followed by a trigonometric simplification gives

$$\Delta \theta_c = \frac{\lambda}{t} \frac{\cos \theta_o}{\sin (\theta_r - \theta_o)} \quad (2-97)$$

The corresponding plot of $\Delta \theta_c$ as a function of the reference angle (Fig. 18) resembles a cosecant curve (which it is for $\theta_o = 0$) and is a generalization of that offered by Smith.⁽¹⁶⁾

Due to the approximations made in the derivation, (2-97) may only be ascribed the status of a first order approximation to the extinction angle.

As an example of interpretation of Fig. 18, consider the case where both object and reference beam are equivalent (i.e. $\theta_i = \theta_o$). The resulting hologram would record a constant intensity, or equivalently, a grating of zero frequency. The resulting reconstruction process would obviously yield a "diffracted" beam of unchanging intensity for all angles of reconstruction incidence. The corresponding extinction angle may thus be interpreted as infinite.

Note also that the extinction angle decreases as the emulsion thickness increases, giving the volume hologram a larger capacity for storing wavefronts.

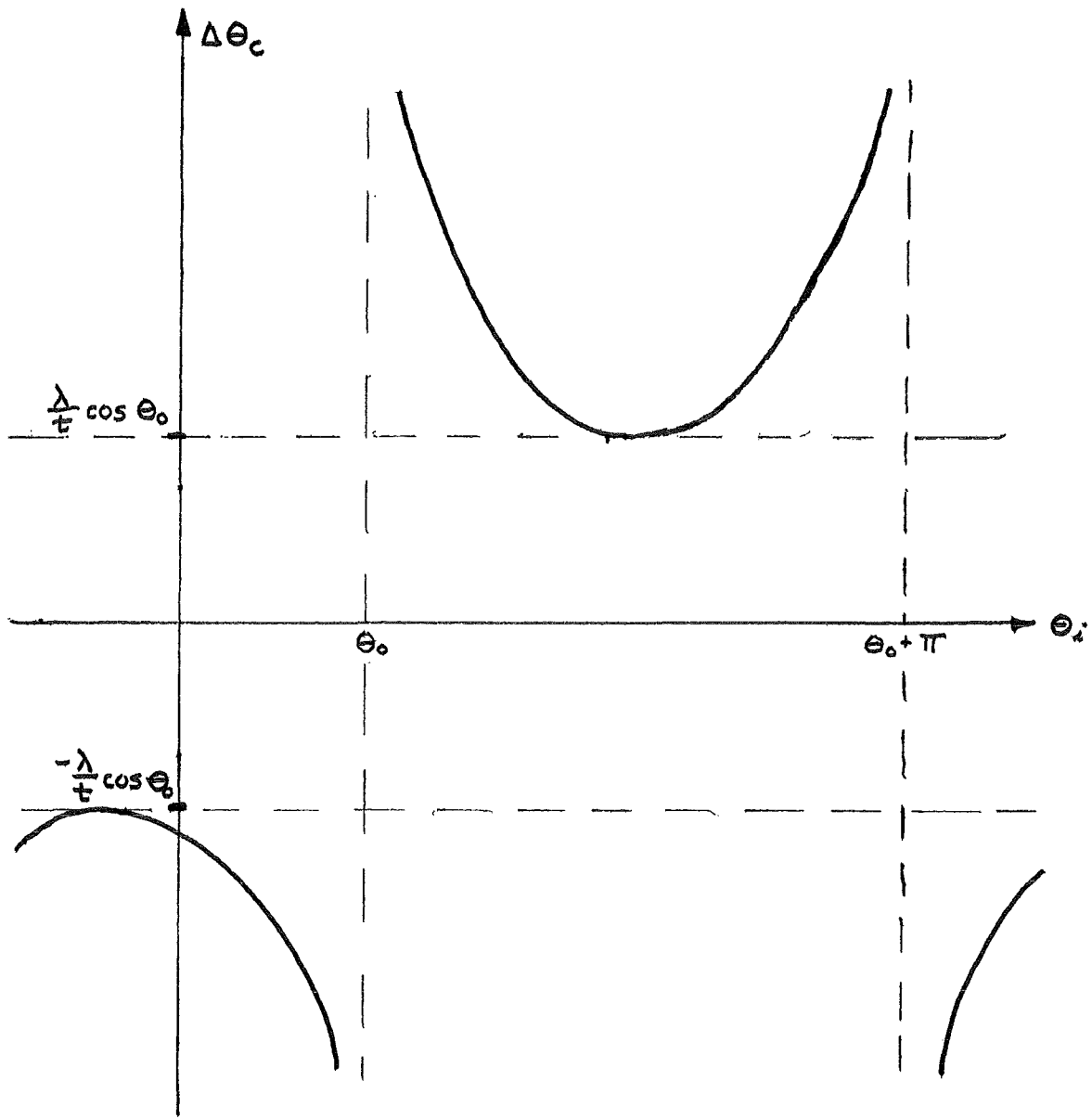


Fig. 18 : A first order approximation of the extinction angle as a function of the angle of incidence of the reconstruction beam.

d) Effects of refraction

To this point all properties of the volume hologram have been expressed in terms of parameters within the emulsion. Due to its importance in later applications, the extinction angle expression is now manipulated to contain only external parameters.

We begin by stating Snell's law described by the geometry of Fig. 19

$$\sin \theta' = n \sin \theta \quad (2-98)$$

where n is the homogeneous refractive index of the emulsion, θ' is the angle of incidence, and θ is the angle of refraction. Here and henceforth, primed variables denote external parameters.

An elementary manipulation of (2-98) gives

$$\theta = \sin^{-1} \left[\frac{1}{n} \sin \theta' \right] \quad (2-99)$$

With appropriate subscripts, substitution into (2-97) yields

$$\Delta \theta_c = \frac{\lambda}{t} \frac{\cos \left[\sin^{-1} \left(\frac{1}{n} \sin \theta'_o \right) \right]}{\sin \left[\sin^{-1} \left(\frac{1}{n} \sin \theta'_r \right) - \sin^{-1} \left(\frac{1}{n} \sin \theta'_o \right) \right]} \quad (2-100)$$

Expanding the denominator we write

$$\Delta \theta_c = \frac{\lambda}{t} \frac{\cos \left[\sin^{-1} \left(\frac{1}{n} \sin \theta'_o \right) \right]}{\cos \left[\sin^{-1} \left(\frac{1}{n} \sin \theta'_o \right) \right] \left[\frac{1}{n} \sin \theta'_r \right] - \cos \left[\sin^{-1} \left(\frac{1}{n} \sin \theta'_r \right) \right] \left[\frac{1}{n} \sin \theta'_o \right]} \quad (2-101)$$

Since

$$\cos \left[\sin^{-1} \left(\frac{1}{n} \sin \theta \right) \right] = \sqrt{1 - \frac{\sin^2 \theta}{n^2}} \quad (2-102)$$

equation (2-101) becomes

$$\Delta \theta_c = \frac{\lambda}{t} \frac{\sqrt{1 - \frac{\sin^2 \theta'_o}{n^2}}}{\sqrt{1 - \frac{\sin^2 \theta'_o}{n^2}} \left[\frac{1}{n} \sin \theta'_r \right] - \sqrt{1 - \frac{\sin^2 \theta'_r}{n^2}} \left[\frac{1}{n} \sin \theta'_o \right]} \quad (2-103)$$

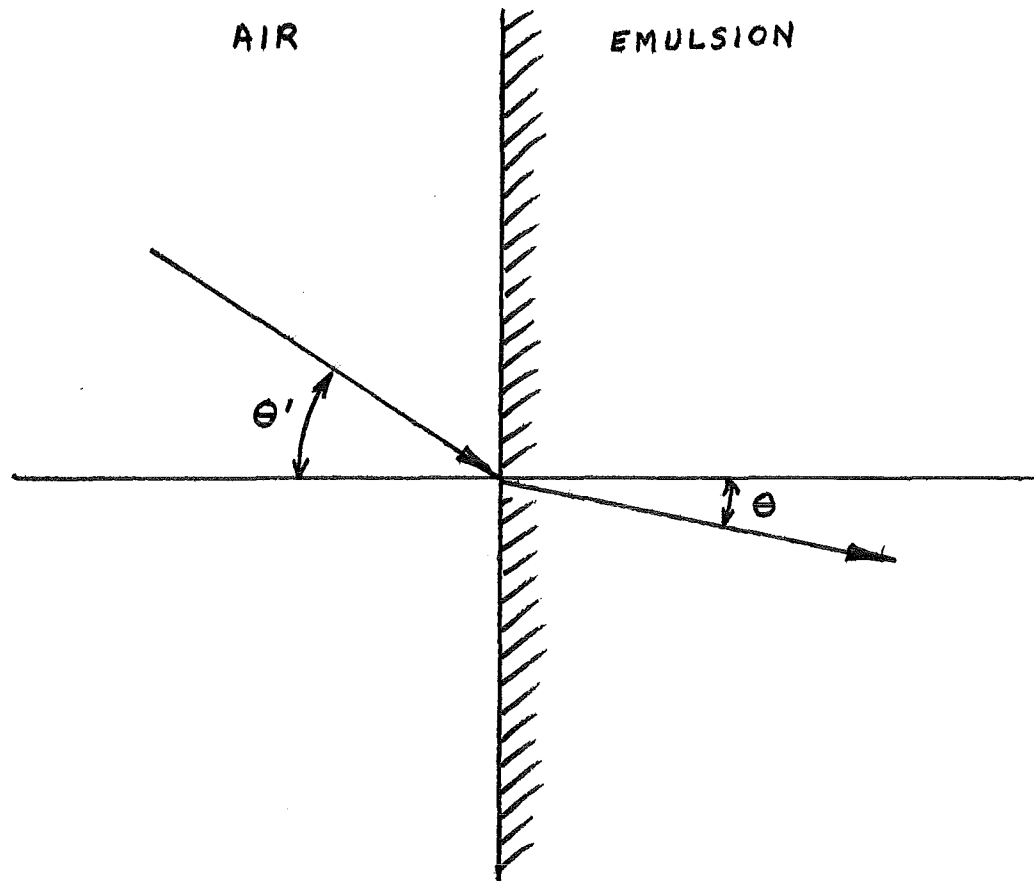


Fig. 19 : Illustration of Snell's law. The ray, entering a medium of homogeneous refractive index n from air with a refractive index of unity, is bent toward the normal in accordance with (2-98)

Before a final simplification, an additional substitution is in order. If a monochromatic wave has wavelength λ_a external to the recording medium (in air), then the wavelength λ within the medium is

$$\lambda = \lambda_a / n \quad (2-104)$$

Substitution into (2-103) followed by simplification gives

$$\Delta \theta_c = \frac{\lambda_a}{t} \frac{n^2 - \sin^2 \theta_o'}{\sqrt{n^2 - \sin^2 \theta_o'} \sin \theta_r' - \sqrt{n^2 - \sin^2 \theta_r'} \sin \theta_o'} \quad (2-105)$$

Let

$$\begin{aligned} l_o' &= \sqrt{n^2 - \sin^2 \theta_o'} & ; & \quad m_o' = \sin \theta_o' \\ l_r' &= \sqrt{n^2 - \sin^2 \theta_r'} & ; & \quad m_r = \sin \theta_r' \end{aligned} \quad (2-106)$$

so that (2-105) simplifies to

$$\Delta \theta_c = \frac{\lambda_a}{t} \frac{l_o'}{l_o' m_r' - l_r' m_o'} \quad (2-107)$$

The quantities in (2-107) may be thought of as effective direction cosines, displaying similar computational status as the direction cosines, (Compare (2-96) and (2-107)) but void of direction cosines properties. Specifically

$$(l_r')^2 + (m_r')^2 = n^2 \neq 1 \quad (2-108)$$

A family of extinction angle curves as a function of object angle and discrete variation of the reference angle is offered in Fig. 20 from (2-107). Recording parameters are for the helium-neon laser ($\lambda_a = 6328 \text{ \AA}$) and Kodak 649F emulsion ($t = 15 \mu\text{M}$; $n \approx 1.5$). A general Fortran computer program allowing variable parameters to generate data for similar curves is

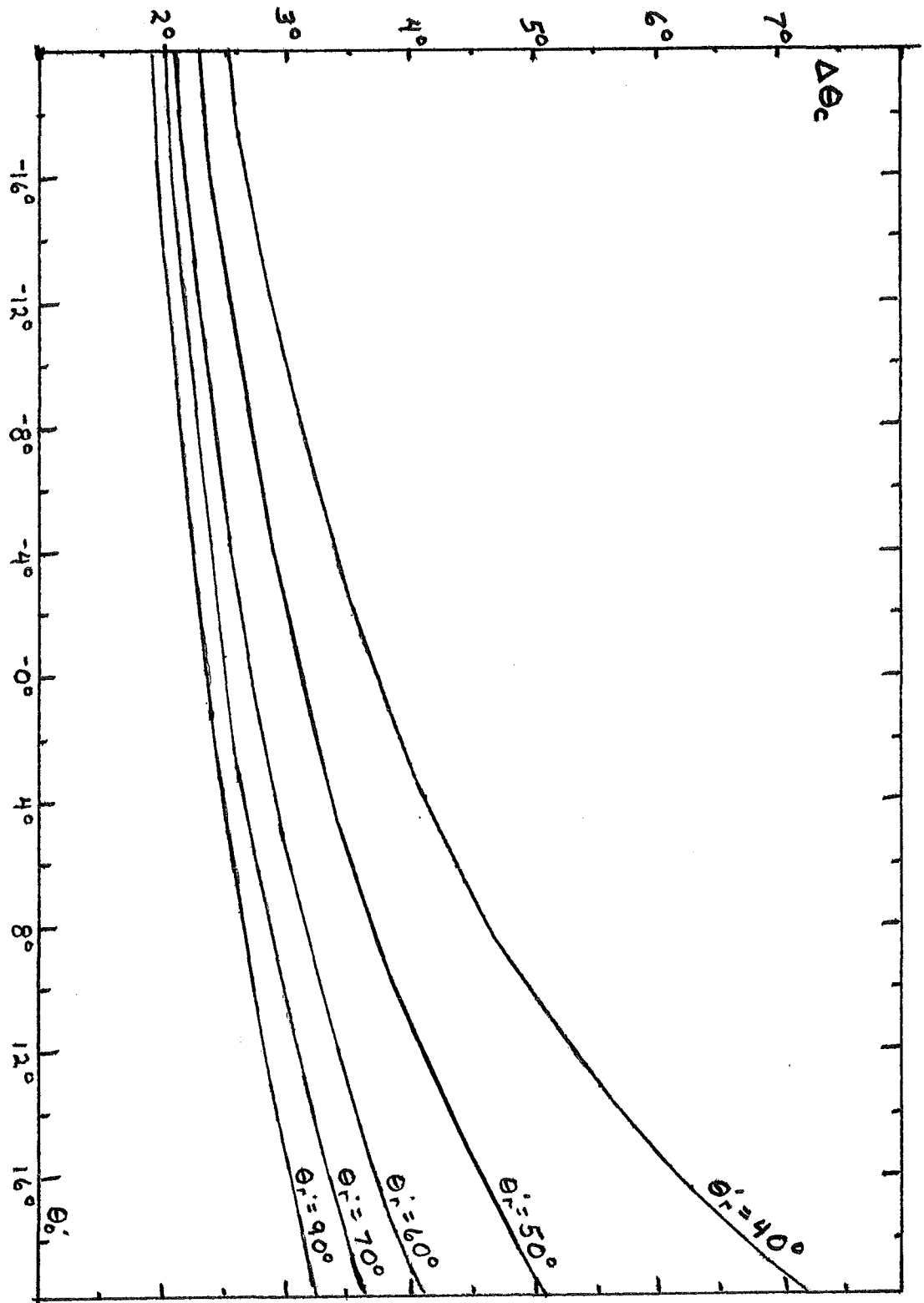


Fig. 20 : The extinction angle from (2-107) for $\lambda_0 = 6328 \text{ \AA}$, $15 \mu\text{M}$, and $n = 1.5$. The reference and object beam propagation directions (θ_i' and θ_o') are measured external to the emulsion.

offered in the appendix.

Due to the refractive nature of the emulsion, there is an obvious limitation placed on the angles within the media.

From (2-98) and (2-31)

$$\alpha = \sin \theta' / n \quad (2-109)$$

Since

$$\alpha^2 + \gamma^2 = 1 \quad (2-110)$$

we may write

$$\gamma = \pm \frac{\sqrt{n^2 - \sin^2 \theta'}}{n} \quad (2-111)$$

The relationships in (2-109) and (2-111), sketched in Fig. 21, clearly limit extinction angle values, since the direction cosines are limited to the intervals

$$|\alpha| \leq 1/n \quad (2-112)$$

and

$$\frac{\sqrt{n^2 - 1}}{n} \leq |\gamma| \leq 1 \quad (2-113)$$

With the concept of volume holography's extinction angle well understood, we now begin exploration of system theory to determine how the extinction angle property might ultimately be used to holographically record a system.

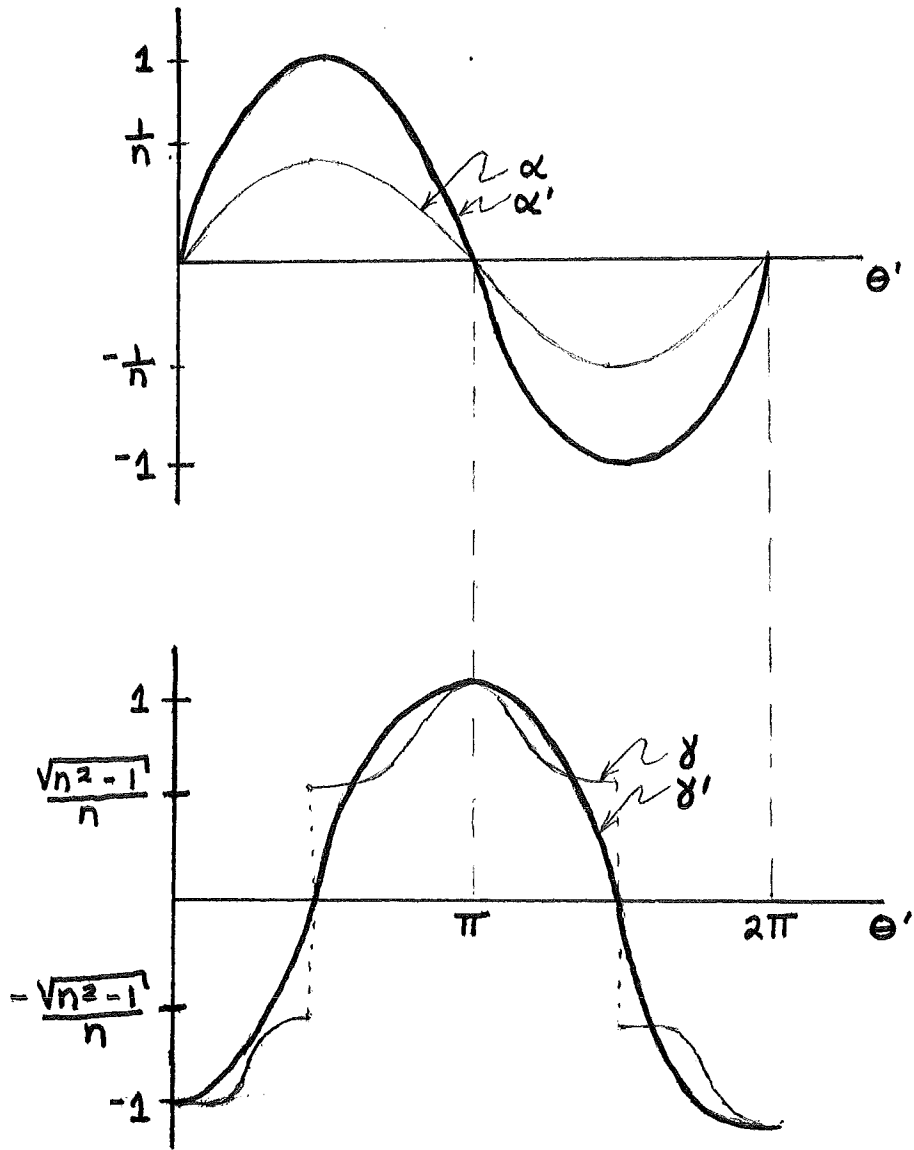


Fig. 21 : Refractive index limitations placed on the direction cosines within a recording medium of refractive index n . Primed variables denote the corresponding direction cosines external to the medium.

(For $n=1.5$, the propagation direction within the emulsion is limited to the interval $|\theta| < 42^\circ$)

III. Linear System Theory

Theory of holographic recording of an optical system stems from classical linear systems theory and the Fourier transforming properties of thin lenses. Problems of practicality lead to approximations, the consequences of which are explored here.

A) Linear Systems⁽¹⁸⁾.

The input-output relationship of a system, as portrayed in Fig. 22, may be modeled by the mathematical operator $\mathcal{S}[\]$

$$g_o(t) = \mathcal{S}[g(t)] \quad (3-1)$$

where $g(t)$ and $g_o(t)$ are respectively the system's input and output. This operation is equivalent to the mapping technique employed in Chapter I to analyze the magnification and Fourier transformation properties of the thin lens.

A system is said to be linear if it obeys the properties of homogeneity and superposition* stated respectively as

$$\mathcal{S}[a g(t)] = a \mathcal{S}[g(t)] \quad (3-2)$$

and

$$\mathcal{S}[g(t) + f(t)] = \mathcal{S}[g(t)] + \mathcal{S}[f(t)] \quad (3-3)$$

* In Chapter I, linearity was assumed for the operations of magnification and Fourier transformation, specifically in the transitions from equations (1-11) to (1-12) and (1-34) to (1-35).

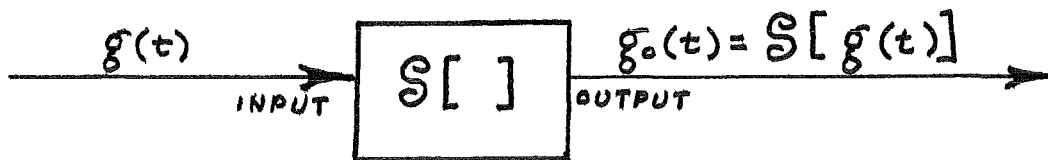


Fig. 22 : The general system model consisting of an input, a system described by the mathematical operator $S[]$, and an output.

where $g(t)$ and $f(t)$ are arbitrary input functions and a is a constant. These criteria may be combined into a single necessary and sufficient condition for linearity

$$\mathcal{S}[a g(t) + b f(t)] = a \mathcal{S}[g(t)] + b \mathcal{S}[f(t)] \quad (3-4)$$

where b is a constant.

1) The superposition integral

A more powerful mathematical treatment of linear systems arises from the sifting property of the Dirac Delta restated here after (1-8):

$$g(t) = \int_{-\infty}^{\infty} g(\xi) \delta(t - \xi) d\xi \quad (3-5)$$

Substituting into (3-1) gives

$$g_o(t) = \mathcal{S} \left[\int_{-\infty}^{\infty} g(\xi) \delta(t - \xi) d\xi \right] \quad (3-6)$$

For linear systems, the integral may be extracted from the operator argument due to superposition.

$$g_o(t) = \int_{-\infty}^{\infty} \mathcal{S} [g(\xi) \delta(t - \xi) d\xi] \quad (3-7)$$

Since the operator is only concerned with functions of t , it views both $g(\xi)$ and $d\xi$ as constant. Thus, due to the homogeneity property of linear systems, these variables may be extracted from the operator's argument leaving

$$g_o(t) = \int_{-\infty}^{\infty} g(\xi) \mathcal{S} [\delta(t - \xi)] d\xi \quad (3-8)$$

The output from a Dirac Delta input is appropriately called the system's impulse response, and is written

$$h(t; \xi) = \mathcal{S}[\delta(t - \xi)] \quad (3-9)$$

Substituting into (3-8) yields the superposition integral

$$g_o(t) = \int_{-\infty}^{\infty} g(\xi) h(t; \xi) d\xi \quad (3-10)$$

To define a general system, the output must be known for every possible input. Assuming linearity, a system is defined by knowledge of all possible impulse inputs by virtue of the superposition integral.

* The infinity of knowledge required for general system definition constitutes the highest order of infinity intuitively (but not mathematically) conceivable. Assumption of linearity reduces the order of the infinite number of defining relationships by one. For an elementary, but interesting discussion on such notions, see Gamov (19).

2) Invariance and convolution

By far the most powerful and most studied subset of linear systems are those which are invariant. For such systems the impulse response is dependent only on the difference of its arguments

$$h(t; \xi) = h(t - \xi) \quad (3-11)$$

Prime examples of such systems are those arising in linear circuit theory. If an input $\delta(t)$ into a linear circuit produces an output of $h(t)$, then an input $\delta(t - t_0)$ will produce $h(t - t_0)$. Such circuits are then time-invariant.

Substitution of the invariance criterion (3-11) into the superposition integral (3-10) results in the convolution integral

$$g_0(t) = \int_{-\infty}^{\infty} g(\xi) h(t - \xi) d\xi \quad (3-12)$$

Thus, for an invariant linear system, a single impulse response suffices for a complete system definition.

$$h(t) = \mathcal{S}[\delta(t)] \quad (3-13)$$

In shorter form, the convolution operation may be expressed as

$$g_0(t) = g(t) * h(t) \quad (3-14)$$

The convolution operation is commutative, associative, and is distributive with respect to addition⁽²⁰⁾

$$g(t) * h(t) = h(t) * g(t) \quad (3-15)$$

$$[g(t) * h(t)] * f(t) = g(t) * [h(t) * f(t)] \quad (3-16)$$

$$g(t) * [h(t) + f(t)] = g(t) * h(t) + g(t) * f(t) \quad (3-17)$$

Another property of the convolution operation which will later prove useful is (with reference to (3-14))

$$\begin{aligned} g_0(t-\xi) &= g(t-\xi) * h(t) \\ &= g(t) * h(t-\xi) \end{aligned} \quad (3-18)$$

3) Fourier relationships

The power of invariant systems rests in their analysis in the frequency domain. From (3-12), it may be shown that

$$G_0(f) = G(f) H(f) \quad (3-19)$$

where $G_0(f)$, $G(f)$, and $H(f)$ are the Fourier transforms of $g_0(t)$, $g(t)$ and $h(t)$, respectively, given by (1-39). The Fourier transform of the system impulse response, $H(f)$, is called the system transfer function. Due to the one-to-one correspondence between function and transform, knowledge of $H(f)$ also suffices for complete definition of an invariant linear system. Mathematically

$$H(f) = \mathcal{F} [h(t)] \quad (3-20)$$

where \mathcal{F} denotes the Fourier transform operation. Important Fourier theorems which will prove useful in later analysis are given below.

(1) Linearity

$$\mathcal{F} [a f(t) + b g(t)] = a \mathcal{F} [f(t)] + b \mathcal{F} [g(t)] \quad (3-21)$$

(2) Similarity

$$\mathcal{F} [g(at)] = \frac{1}{|a|} G(f/a) \quad (3-22)$$

(3) Shift theorem

$$\mathcal{F} [g(t-\xi)] = G(f) e^{-j2\pi\xi f} \quad (3-23)$$

(4) Recurrence

$$\mathcal{F}[\mathcal{F}\{g(t)\}] = g(-t) \quad (3-24)$$

Proofs of these theorems (except 4) plus the convolution-Fourier transform relationship are offered by Goodman⁽²¹⁾.

B) Linear Optical Systems

Linear imaging systems afford parallel processing; thus previous notions must be extended to two dimensions and appropriate nomenclature must be applied. Most optical systems may be thought of as consisting of an input plane, a system, and an output plane (see Fig. 23).

The one- and two-dimensional impulse responses of such a system are optically called the point spread and line spread functions, which are obtained respectively from (3-13) as

$$\mathcal{S}[\delta(x-\xi, y-\eta)] = h(x, y; \xi, \eta) \quad (3-25)$$

and

$$\mathcal{S}[\delta(x-\xi)] = h(x; \xi) \quad (3-26)$$

The line-spread function is employed where one dimensional analysis loses no generality.

In two dimensions, the superposition integral becomes (from (3-10))

$$g_o(x, y) = \int_{-\infty}^{\infty} \int_{-\infty}^{\infty} g(\xi, \eta) h(x, y; \xi, \eta) d\xi d\eta \quad (3-27)$$

and convolution from (3-11) and (3-12)

$$g_o(x, y) = \int_{-\infty}^{\infty} \int_{-\infty}^{\infty} g(\xi, \eta) h(x-\xi, y-\eta) d\xi d\eta \quad (3-28)$$

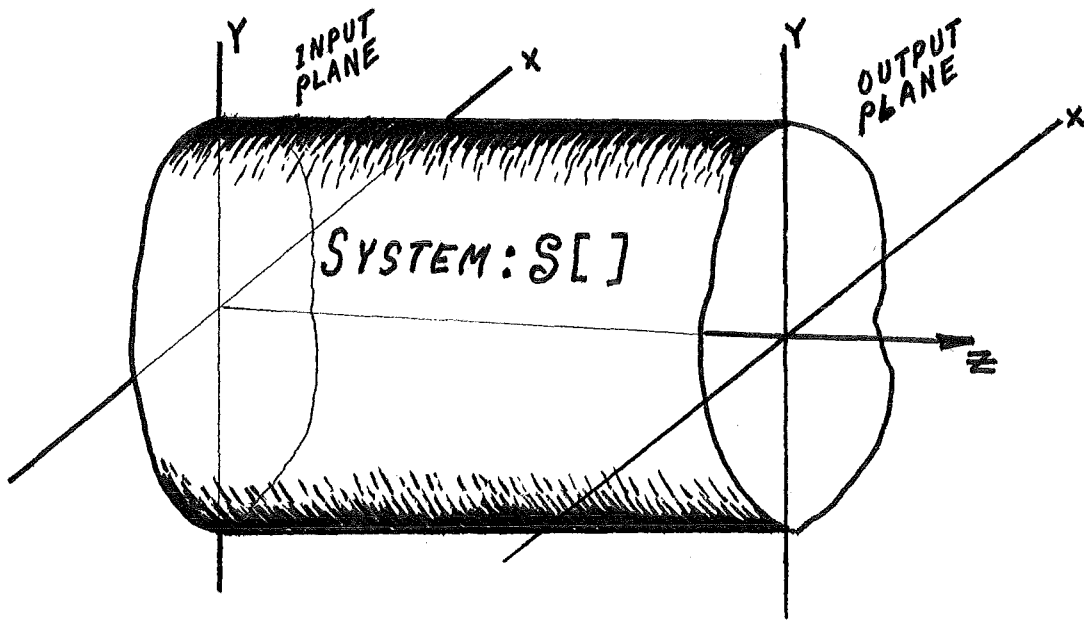


Fig. 23 : General portrayal of an optical system consisting of an input plane, a system, and an output plane.

The two dimensional Fourier transform is here repeated from (1-38)

$$\begin{aligned} G(f_x, f_y) &= \mathcal{F} [g(x, y)] \\ &= \int_{-\infty}^{\infty} \int_{-\infty}^{\infty} g(\xi, \eta) e^{-j2\pi(f_x \xi + f_y \eta)} d\xi d\eta \end{aligned} \quad (3-29)$$

When Fourier transforming is done with a thin double convex lens, the spatial frequencies are given as

$$f_x = \frac{x_f}{\lambda f} \quad ; \quad f_y = \frac{y_f}{\lambda f} \quad (3-30)$$

where the transform falls on the (x_f, y_f) plane.

(1) Isoplanicity

Optical system invariance is called space invariance or isoplanicity. For isoplanatic systems, a single impulse suffices for a complete system definition. It is indeed unfortunate that optical systems in general are space variant.

We pause here to cite two common optical systems which are not isoplanatic and which will henceforth be used as running examples.

Consider first a simple thin lens Fourier transformer. The impulse response for such a system is given as:

$$\begin{aligned} S[\delta(x-\xi, y-\eta)] &= \mathcal{F}[\delta(x-\xi, y-\eta)] \\ &= e^{-j2\pi(f_x \xi + f_y \eta)} \end{aligned}$$

Applying (3-30) and (3-25) we write the point spread function as:

$$h(x, y; \xi, \eta) = e^{-\frac{j2\pi}{\lambda f}(x\xi + y\eta)} \quad (3-31)$$

Clearly the complex argument of the exponential cannot be manipulated to produce $h(x - \xi, y - \eta)$. The system is thus not isoplanatic. It is indeed ironic that the Fourier transforming operation used so widely in the study of invariant linear systems is itself variant.

A second common variant optical system is the simple magnifier. We here rewrite its input-output relationship from (1-17) as

$$g_o(x, y) = \frac{1}{M^2} g\left(\frac{x}{M}, \frac{y}{M}\right) \quad (3-32)$$

Placing the point source $\delta(x - \xi, y - \eta)$ on the input plane, we then have

$$\begin{aligned} h(x, y; \xi, \eta) &= \frac{1}{M^2} \delta\left[\frac{x}{M} - \xi, \frac{y}{M} - \eta\right] \\ &= \delta[x - M\xi, y - M\eta] \end{aligned} \quad (3-33)$$

Here again there exists no algebraic trickery to produce $h(x - \xi, y - \eta)$ except for the trivial case of unity magnification.

The space variant nature of these elementary optical systems suggests that most linear optical systems are indeed not isoplanatic.

2) Measurement of spatial variance

In previous notions, a linear system was tagged discretely as invariant or variant. A classic paper by Lohmann and Paris⁽²²⁾ introduces the idea of relative degrees of invariance to linear systems. Without loss of generality, attention is restricted to one-dimensional analysis. All systems are assumed linear.

We begin by redefining the line spread function as

$$h(x - x_0; x_0) = \mathcal{S} [\delta(x - x_0)] \quad (3-34)$$

(Compare with 3-25). There are two advantages to this notation. First, when the line spread function is no longer a function of its second argument, the system is completely isoplanatic. Secondly, in order to extend the idea of the transfer function from line spread functions originating from line sources not located at the origin, we define from (3-20) and (3-34)

$$H(f_x; x_0) = \mathcal{F} [h(x; x_0)] \quad (3-35)$$

To begin assignment of various degrees of isoplanicity to linear systems, the cross-correlation of the line spread functions originating from line sources x_1 and x_2 on the input plane is defined as

$$\begin{aligned} C(\xi, x_1, x_2) &= \int_{-\infty}^{\infty} h(x + \frac{\xi}{2} - x_1; x_1) h^*(x - \frac{\xi}{2} - x_2; x_2) \\ &= C^*(-\xi, x_2, x_1) \end{aligned} \quad (3-36)$$

The degree of space invariance is then defined as

$$\sigma(x_1, x_2) = \frac{C(x_1 - x_2, x_1, x_2)}{[C(0, x_1, x_1) C(0, x_2, x_2)]^{1/2}} \quad (3-37)$$

or equivalently

$$\sigma(x_1, x_2) = \frac{\int_{-\infty}^{\infty} h(x - \frac{x_1 + x_2}{2}; x_1) h^*(x - \frac{x_1 + x_2}{2}; x_2) dx}{[\int_{-\infty}^{\infty} |h(x - x_1; x_1)|^2 dx \int_{-\infty}^{\infty} |h(x - x_2; x_2)|^2 dx]^{\frac{1}{2}}} \quad (3-38)$$

Schwarz's inequality may be written as

$$\frac{|\int_{-\infty}^{\infty} \int_{-\infty}^{\infty} XY d\xi d\eta|^2}{\int_{-\infty}^{\infty} \int_{-\infty}^{\infty} |X|^2 d\xi d\eta \int_{-\infty}^{\infty} \int_{-\infty}^{\infty} |Y|^2 d\xi d\eta} \leq 1 \quad (3-39)$$

where X and Y are complex functions of ξ and η . Direct comparison with (3-38) gives

$$|\sigma(x_1, y_1)| \leq 1 \quad (3-40)$$

Equality in (3-39) is achieved when

$$Y = X^* \quad (3-41)$$

Thus a value of unity is assigned $|\sigma(x_1, y_1)|$ when

$$h(x; x_1) = h(x; x_2) \quad (3-42)$$

or equivalently when the system is isoplanatic in the conventional sense. On the other hand when $\sigma = 0$, the system may be said to have no trace of isoplanicity.

To include cases not covered by (3-38), we define $\sigma = 0$ if one and only one of the line spread functions is zero, and $\sigma = 1$ if both are zero.

The degree of space invariance may also be expressed in the frequency domain, in terms of transfer functions. Parseval's theorem states:

$$\int_{-\infty}^{\infty} |g(x)|^2 dx = \int_{-\infty}^{\infty} |G(f_x)|^2 df_x \quad (3-43)$$

where

$$G(f_x) = \mathcal{F}[g(x)] \quad (3-44)$$

It is evident that

$$\int_{-\infty}^{\infty} |h(x-x_i; x_i)|^2 dx = \int_{-\infty}^{\infty} |h(x; x_i)|^2 dx \quad (3-45)$$

and can be shown that

$$\begin{aligned} \int_{-\infty}^{\infty} h\left(x - \frac{x_1+x_2}{2}; x_1\right) h^*\left(x - \frac{x_1+x_2}{2}; x_2\right) dx \\ = \int_{-\infty}^{\infty} H(f_x; x_1) H^*(f_x; x_2) df_x \end{aligned} \quad (3-46)$$

so that (3-38) becomes

$$\sigma(x_1, x_2) = \frac{\int_{-\infty}^{\infty} H(f_x; x_1) H^*(f_x; x_2) df_x}{\left[\int_{-\infty}^{\infty} |H(f_x; x_1)|^2 df_x \int_{-\infty}^{\infty} |H(f_x; x_2)|^2 df_x \right]^{1/2}} \quad (3-47)$$

It has been pointed out that the Lohmann-Paris method will yield complete isoplanicity only if the linear system is isoplanatic for all inputs⁽²³⁾. For example, direct application of the above expressions for the degree of isoplanicity to both the simple magnifier and Fourier transformer gives:

$$|\sigma(x_1, x_2)| = \begin{cases} 1 & ; x_1 = x_2 \\ 0 & ; x_1 \neq x_2 \end{cases} \quad (3-48)$$

This occurs due to the infinite integral limits in the frequency or spatial expressions of the degree of space variance, which in practice do not extend over the entire planes. Thus appropriate applications of (3-38) and (3-47) are respectively to object width limited and band limited line spread functions. When analytical computation of line spread functions become overly complex, an experimental method for determining the cross-correlation function given by (3-36) is offered by Lohmann and Paris⁽²²⁾.

We now venture to derive the isoplanicity of the systems used herein as running examples. Consider, first, the simple magnifier which is used solely for magnification of band-limited functions. Redefining the magnifier's line spread function [(3-33)] in terms of (3-34) gives

$$\begin{aligned} h(x-x_i; x_i) &= \delta [x - Mx_i] \\ &= \delta [(x-x_i) - (M-1)x_i] \end{aligned} \quad (3-49)$$

or equivalently

$$h(x; x_i) = \delta [x - (M-1)x_i] \quad (3-50)$$

The corresponding transfer function is then

$$H(f_x; x_i) = e^{-j 2\pi (M-1) x_i f_x} \quad (3-51)$$

Assuming that we limit the frequency of all input functions to be zero outside the interval

$$-\omega \leq f_x \leq \omega \quad (3-52)$$

and noting

$$|e^{j\phi(x)}|^2 = 1 \quad (3-53)$$

we have from (3-47)

$$\sigma(x_1, x_2) = \frac{\int_{-\omega}^{\omega} e^{-j 2\pi (M-1)(x_1 - x_2) f_x} df_x}{\int_{-\omega}^{\omega} df_x} \quad (3-54)$$

Evaluation of this expression gives

$$\sigma(x_1, x_2) = \text{sinc} [2(M-1)(x_1 - x_2)\omega] \quad (3-55)$$

where

$$\text{sinc}(x) = \frac{\sin(\pi x)}{\pi x} = \text{sinc} \left(\frac{x}{\pi} \right) \quad (3-56)$$

We note from (3-55) as before, the magnifier is completely isoplanatic for the case of unit magnification. The isoplanaticity is also directly a function of the distance between the lines of interest in the input plane. Note also, in the limit as ω approaches infinity, the statement made in (3-48) is verified.

Consider now the Fourier transformer. Redefining the line spread function (3-31) via (3-34) we have

$$h(x - x_i; x_i) = e^{-j 2\pi f_i x} \quad (3-57)$$

where

$$f_i = x_i / \lambda f$$

or equivalently

$$h(x; x_i) = e^{-j 2\pi f_i x} e^{-j 2\pi f_i x_i} \quad (3-58)$$

All input functions are now restricted to the interval

$$-a \leq x \leq a \quad (3-59)$$

Substituting the line spread function into the spatial expression for the degree of space variance [(3-38)], and manipulating gives

$$\sigma(x_1, x_2) = \frac{1}{2a} e^{-j\pi(f_1 x_1 - f_2 x_2)} \int_{-a}^a e^{-j2\pi(f_1 - f_2)x} dx \quad (3-60)$$

Evaluation of (3-60) gives

$$\sigma(x_1, x_2) = \text{sinc} \left[\frac{2(x_1 - x_2)a}{\lambda f} \right] e^{-j\pi(f_1 x_1 - f_2 x_2)} \quad (3-61)$$

The magnitude of the space variance of the optical Fourier transformer is seen to change more quickly with $(x_1 - x_2)$ than that of the magnifier due to the small value of λf , which has an order of magnitude of 10^{-5} meters squared for visible light. Note here, as always,

$$\sigma(x_1, x_2) = 1 \quad \text{IF } x_1 = x_2 \quad (3-62)$$

A final isoplanatic measure offered by Lohmann and Paris⁽²²⁾ assigns a numerical value to a system's space variance. The average degree of isoplanicity is defined as

$$\rho = \frac{\int_H \int_H \sigma(x_1, x_2) dx_1 dx_2}{\int_H \int_H dx_1 dx_2} \quad (3-63)$$

where integration is over a region of interest in the input plane. In a fashion similar to that employed earlier in this section, it can be shown that

$$|\rho| \leq 1 \quad (3-64)$$

c) The piecewise isoplanatic approximation

No matter what degree of isoplanicity is assigned to a variant linear system, an infinite number of spread functions is needed for complete system definition. Those systems, however, whose space variance changes slowly over a small increment in the input plane may be approximated as piecewise isoplanatic. In essence, the space variant system is divided into a number of isoplanatic systems, each specified by a patch on the input plane. Lohmann and Paris⁽²²⁾ after Fellgett and Linfoot, define such an isoplanatic patch from

$$|\sigma(x_1, x_2) - 1| \leq \epsilon \quad (3-65)$$

where ϵ is the maximum magnitude change in isoplanicity allowed a patch.

We now explore the modeling of a space variant linear system as piecewise isoplanatic and the corresponding consequences.

(1) The system model

In general terms, the input plane of a space variant system may be expressed as

$$\sum_n \text{rect} \left[\frac{x - x_n}{2\Delta x_n} \right] \quad (3-66)$$

where

$$\text{rect}(x) = \begin{cases} 1 & ; -\frac{1}{2} \leq x \leq \frac{1}{2} \\ 0 & ; \text{OTHERWISE} \end{cases} \quad (3-67)$$

and

$$x_n + \Delta x_n = x_{n+1} - \Delta x_{n+1} \quad (3-68)$$

The nth spatial pulse in (3-66) represents the location of the nth isoplanatic patch centered at $x = x_n$ and with width $2 \Delta x_n$. Summation is assumed to cover the region of interest on the input plane. The criterion in (3-68) is made to insure that there are no "holes", or overlap between two adjacent isoplanatic patches.

In order to completely define a piecewise isoplanatic system, knowledge of the spread-function of each patch needs to be known. We assume line sources are placed conveniently at the midpoints of each patch at x_n and we have knowledge of

$$h(x - x_n; x_n) = \mathcal{S}[\delta(x - x_n)] \quad (3-69)$$

for all n .

Considered now is the input-output relationship of a piecewise isoplanatic system. An input function $g(x)$ must first be divided into isoplanatic regions. Specifically

$$g(x) = \sum_n g_n(x - x_n) \quad (3-70)$$

where

$$g_n(x - x_n) = g(x) \text{ rect} \left[\frac{x - x_n}{2 \Delta x_n} \right] \quad (3-71)$$

or equivalently

$$g_n(x) = g(x + x_n) \text{ rect} \left[\frac{x}{2 \Delta x_n} \right] \quad (3-72)$$

Note that, by definition, each $g_n(x)$ is centered at the origin (Fig. 24). Also to be noted is the analogy between the "function sifting" in (3-71) and the sifting property of the Dirac Delta [(3-5)].

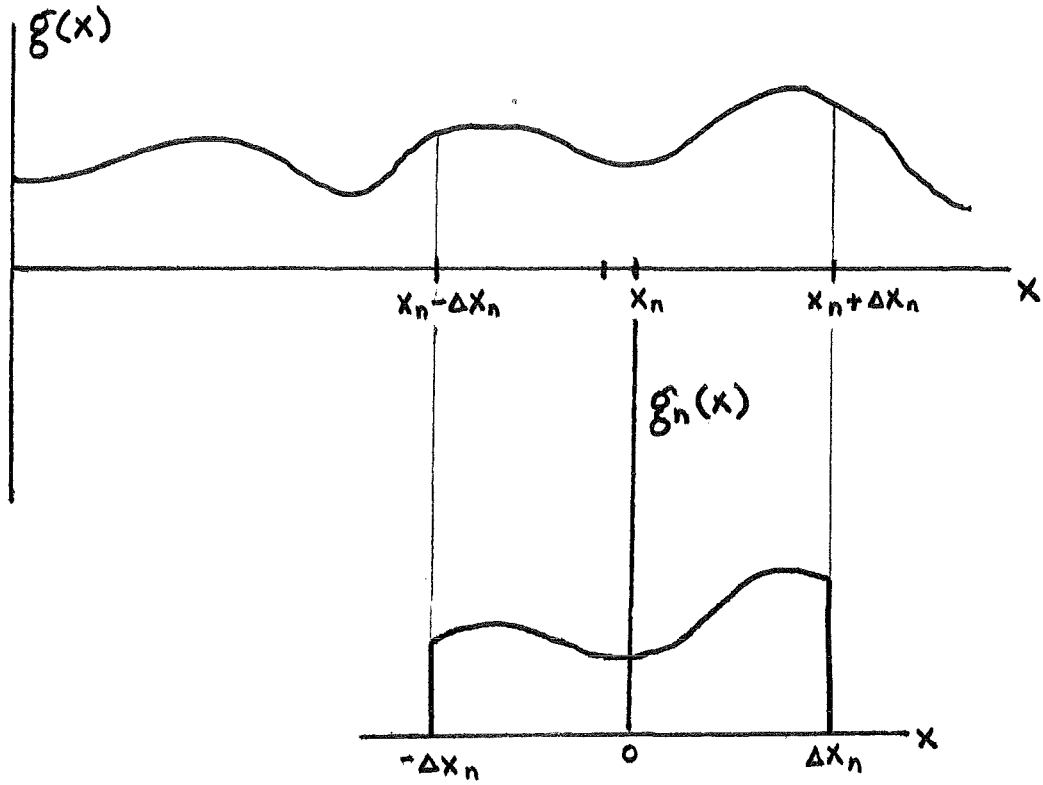


Fig. 24 : Extraction of the n th isoplanatic region from $g(x)$.

To determine the output of a piecewise isoplanatic system, $\tilde{g}_o(x)$, due to an input $g(x)$, the system operator [(3-1)] is recalled. Substitution of (3-70) into (3-1) gives

$$\tilde{g}_o(x) = \mathfrak{S} \left[\sum_n g_n(x-x_n) \right] \quad (3-73)$$

The system is assumed linear so that the principle of superposition [(3-3)] may be applied:

$$g_o(x) = \sum_n \mathfrak{S} [g_n(x-x_n)] \quad (3-74)$$

Each argument of the system operator is now isoplanatic and can be expressed via the convolution integral [(3-12)]. That is:

$$\mathfrak{S} [g_n(x-x_n)] = \int_{-\infty}^{\infty} g_n(\xi-x_n) h(x-\xi; x_n) d\xi \quad (3-75)$$

or in shorthand form, from (3-14)

$$\mathfrak{S} [g_n(x-x_n)] = g_n(x-x_n) * h(x; x_n) \quad (3-76)$$

Substituting into (3-75) gives

$$\tilde{g}_o(x) = \sum_n g_n(x-x_n) * h(x; x_n) \quad (3-77)$$

or equivalently from (3-18)

$$\tilde{g}_o(x) = \sum_n g_n(x) * h(x-x_n; x_n) \quad (3-78)$$

The input-output relationship of a piecewise isoplanatic system can thus be expressed as a superposition of convolutions, and is the hybrid of variance and invariance. For example, one heuristically sees

$$\lim_{\substack{n \rightarrow \infty \\ \Delta x_n \rightarrow 0}} \sum_n g_n(x) * h(x - x_n; x_n) = \int_{-\infty}^{\infty} g(x) h(x - x_n; x_n) dx \quad (3-79)$$

that is, the system becomes completely space variant as the width of each isoplanatic patch approaches zero. This necessitates system description solely by superposition.

The ideas presented by Lohmann and Paris can now be seen as possible criteria for determining which invariant linear systems can be successfully modeled as piecewise isoplanatic.

The input-output relationship of a piecewise isoplanatic system may also be expressed in the frequency domain. From the shift theorem [(3-23)] and the convolution-Fourier transform relationship, the frequency expression for both (3-77) and (3-78) is

$$\tilde{G}_o(f_x) = \sum_n G_n(f_x) H(f_x; x_n) e^{-j 2 \pi f_x x_n} \quad (3-80)$$

where

$$G_n(f_x) = \mathcal{F}[g_n(x)] \quad (3-81)$$

and

$$H(f_x; x_n) = \mathcal{F}[h(x; x_n)] \quad (3-82)$$

A problem encountered in implementation of the piecewise isoplanatic approximation is avoidance of the nth isoplanatic region transform from multiplying other than the nth transfer function. For this reason, we formulate the cross-talk elimination criterion as

$$H(f_x; x_n) G_m(f_x) = 0 \quad \text{IF } m \neq n \quad (3-83)$$

(2) Consequences of the piecewise isoplanatic approximation

The effects of modeling a system as piecewise isoplanatic are best illustrated by example.

Consider first the simple magnifier. We conveniently choose for an input (Fig. 25a)

$$g(x) = \text{rect} \left[\frac{x}{2a} \right] \quad (3-84)$$

where the rect function is given by (3-67). From the input-output relationship of the simple magnifier [(1-18)] one would expect an output (Fig. 25c)

$$g_0(x) = \frac{1}{|M|} \text{rect} \left[\frac{x}{2Ma} \right] \quad (3-85)$$

In order to apply the piecewise isoplanatic approximation, the input is divided into $2k + 1$ isoplanatic patches, all of width $2 \Delta x$, centered at

$$x_n = 2n \Delta x \quad (3-86)$$

Noting that

$$a = (2k + 1) \Delta x \quad (3-87)$$

we then have

$$g(x) = \sum_{n=-k}^k \text{rect} \left[\frac{x - 2n \Delta x}{2 \Delta x} \right] \quad (3-88)$$

so that from (3-72)

$$g_n(x) = \text{rect} \left[\frac{x}{2 \Delta x} \right] \quad (3-89)$$

From (3-50) the line spread function for the simple magnifier is

$$\begin{aligned} h(x - x_n; x_n) &= \delta [x - Mx_n] \\ &= \delta [x - 2nM \Delta x] \end{aligned} \quad (3-90)$$

From (3-78) the piecewise isoplanatic approximation for the output is thus

$$\tilde{g}_0(x) = \sum_{n=-k}^k \text{rect} \left[\frac{x}{2\Delta x} \right] * \delta[x - 2n\Delta x M] \quad (3-91)$$

Through the sifting property of the Dirac Delta and the convolution integral, it may be shown that

$$g(x) * \delta(x - x_0) = g(x - x_0) \quad (3-92)$$

Thus, (3-91) becomes

$$\tilde{g}_0(x) = \sum_{n=-k}^k \text{rect} \left[\frac{x - 2n\Delta x M}{2\Delta x} \right] \quad (3-93)$$

The cases for $|M| > 1$ and $\frac{1}{2} \leq |M| \leq 1$ are illustrated respectively in Figures 25d and e. In both cases one can see the attempts of the piecewise isoplanatic approximation to mimic the true output in terms of width and area.

A generalization of the piecewise isoplanatic magnifier's output follows. Substitution of the line spread function [(3-90)] into the piecewise isoplanatic approximation [(3-78)] gives

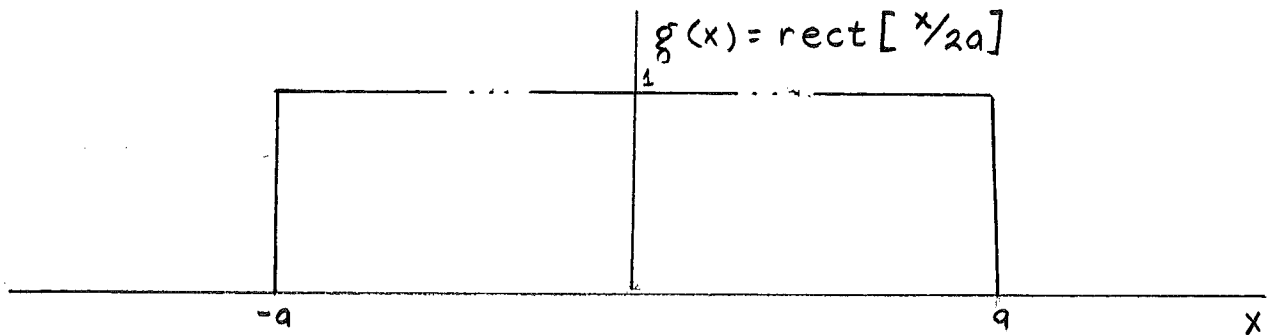
$$\tilde{g}_0(x) = \sum_n g_n(x) * \delta(x - Mx_n) \quad (3-94)$$

or equivalently, from (3-72)

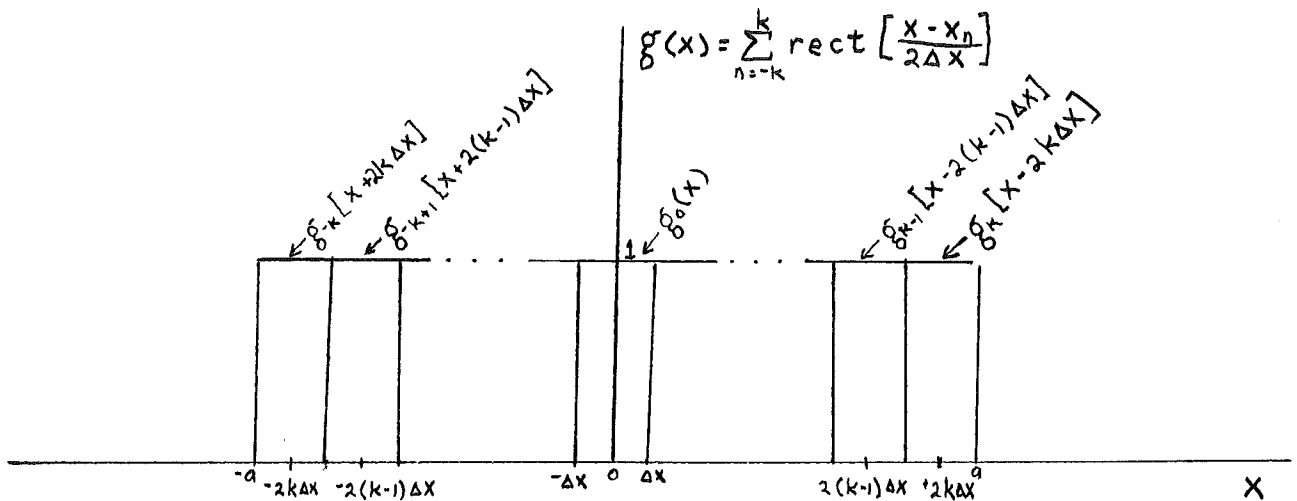
$$\tilde{g}_0(x) = \sum_n g(x + x_n) \text{rect} \left[\frac{x}{2\Delta x_n} \right] * \delta(x - Mx_n) \quad (3-95)$$

Noting (3-92), the final desired relationship is

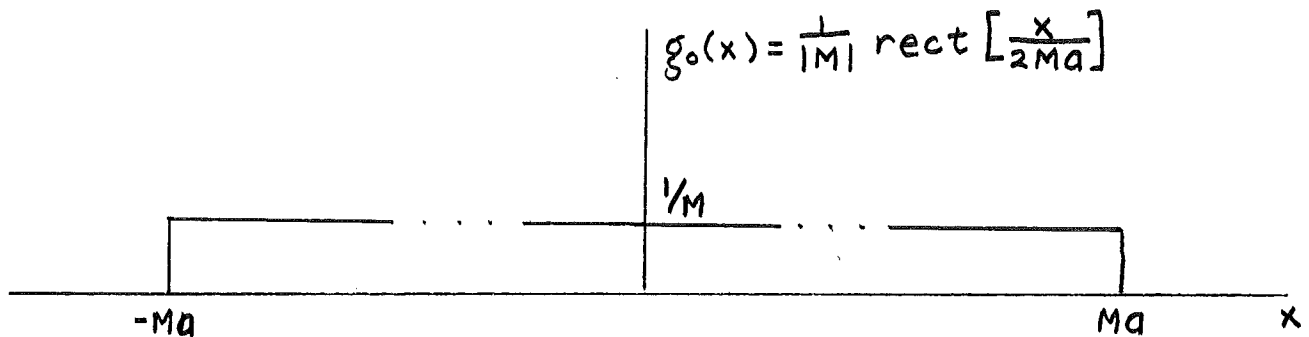
$$\tilde{g}_0(x) = \sum_n g[x - (M-1)x_n] \text{rect} \left[\frac{x - Mx_n}{2\Delta x_n} \right] \quad (3-96)$$



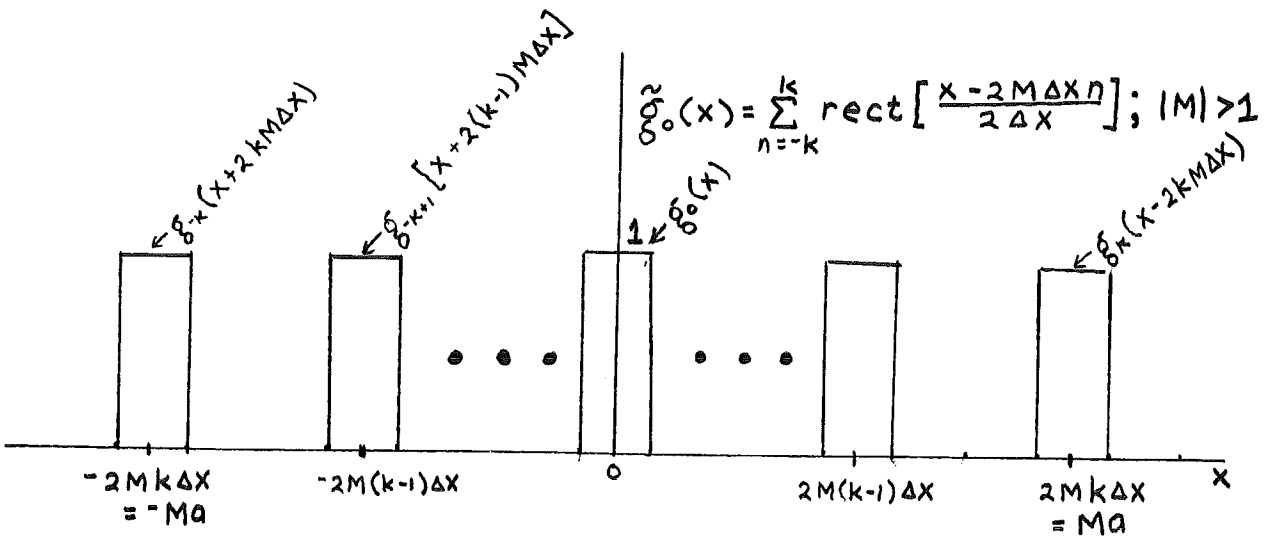
a) The input rect function.



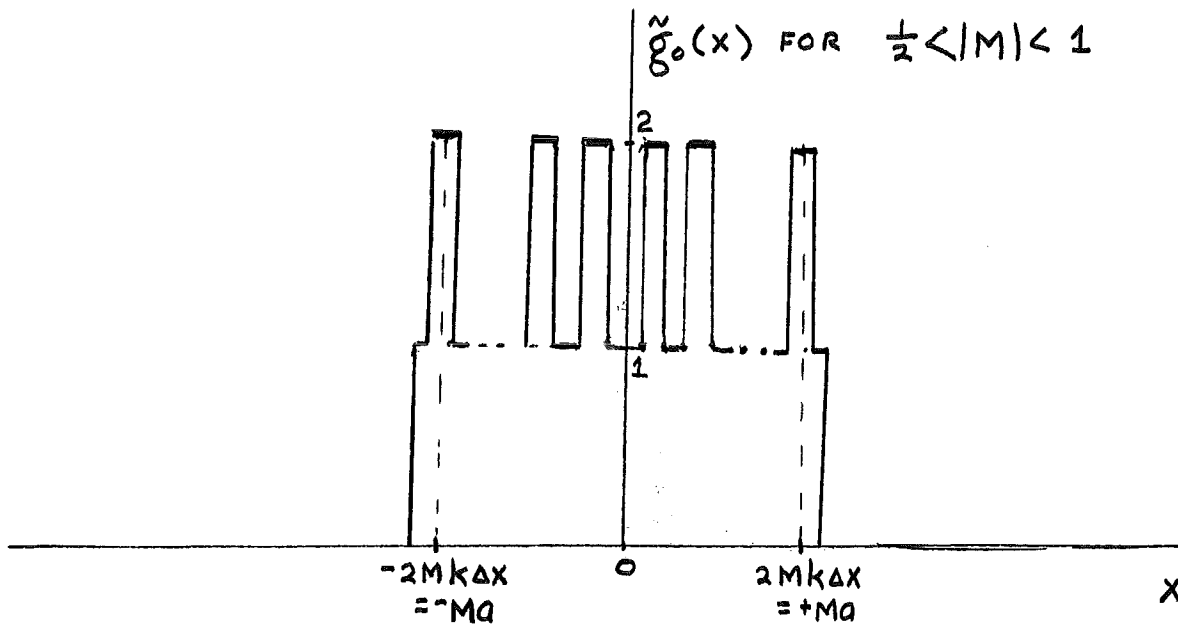
b) Dividing the input in (a) into isoplanatic patches. Each patch has width $2\Delta x$.



c) The true output for the simple magnifier for the input given in (a).



d) Piecewise isoplanatic approximated output for the simple magnifier for $|M| > 1$. Each pulse has width $2\Delta x$.



e) Piecewise isoplanatic approximated output for $\frac{1}{2} < |M| < 1$.

Fig. 25: Piecewise isoplanatic approximation for the simple magnifier with a pulse input.

Here again, each isoplanatic patch is "magnified" by being shifted by a factor of Mx_n (Fig. 26).

Next to be explored is the consequence of modeling the Fourier transformer as piecewise isoplanatic. We begin by assuming the rect function input as before [(3-84)] with generalization to follow. From the Fourier integral [(1-39)], it may be shown that

$$\mathcal{F}[\text{rect}(x)] = \text{sinc}(fx) \quad (3-97)$$

From the similarity theorem [(3-22)] one would then expect an output of

$$\begin{aligned} g_o(x) &= \mathcal{F}[\text{rect}(\frac{x}{2a})] \\ &= 2a \text{sinc}[\frac{2ax}{\lambda f}] \end{aligned} \quad (3-98)$$

where we have employed the spatial equivalence to frequency [(1-36)] for notational consistency.

The line spread function of the nth isoplanatic patch is [(3-58)]:

$$h(x; x_n) = e^{-j2\pi x f_n} e^{-j2\pi f_n x_n} \quad (3-99)$$

From the recurrence theorem, [(3-24)], the corresponding transfer function is

$$H(f_x; x_n) = \delta(f_x + f_n) e^{-j2\pi f_n x_n} \quad (3-100)$$

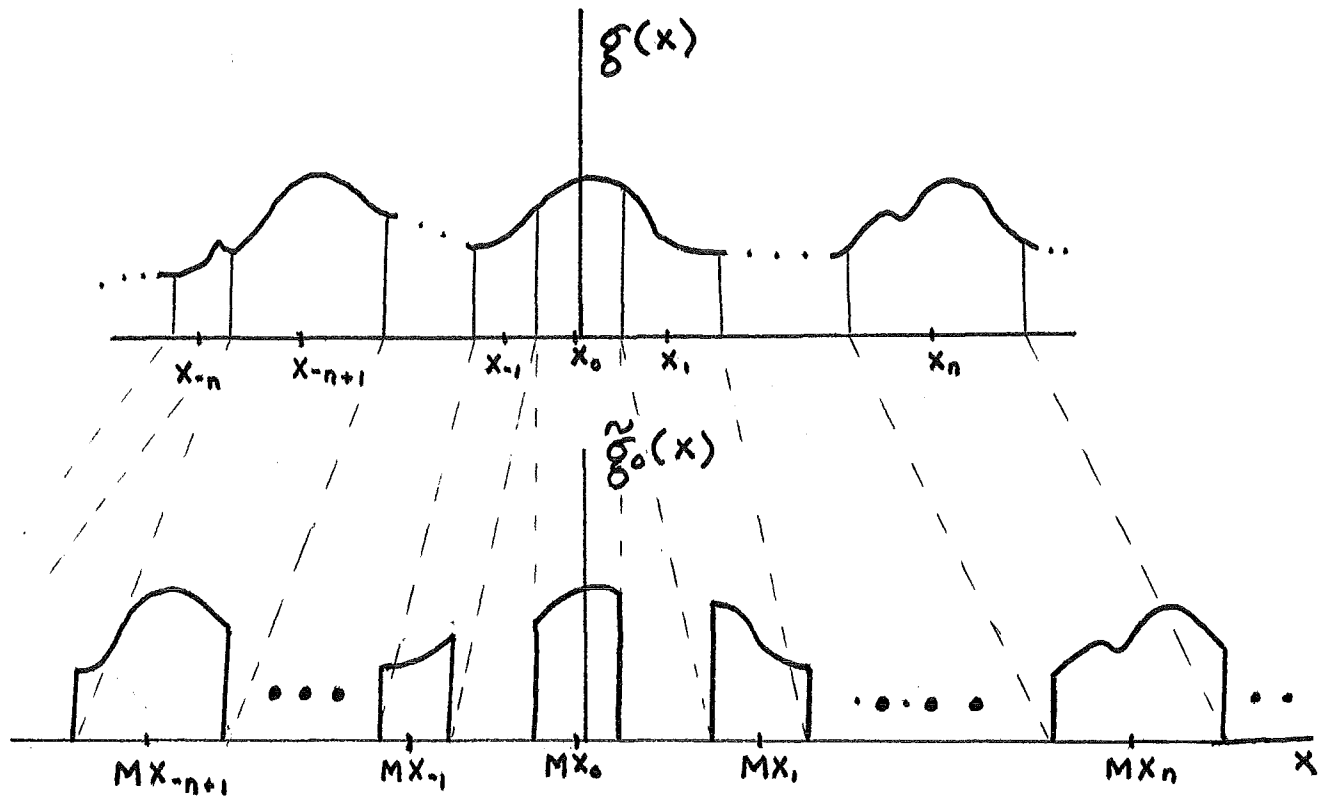


Fig. 26 : Generalized piecewise isoplanatic approximation to the simple magnifier (3-96). Each isoplanatic region is "magnified" by being shifted a factor of MX_n .

where

$$f_n = x_n / \lambda f \quad (3-101)$$

If we choose to divide the input rect function in the same manner as before [(3-89)] the similarity theorem dictates

$$\begin{aligned} G_n(f_x) &= \mathcal{F}[\text{rect}(\frac{x}{2\Delta x})] \\ &= 2\Delta x \text{sinc}(2\Delta x f_x) \end{aligned} \quad (3-102)$$

Substituting this isoplanatic patch spectrum and the transfer function [(3-100)] into the frequency expression for the piecewise isoplanatic approximation [(3-80)] gives

$$\tilde{G}_o(f_x) = 2\Delta x \sum_{n=-k}^k \text{sinc}(2\Delta x f_x) \delta(f_x + f_n) e^{-j2\pi f_n x_n} e^{-j2\pi f_x x_n} \quad (3-103)$$

Due to the Delta function, each term is non-zero only when

$$f_x = -f_n \quad (3-104)$$

Thus, (3-103) becomes

$$\tilde{G}_o(f_x) = 2\Delta x \sum_{n=-k}^k \text{sinc}(2\Delta x f_n) \delta(f_x + f_n) \quad (3-105)$$

Inverse transformation gives

$$\tilde{g}_o(x) = 2\Delta x \sum_{n=-k}^k \text{sinc}(2\Delta x f_n) e^{-j2\pi f_n x} \quad (3-106)$$

Since

$$x_n = -x_{-n} \quad (3-107)$$

equation (3-106) becomes

$$\begin{aligned} \tilde{g}_0(x) &= 2\Delta x \left[1 + \sum_{n=1}^k \operatorname{sinc}(2\Delta x f_n) \right. \\ &\quad \left. \times \{ e^{j2\pi f_n x} + e^{-j2\pi f_n x} \} \right] \\ &= 2\Delta x \left[1 + 2 \sum_{n=1}^k \operatorname{sinc}(2\Delta x f_n) \cos(2\pi f_n x) \right] \end{aligned} \quad (3-108)$$

or, equivalently, from (3-86) and (3-101)

$$\begin{aligned} \tilde{g}_0(x) &= 2\Delta x \left[1 + 2 \sum_{n=1}^k \operatorname{sinc} \left(\frac{4n\Delta x^2}{\lambda f} \right) \right. \\ &\quad \left. \times \cos \left(\frac{4n\pi\Delta x x}{\lambda f} \right) \right] \end{aligned} \quad (3-108)$$

This is the final piecewise isoplanatic approximation to the Fourier transform of a spatial pulse. In the limit, as k approaches infinity, one would expect (3-108) to become the true sinc output given in (3-102). This is graphically illustrated in Fig. 27 where (3-108) is plotted for various values of k . The computer program from which these curves were generated is offered in the appendix.

The generalized input-output relationship of the piecewise isoplanatic approximation of the Fourier transformer follows. From (3-72) we write

$$G_n(f_x) = \mathcal{F} \left[g(x + \Delta x_n) \operatorname{rect} \left(\frac{x}{2\Delta x_n} \right) \right] \quad (3-109)$$

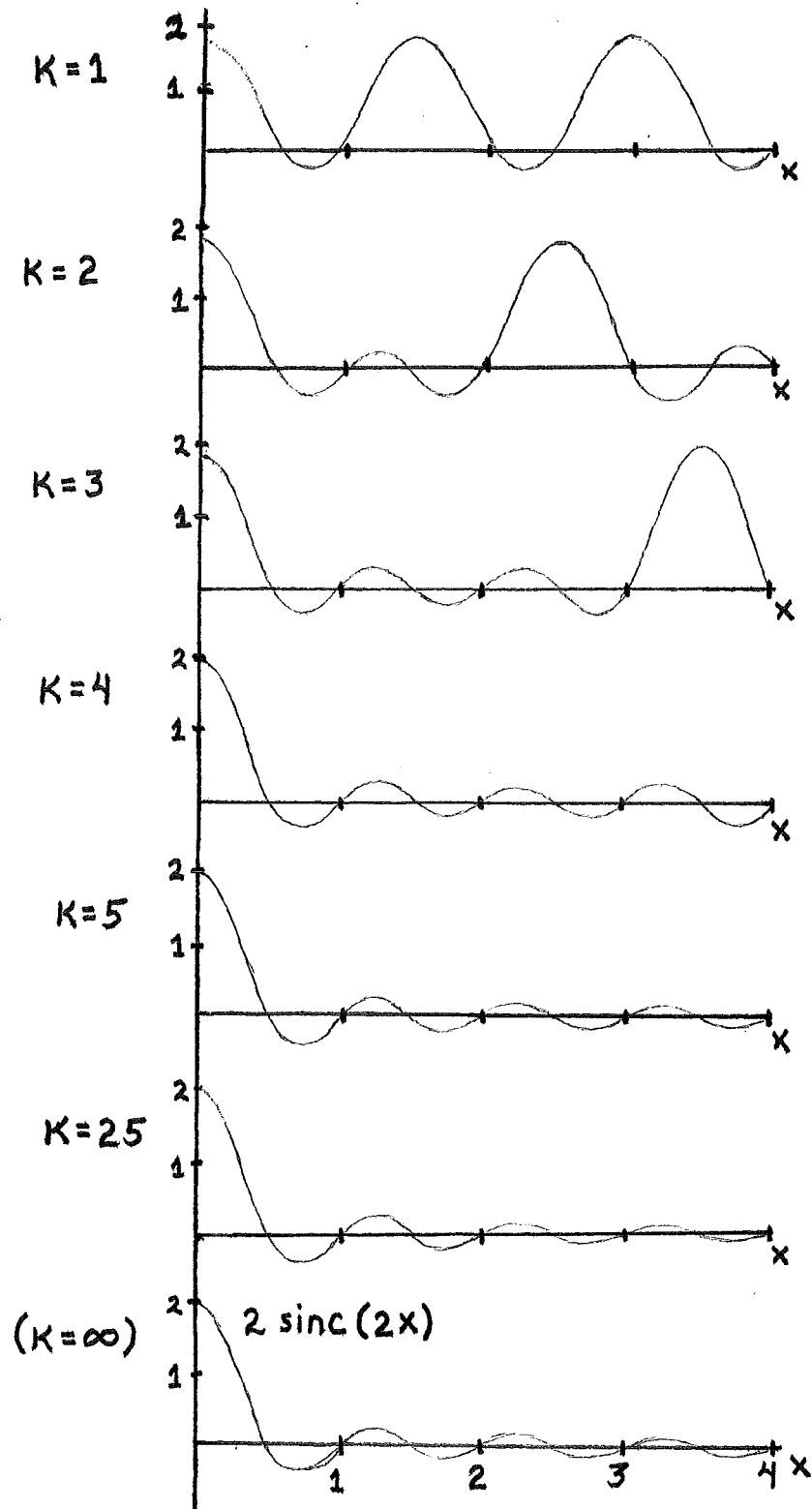


Fig. 27 : Piecewise isoplanatic approximated output of a Fourier Transformer with an input $\operatorname{rect}[x/2]$ as given by (3-108). The input pulse was divided into $2k+1$ isoplanatic patches. The true output is $2 \operatorname{sinc}(2x/\lambda f)$. (The above curves are for $\lambda f = 1$)

Substituting this and the Fourier transformer's transfer function [(3-100)] into the frequency domain expression for the piecewise isoplanatic approximation [(3-80)] gives

$$\tilde{g}_o(f_x) = \sum_n \mathcal{F} [g(x + \Delta x_n) \text{rect} (\frac{x}{2\Delta x_n})] \Big|_{f_x = -f_n} \times \delta(f_x + f_n) \quad (3-110)$$

or equivalently in the spatial domain

$$\tilde{g}_o(x) = \sum_n \mathcal{F} [g(x + \Delta x_n) \text{rect} (\frac{x}{2\Delta x_n})] \Big|_{f_x = -f_n} \times e^{-j2\pi f_n x} \quad (3-111)$$

There exists an interesting analogy to the piecewise isoplanatic approximation of the Fourier transformer and the Fourier series expansion of a function. Any periodic function $g_{on}(x)$ with fundamental frequency f , may be expressed as

$$g_{on}(x) = \sum_{n=-\infty}^{\infty} \alpha_n e^{j2\pi n f x} \quad (3-112)$$

where

$$\alpha_n = \int_x^{x+1/f} g_{on}(x) e^{-j2\pi n f x} dx \quad (3-113)$$

and where the periodic nature of $g_{on}(x)$ is assured by

$$g_{on}(x) = g_{on}(x + 1/f) \quad (3-114)$$

The α_n coefficient is recognized as the Fourier transform of a single period of $g_{on}(x)$ evaluated at nf , and may be written as

$$\alpha_n = \mathcal{F}[g_{op}(x)] \Big|_{f_x = nf} \quad (3-115)$$

where $g_{op}(x)$ is a single period of g_{on} :

$$g_{op}(x) = g_{on}(x) \text{rect}[f(x-x_0)] \quad (3-116)$$

and x_0 is constant.

The frequency domain equivalent of the Fourier series expression [(3-112)] is

$$\begin{aligned} G_{on}(f_x) &= \mathcal{F}[g_{on}(x)] \\ &= \sum_{n=-\infty}^{\infty} \alpha_n \delta(f_x - nf) \end{aligned} \quad (3-117)$$

Substitution of (3-115) gives

$$G_{on}(f_x) = \sum_{n=-\infty}^{\infty} \mathcal{F}[g_{op}(x)] \Big|_{f_x = nf} \delta(f_x - nf) \quad (3-118)$$

Note the striking computational similarities between the Fourier series [(3-118)] and piecewise isoplanatic approximation synthesis [(3-110)] of a function. Both relationships are expressed in the frequency domain as an impulse chain weighted by a Fourier transform expression of the described function. A notable difference is the limitation of the Fourier series to describe non-periodic functions which are zero outside a certain finite interval. Such is not the case for the piecewise isoplanatic synthesis. Another notable difference is the Fourier

series' employment of harmonics for function synthesis. For non-uniform isoplanatic patch calibration ($\Delta x_n \neq \text{constant}$ for all n) this is not the case for the piecewise isoplanatic synthesis.

(3) Isoplanatic linear systems

We now examine the effects of modeling an isoplanatic linear system as piecewise isoplanatic. The most obvious of isoplanatic systems are those performing operations encountered in elementary calculus. Consider first the integrator, which may be expressed in system notation as

$$\begin{aligned} g_o(x) &= \mathcal{S}[g(x)] \\ &= \int_{-\infty}^x g(x) dx \end{aligned} \quad (3-119)$$

The line spread function (3-34) of the optical integrator is then

$$h(x-x_0; x_0) = \int_{-\infty}^{\infty} \delta(x-x_0) dx = \mu(x-x_0) \quad (3-120)$$

where $\mu(x)$ is the unit step function. We see that the optical integrator is isoplanatic, since the line spread function is solely a function of the difference $(x - x_0)$. The transfer function of the integrator is

$$\begin{aligned} H(f_x) &= \mathcal{F}_1[\mu(x)] \\ &= \frac{1}{2} \delta(f_x) - \frac{j}{2\pi f_x} \end{aligned} \quad (3-121)$$

The optical differentiator is also isoplanatic, with an input-output relation given as

$$\begin{aligned} g_o(x) &= \mathcal{S}[g(x)] \\ &= \frac{d}{dx} g(x) \end{aligned} \quad (3-122)$$

The differentiator's line spread function is then

$$h(x-x_o; x_o) = \frac{d}{dx} \delta(x-x_o) = \delta'(x-x_o) \quad (3-123)$$

where $\delta'(x)$ represents the unit doublet⁽²⁴⁾. The unit doublet may be defined through an operation analogous to the sifting property of the Dirac Delta [(3-5)]:

$$\int_{-\infty}^{\infty} f(x) \delta'(x-x_o) dx = - \frac{df(x_o)}{dx} \quad (3-124)$$

The transfer function of the differentiator is

$$\begin{aligned} H(f_x) &= \mathcal{F}[\delta'(x)] \\ &= \int_{-\infty}^{\infty} \delta'(x) e^{-j2\pi f_x x} dx \end{aligned} \quad (3-125)$$

From (3-124)

$$\begin{aligned} H(f_x) &= - \left[\frac{d}{dx} e^{-j2\pi f_x x} \right] \Big|_{x=0} \\ &= j2\pi f_x \end{aligned} \quad (3-126)$$

From the above considerations, one may generalize transfer functions for multiple integration and differentiation. All will be isoplanatic.

An intuitively comforting relationship is the equivalence of $\tilde{g}_0(x)$ and $g(x)$ where a system is completely isoplanatic.

For such systems

$$h(x; x_n) = h(x) \quad (3-127)$$

The piecewise isoplanatic approximation [(3-77)] then becomes

$$\tilde{g}_0(x) = \sum_n g_n(x - x_n) * h(x) \quad (3-128)$$

Through the commutative [(3-15)] and distributive [(3-17)] properties of the convolution operation

$$\tilde{g}_0(x) = h(x) * \left[\sum_n g_n(x - x_n) \right] \quad (3-129)$$

which from (3-70) reduces to

$$\tilde{g}_0(x) = g(x) * h(x) = g_0(x) \quad (3-130)$$

This is the promised result.

We now examine the equivalence of the piecewise isoplanatic approximation for the specific cases of integrator and differentiator. For the former, we have from (3-128) and (3-120)

$$\tilde{g}_0(x) = \sum_n g_n(x - x_n) * \mu(x) \quad (3-131)$$

or equivalently

$$\tilde{g}_0(x) = \sum_n \int_{-\infty}^x g_n(x - x_n) dx \quad (3-132)$$

Each region is thus integrated. A geometrical illustration of this process is offered in Fig. 28a for the case of a spatial pulse divided into three arbitrary isoplanatic regions.

The superposition of all processed patches is seen to produce the true integrator output.

The same predicted equivalence of true and approximated output occurs with the invariant differentiator. Substitution of (3-123) into (3-128) gives

$$\tilde{g}_0(x) = \sum_n g_n(x-x_n) * \delta'(x) \quad (3-127)$$

or equivalently

$$\tilde{g}_0(x) = \sum_n \frac{d}{dx} g_n(x-x_n) \quad (3-128)$$

From (3-71)

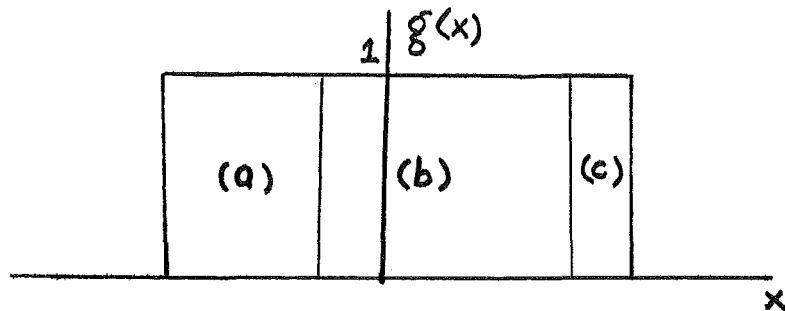
$$\tilde{g}_0(x) = \sum_n \frac{d}{dx} g(x) \text{rect} \left[\frac{x-x_n}{2\Delta x_n} \right] \quad (3-129)$$

since

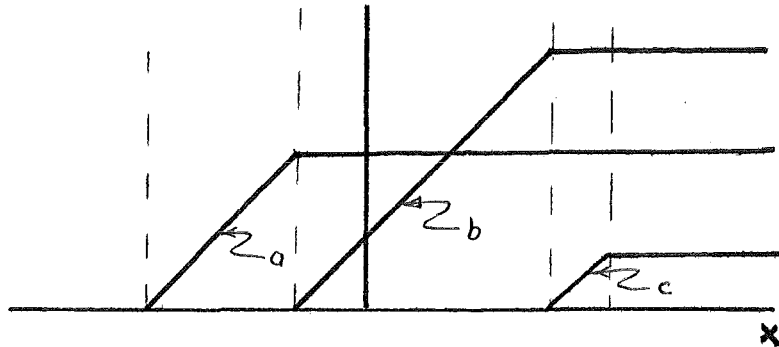
$$\frac{d}{dx} \text{rect} \left[\frac{x-x_n}{2\Delta x_n} \right] = \delta(x-x_n-\Delta x_n) - \delta(x-x_n+\Delta x_n) \quad (3-130)$$

The nth processed patch (the nth term in 3-129) may be written

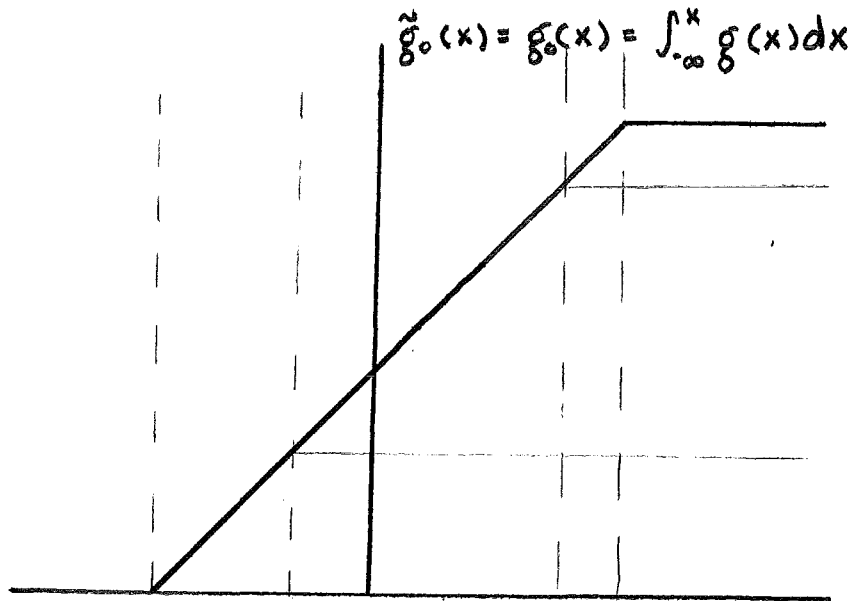
$$\begin{aligned} & \frac{d}{dx} g(x) \text{rect} \left[\frac{x-x_n}{2\Delta x_n} \right] \\ &= \text{rect} \left[\frac{x-x_n}{2\Delta x_n} \right] \frac{d}{dx} g(x) \\ & \quad + g(x_n-\Delta x_n) \delta(x-x_n+\Delta x_n) \\ & \quad - g(x_n+\Delta x_n) \delta(x-x_n-\Delta x_n) \end{aligned} \quad (3-131)$$



i) Input pulse divided into three isoplanatic regions.

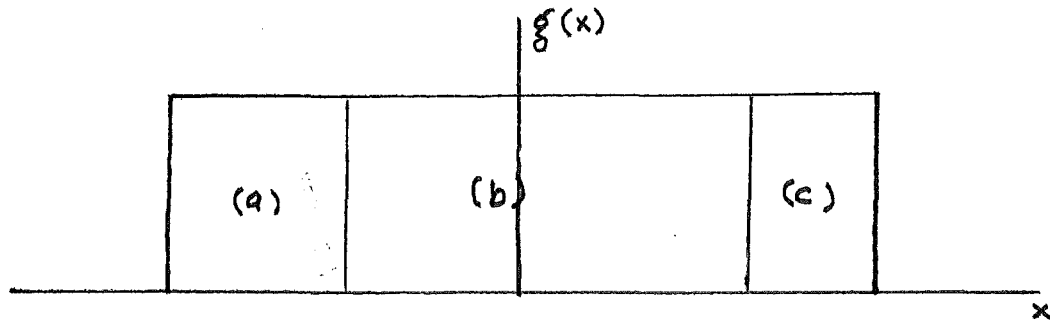


ii) Corresponding processed patches. Each ramp has a slope of unity.

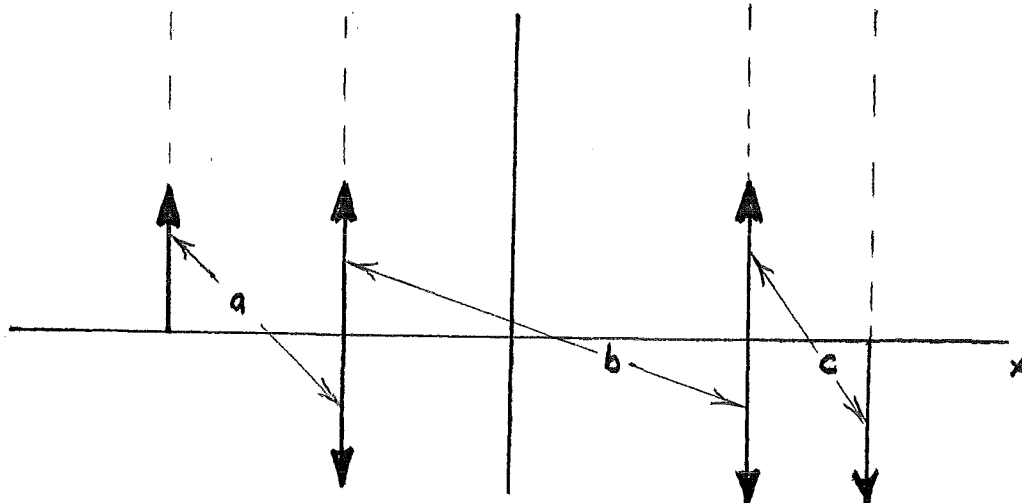


iii) Summation of each processed patch gives the true integral of the spatial pulse.

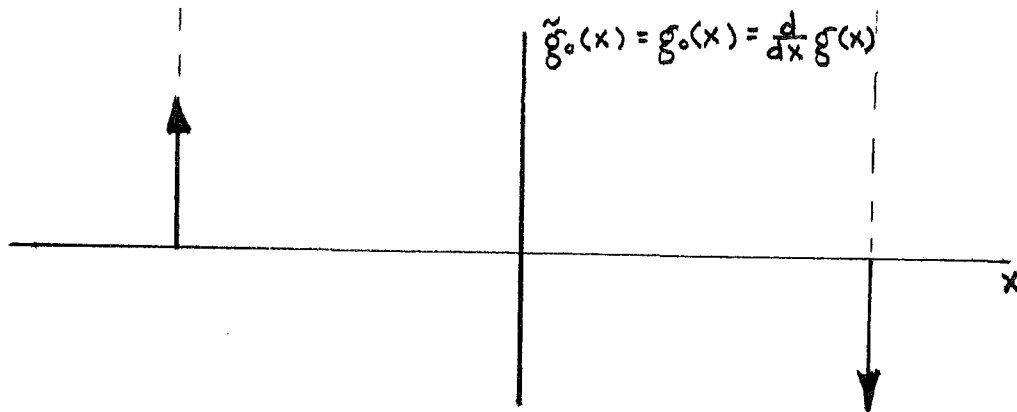
a) The piecewise isoplanatic approximation to the space invariant integrator from a spatial pulse divided into three arbitrary isoplanatic regions labeled a, b, and c. The "approximation" is equivalent to the true output.



i) Input pulse divided into three isoplanatic regions.



ii) Corresponding processed patches. Each impulse has a magnitude of unity.



iii) Summation of each processed patch gives the true derivative of the input.

b) The piecewise isoplanatic approximation to the space invariant differentiator.

Fig. 28 : Illustration of the equivalence of the true and piecewise isoplanatic approximated outputs of an invariant system for the case of the integrator and differentiator. Spatial pulses divided into three arbitrary isoplanatic patches are chosen for the inputs to both.

In the summation process in (3-129), the unwanted delta terms in (3-131) cancel from corresponding delta terms generated in adjacent patches. This occurs because we have already specified in (3-68) that

$$X_n + \Delta X_n = X_{n+1} - \Delta X_{n+1} \quad (3-132)$$

An illustration of this process for the specific case of a spatial pulse divided into three isoplanatic regions is offered in Fig. 28b. Again, the approximated output is equivalent to the true output due to the isoplanatic nature of the system.

(4) Generalizations and reflections

The preceding methods of analysis for determining the consequences of modeling the magnifier and Fourier transformer as piecewise isoplanatic may be directly applied to any invariant linear system. The following is a generalized summary of this technique:

- 1) Divide the system into a number of non-overlapping invariant regions. For example, optical system inputs are divided into isoplanatic patches. A linear invariant circuit input would be divided into a number of invariant time intervals.
- 2) Find the impulse response (and thus the transfer function) of each region. This is done by placing an impulse within the nth region at the system's input and noting the corresponding output.

- 3) Divide an arbitrary input function into invariant regions as in (1). Convolve each region with the corresponding impulse response. The summation of all processed regions is the piecewise invariant approximation of the output.
- 4) Determine the true output of the linear system by means of superposition and compare with the approximated output for goodness of fit.

The piecewise invariant approximation is one dimensional when applied to linear circuitry and two dimensional when applied in optics. Extension suggests generalization may be applied to describe any variant linear system in any finite number of dimensions.

The system analysis presented in this section is not complete. The following topics are in need of further investigation concerning the piecewise isoplanatic approximation:

- 1) A measure of the rate that a given piecewise isoplanatic approximation approaches the true output is needed.
- 2) Allowance for arbitrary isoplanatic patch width has been allowed in this section. Some patch distributions would seem to produce better output approximations than others. This suggests an investigation of optimal isoplanatic patch calibration.

3) All line spread functions in this section were found from the system response to an impulse placed at the midpoint of each isoplanatic patch while the very nature of isoplanicity suggests the spread function may be found from an impulse placed anywhere within the patch. This reflection suggests a study of the optimal placement of the impulse in each isoplanatic region.

4) Lastly, a method to determine which systems may be successfully modeled as piecewise isoplanatic is needed.

A possible solution to these problems rests in the system theory presented by Lohmann and Paris⁽²²⁾. Another possible method could arise from comparison of the true and approximated outputs. To date, the author's investigation of these methods has only been mildly successful.

A final note of interest rests in the amount of information needed to define a piecewise isoplanatic system. As previously stated, a general non-linear system demands knowledge of every output for every input. The infinity of defining relationship needed is of the highest order intuitively conceivable, constituting a one-to-one mapping with the set of all geometrical curves. Assumption of linearity decreases the order of the infinity of defining relationships which now may be mapped on a one-to-one basis with the set of all real numbers. A piecewise isoplanatic linear system (for which one is concerned with the entire input plane) also demands an infinity of defining relationships.

This particular infinity, however, has a one-to-one mapping with the positive integers and is thus an order below that demanded solely by assumption of linearity. Lastly, if a system is both linear and invariant, only a single defining relationship (the spread function) is needed for complete system definition.

Having explored these pure mathematical curiosities of system analysis, we now explore the possibility of implementing the piecewise isoplanatic approximation through holographic techniques.

IV. Recording Theory and Implementation

With the properties of the thin lens, the concepts of planar and volume holography, and an understanding of linear optical systems, we venture now to derive and implement procedures for holographically recording space variant linear systems, exploring the consequences, limitations, and implementation problems of each.

A) Generating Spread and Transfer Functions

To this point, mathematical models have been presented to analyze the linear optical system. Methods of realization of these concepts are now presented.

(1) The Dirac Delta and spread functions.

The two dimensional generalization of the point spread function [(3-34)] is

$$h(x-x_n; y-y_m; x_n, y_m) = \mathcal{S}[\delta(x-x_n, y-y_m)] \quad (4-1)$$

The Dirac Delta is used here and elsewhere in system analysis primarily for mathematical convenience. The physical existence of such a function is impossible due to its infinite "height" and discontinuity.

A fair optical approximation of the Dirac Delta may be made by focusing a plane wave to a "point" with a thin lens (Fig. 29). Noting that the thin lens is circular, we define

$$\text{circ } \sqrt{x^2 + y^2} = \begin{cases} 1 & ; \sqrt{x^2 + y^2} \leq 1 \\ 0 & ; \text{OTHERWISE} \end{cases} \quad (4-2)$$

The Fourier transform approximation of the field in the back focal plane is

$$\mathcal{F} \left[\text{circ } \frac{\sqrt{x^2 + y^2}}{a} \right] = \frac{a}{\rho} J_1(2\pi a \rho) \quad (4-3)$$

where a is the lens radius, J_1 is the Bessel Function of the first kind, order one, and

$$\rho = \frac{\sqrt{x^2 + y^2}}{\lambda f} \quad (4-4)$$

Goodman⁽⁸⁾ offers the following possible definition of the Dirac Delta

$$\delta(x, y) = \lim_{a \rightarrow \infty} \frac{a}{\rho} J_1(a 2\pi \rho) \quad (4-5)$$

The focused plane wave thus suffices for a Dirac Delta, for sufficiently large values of a .

The point spread function, (4-1), may easily be realized with $\delta(x - x_n, y - y_n)$ at one's disposal. Recalling the general optical system model pictured in Fig. 23, one need merely "focus" a point source on the input plane at (x_n, y_n) . The field

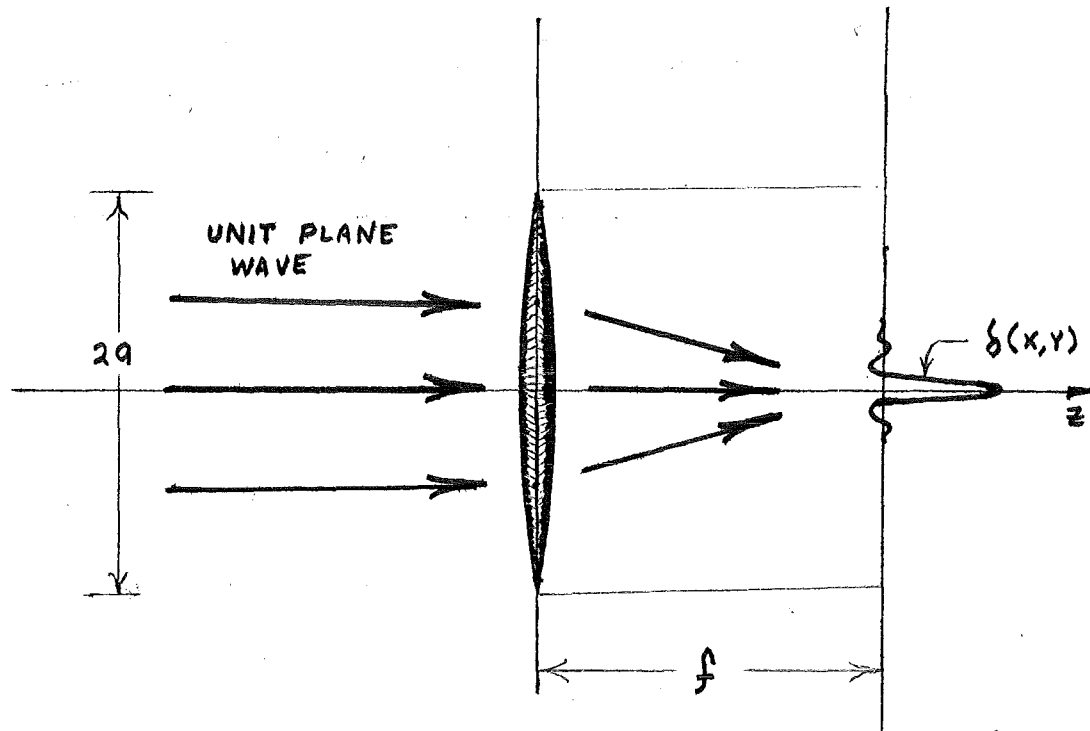


Fig. 29 : Generating the dirac delta by focusing a plane wave to a point source on the back focal plane of a thin lens.

distribution on the output plane is the corresponding point spread function. (Fig. 30).

Generation of the line spread function is possible in an analogous manner employing a double convex cylindrical (as opposed to spherical) lens. Such a lens would essentially focus an incident unit amplitude plane wave to $\delta(x)$ on its back focal plane and perform Fourier transforms in the sense of

$$G\left(\frac{x_f}{\lambda f}, \gamma\right) = \int_{-\infty}^{\infty} g(x, \gamma) e^{-j2\pi\left(\frac{x_f}{\lambda f}\right)x} dx \quad (4-6)$$

In order to completely specify a variant system, point spread functions from each isoplanatic patch need to be known. Intuitively, this information would be included from a knowledge of the responses of "criss-crossed" line sources on the system input, reducing the number of defining spread functions by twice a square root. This hypothesis is left for future consideration.

(2) The transfer function.

One possible procedure to determine the transfer function of a linear circuit is to first place an impulse at the circuit's input terminal and then perform a Fourier transform on the corresponding output. This operation finds some happy optical analogs due to the Fourier transforming properties of the thin lens.

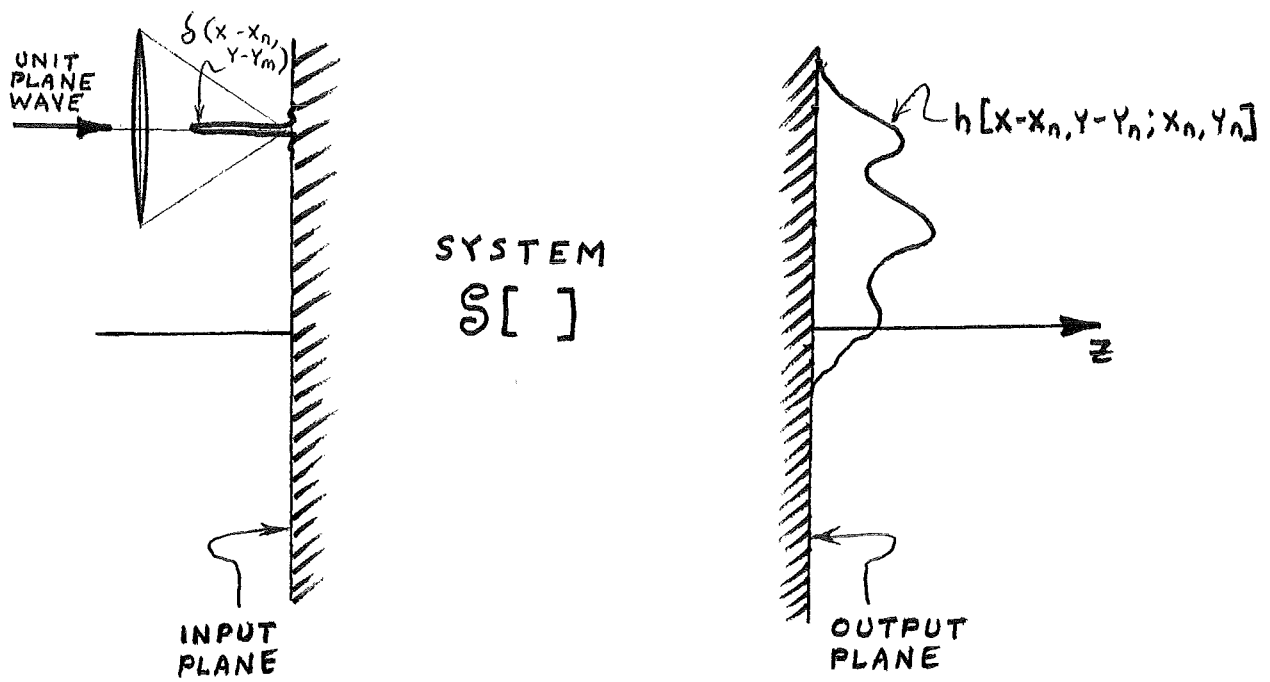


Fig. 30 : Generating a system's point spread function. A point source is focused at co-ordinates (x_n, y_m) of the system's input plane. The resulting distribution on the output plane is $h_{nm}(x-x_n, y-y_m)$.

If one were to perform a Fourier transform of a system's line spread function with a lens centered on the system axis, the result would be

$$\mathcal{F}[h_{nm}(x-x_n, y-y_m)] = H_{nm}(f_x, f_y) e^{-j2\pi(f_x x_n + f_y y_m)} \quad (4-7)$$

where we have adopted the notation

$$f(x, y; x_n, y_m) = f_{nm}(x, y) \quad (4-8)$$

To determine the Fourier transforming properties of a lens centered at (x_n, y_m) , we define

$$\mathcal{F}_{[x-x_n, y-y_m]} \{g(x, y)\} = \int_{-\infty}^{\infty} g(x, y) e^{-j2\pi[(x-x_n)(f_x-f_n) + (y-y_m)(f_y-f_m)]} dx dy \quad (4-9)$$

where

$$f_n = \frac{x_n}{\lambda f} \quad ; \quad f_m = \frac{y_m}{\lambda f} \quad (4-10)$$

The advantages to this notation are obvious when one notes

$$\mathcal{F}_{[x-x_n, y-y_m]} [h_{nm}(x-x_n, y-y_m)] = H_{nm}(f_x - f_n, f_y - f_m) \quad (4-11)$$

This is, in fact, the transform of the line spread function of a system resulting from a lens centered at (x_n, y_m) .

In the most general case, the transform of the shifted line function, (4-1), with a lens centered at (a, b) gives

$$\begin{aligned} \bar{H}_{nm}(f_x) &= \mathcal{F}_{[x-a, y-b]} [h_{nm}(x-x_n, y-y_m)] \\ &= H_{nm}(f_x - f_a, f_y - f_b) e^{j2\pi[(f_x - f_a)(x_n - a) + (f_y - f_b)(y_n - b)]} \end{aligned} \quad (4-12)$$

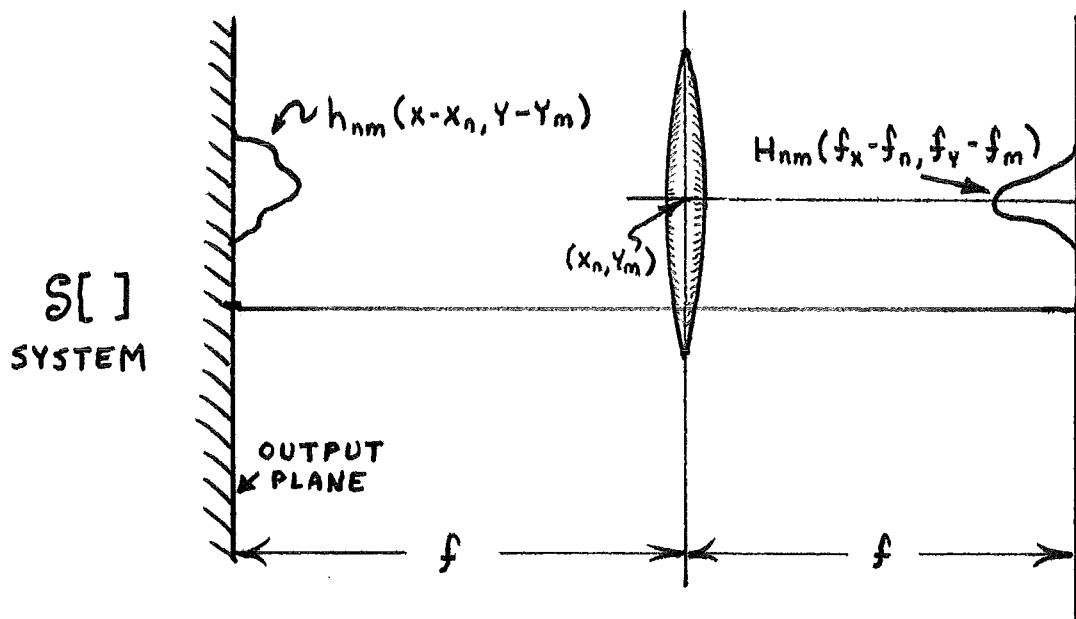
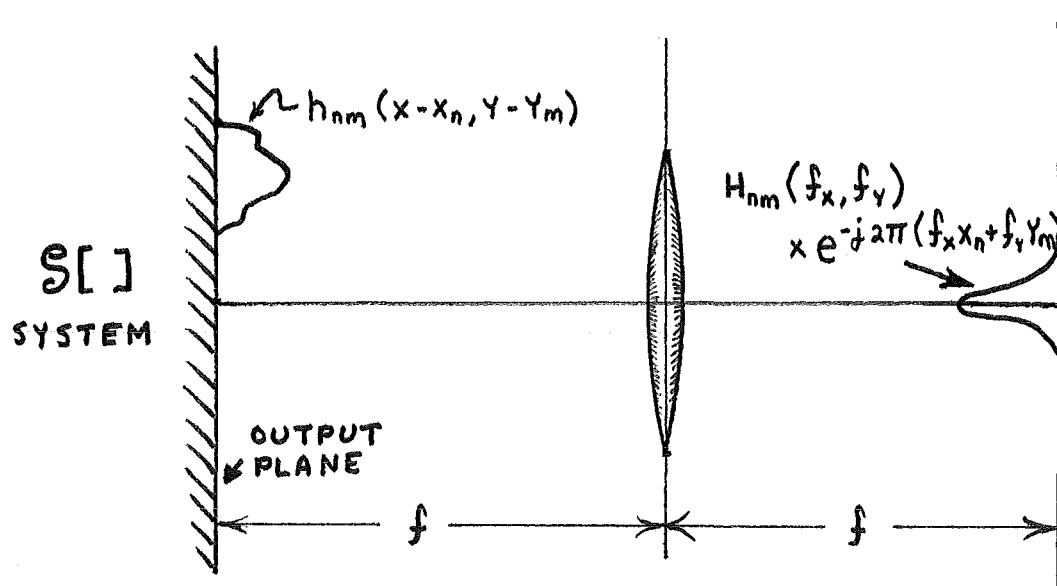


Fig. 31 : Two methods to generate transfer function expressions. The point spread function, as generated in Fig. 30, is Fourier Transformed by a thin lens placed at co-ordinates

- a) $(0, 0)$
- b) (x_n, y_m)

where the notation $\bar{f}(x,y)$ denotes shifted versions of $f(x,y)$ possibly accompanied by a linear or constant multiplicative phase factor.

As can be seen, there exist a number of ways to generate transfer function expressions. In future considerations, we choose from this abundance in accordance with need.

(3) Holographic recording of the transfer function

a) Availability of form

When holographically recorded, a transfer function expression may be further altered by physically shifting the developed hologram to different reconstruction locations. Of additional interest is the altering of the multiplicative phase term from the reference beam resulting from this shifting.

In order to record the magnitude and phase of an information bearing wave, a reference beam needs to be employed. The most general expression for a reference beam for recording the nmth transfer function would be

$$U_{nm}(f_x, f_y) = A_{nm}(f_x, f_y) e^{-j\phi_{nm}(f_x, f_y)} \quad (4-13)$$

It becomes convenient to assign the amplitude of the reference beam a value of unity, and keep the phase linear,

$$\phi_{nm}(f_x, f_y) = 2\pi(\xi f_x + \eta f_y) \quad (4-14)$$

The reference wave then results from a plane wave with direction cosines [(1-26)]

$$\begin{aligned} \alpha_{nm} &= \xi_n / r \\ \beta_{nm} &= \eta_m / r \\ \gamma_{nm} &= \frac{1}{r} \sqrt{r^2 - \xi_n^2 - \eta_m^2} \end{aligned} \quad (4-15)$$

Note that by virtue of the subscripts, different reference beams are being allowed for each transfer function.

If the reference beam is beat with the corresponding transfer function [(4-12)], the resulting intensity on the surface of a photosensitive media would be (from (2-4))

$$\begin{aligned} I(f_x, f_y) = & |H_{nm}(f_x, f_y)|^2 + 1 \\ & + \bar{H}_{nm}(f_x, f_y) e^{-j2\pi(f_x \xi_n + f_y \eta_m)} \\ & + \bar{H}_{nm}^*(f_x, f_y) e^{j2\pi(f_x \xi_n + f_y \eta_m)} \end{aligned} \quad (4-16)$$

Since one ultimately wishes to work with the transfer function, and not its conjugate, attention is restricted to the third term in the intensity distribution.

$$I_3(f_x, f_y) = \bar{H}_{nm}(f_x, f_y) e^{-j2\pi(f_x \xi_n + f_y \eta_m)} \quad (4-17)$$

Or equivalently, from (4-12):

$$\begin{aligned} I_3(f_x, f_y) = & H_{nm}(f_x - f_a, f_y - f_b) \\ & \times e^{j2\pi[(f_x - f_a)(x_n - a) + (f_y - f_b)(y_m - b)]} \\ & \times e^{-j2\pi[f_x \xi_n + f_y \eta_m]} \end{aligned} \quad (4-18)$$

The more specific cases of interest are when the transform lens is centered on the system axis [(4-7)] or at coordinates (x_n, y_m) [(4-11)] as pictured in Fig. 31. The corresponding intensity distributions of interest are respectively

$$I_3(f_x, f_y) = H_{nm}(f_x, f_y) e^{-j2\pi[(x_n + \xi_n)f_x + (y_m + \eta_m)f_y]} \quad (4-19)$$

and

$$I_3(f_x, f_y) = H_{nm}(f_x - f_n, f_y - f_m) e^{-j2\pi(\xi_n f_x + \eta_m f_y)} \quad (4-20)$$

Further expressions containing the transfer function are available by physically shifting the developed hologram. In the most general case, shifting the intensity distribution given by (4-18) to coordinates (p, q) on the Fourier plane would put at one's disposal the expression

$$\begin{aligned}
 I_3(f_x - f_p, f_y - f_q) &= H_{nm}(f_x - f_a - f_q, f_y - f_b - f_q) \\
 &\times e^{j2\pi[(f_x - f_a - f_q)(x_n - a) + (f_y - f_b - f_q)(y_n - b)]} \\
 &\times e^{-j2\pi[(f_x - f_p)\xi_n + (f_y - f_q)\eta_m]} \quad (4-21)
 \end{aligned}$$

Specific cases of interest are first, shifting the on-axis transform intensity distribution [(4-19)] to coordinates (x_n, y_m) on the Fourier plane to give

$$\begin{aligned}
 I_3(f_x - f_n, f_y - f_m) &= H_{nm}(f_x - f_n, f_y - f_m) \\
 &\times e^{-j2\pi[(x_n + \xi_n)(f_x - f_n) + (y_m + \eta_m)(f_y - f_m)]} \quad (4-22)
 \end{aligned}$$

and secondly, shifting the specific off-axis transform intensity distribution [(4-20)] to the origin

$$\begin{aligned}
 I_3(f_x + f_n, f_y + f_m) &= H_{nm}(f_x, f_y) \\
 &\times e^{-j2\pi[(x_n + \xi_n)(f_x + f_n) + (y_m + \eta_m)(f_y + f_m)]} \quad (4-23)
 \end{aligned}$$

Obviously, there then exist a number of ways to generate intensity distributions containing the transfer function. In each case presented above, the transfer function is shifted and/or accompanied by a multiplicative linear phase factor. This diversity will later prove useful for choosing appropriate expressions to fulfill the piecewise isoplanatic approximation.

b) Desired Fourier plane expressions

The non-existence of the inverse Fourier transform in optical processing is overcome by the recurrence theorem [(3-24)]. As such the Fourier expression of the piecewise isoplanatic approximation (P.I.A.) must be remassaged. Specifically, we desire on the Fourier plane the inverse transform of the P.I.A. in the spatial domain. That is

$$\mathcal{F}^{-1}[h_{nm}(x, y) * g_{nm}(x-x_n, y-y_m)] = G_{nm}(-f_x, -f_y) H_{nm}(-f_x, -f_y) \times e^{j2\pi[f_x x_n + f_y y_m]} \quad (4-24)$$

or equivalently

$$\mathcal{F}^{-1}[\tilde{g}_0(x, y)] = \tilde{G}_0(-f_x, -f_y) \quad (4-24)$$

Since a rotation of 180° is also acceptable on the output, we may also have on the Fourier plane

$$\mathcal{F}^{-1}[\tilde{g}_0(-x, -y)] = \tilde{G}_0(f_x, f_y) \quad (4-25)$$

While appearing rather innocent in this context, the above considerations become critical in later recording schemes.

3) Limitations on Recordable Waveforms

A note is in order concerning the physical limitations on waveforms which may be holographically recorded. Film is a passive optical element affording a normalized attenuation between opaque (1) and transparent (0). Recorded intensity [(2-4)] is then limited by

$$0 \leq I(x, y) \leq 1 \quad (4-25)$$

This restriction, for example, precludes conventional holographic recording of the transfer functions of the Fourier transformer [(3-100)] or the integrator [(3-121)], both of which contain the Dirac Delta. Acceptable synthesis of these frequency domain transmittances necessitates the use of active optical elements.

B) System Recording Employing the Extinction Angle

In previous holographic considerations, distinction is made between the object and reference beams, while in truth, the system has no such method of differentiation. This becomes self evident when one considers the case of two plane waves.

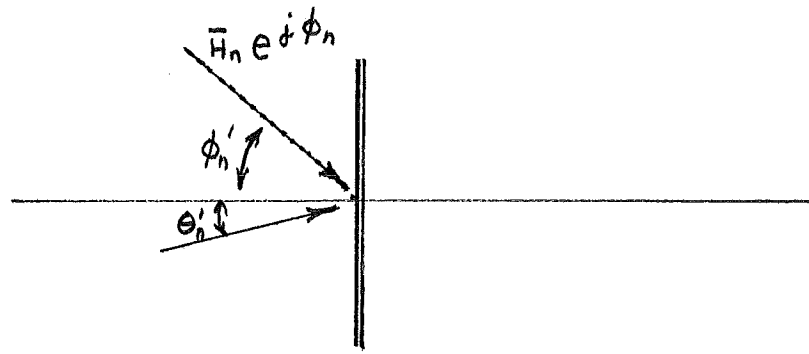
Consider Fig. 32a where $\bar{H}_n(f_x)$ [(4-12)], accompanied by a multiplicative linear phase term, is beat with a planar reference beam. The former may be thought of as a modulated plane wave propagating at an angle ϕ' with respect to the system axis. Employing the labeled parameters in Fig. 32a, the film essentially records an intensity distribution given as

$$I = 1 + |H_n|^2 + H_n e^{j\phi_n} e^{-j\theta_n} + H_n^* e^{-j\phi_n} e^{j\theta_n} \quad (4-26)$$

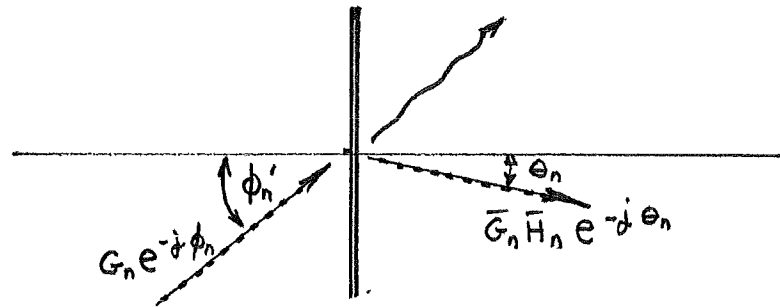
Attention is restricted to the third term which contains the desired transfer function information:

$$I_3 = \bar{H}_n e^{j\phi_n} e^{-j\theta_n} \quad (4-27)$$

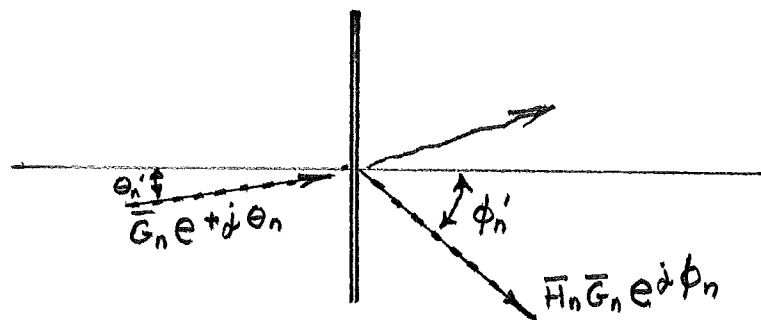
Once developed, the hologram will be illuminated with tilted versions of $\bar{G}_n(f_x)$. As with the transfer function notation, $\bar{G}_n(f_x)$ is a generalization of all shifted versions of $G_n(f_x)$ which may be accompanied by a linear multiplicative phase term.



a) Recording of $H_n e^{j\phi_n}$ with planar reference beam $e^{j\theta_n}$



b) Reconstruction with $G_n e^{-j\phi_n}$ to give $H_n \bar{G}_n e^{-j\theta_n}$



c) Reconstruction with $\bar{G}_n e^{j\theta_n}$ to give $H_n \bar{G}_n e^{j\phi_n}$

Fig. 32 : Methods of obtaining $\bar{G}_n \bar{H}_n$ from a holographic recording.

We first illuminate with $\bar{G}_n e^{-j\phi_n}$ (Fig. 32b). With no regard to diffraction efficiency, this term multiplies (4-27) to give

$$U_{\theta_n} = \bar{H}_n \bar{G}_n e^{-j\theta_n} \quad (4-28)$$

In a similar fashion, illumination with $\bar{G}_n e^{j\theta_n}$ (Fig. 32c) gives

$$U_{\phi_n} = \bar{H}_n \bar{G}_n e^{j\phi_n} \quad (4-29)$$

Thus, in the most general of terms, there are two ways to extract the desired information from the hologram. Note also the similarity of the above expressions and the terms of the piecewise isoplanatic approximation expressed in the Fourier domain [(3-80)].

In order to determine how one might employ diffraction efficiency to separate adjacent functions on recording and reconstruction, a brief detour into the angular incidence interval occupied by a waveform is necessitated.

1) Angular intervals of waveforms

As stated previously in the thin lens section, a waveform may be decomposed into a number of rays. In many cases, the propagation directions of these rays fall into an angular interval

$$\begin{aligned} \psi_n \pm \Delta\psi_n \\ \Delta\psi_n \geq 0 \end{aligned} \quad (4-30)$$

Consider first the transfer function of the non-inverting magnifier

$$H_n(f_x) = e^{-j2\pi(M-1)x_n f_x} \quad (4-31)$$

This expression results from a plane wave with a single propagation direction, and may be shown to lie in the zero width angular interval given by

$$\psi_n = a \tan \left(\frac{Mx}{f} \right) \quad (4-32)$$

$$\Delta \psi_n = 0$$

The transfer function of the Fourier transformer is again

$$H_n(f_x) = \delta(f_x + f_n) e^{-j 2\pi x_n f_n} \quad (4-33)$$

Generating the Dirac Delta term by focusing a plane wave to a point suggests a value of $\Delta \psi_n$ between 90° and, say, 10° , depending on the goodness of approximation desired.

As a third example, consider the transformation of $g_n(x-x_n)$ as depicted in Fig. 33. The end points at $x_n \pm \Delta x_n$ on the input plane essentially give rise to spherical waves which are collimated by the lens. All other points within the input strip yield plane waves propagating within the resulting angular interval. As such

$$\psi_n + \Delta \psi_n = a \tan \frac{-(x_n + \Delta x_n)}{f} \quad (4-34)$$

$$\psi_n - \Delta \psi_n = a \tan \frac{-(x_n - \Delta x_n)}{f}$$

This is true when $g_n(x-x_n)$ extends the entire strip width and is the maximum angular interval. For example, if the input was $\delta(x-x_n)$, the result would be a plane wave with $\Delta \psi_n = 0$.

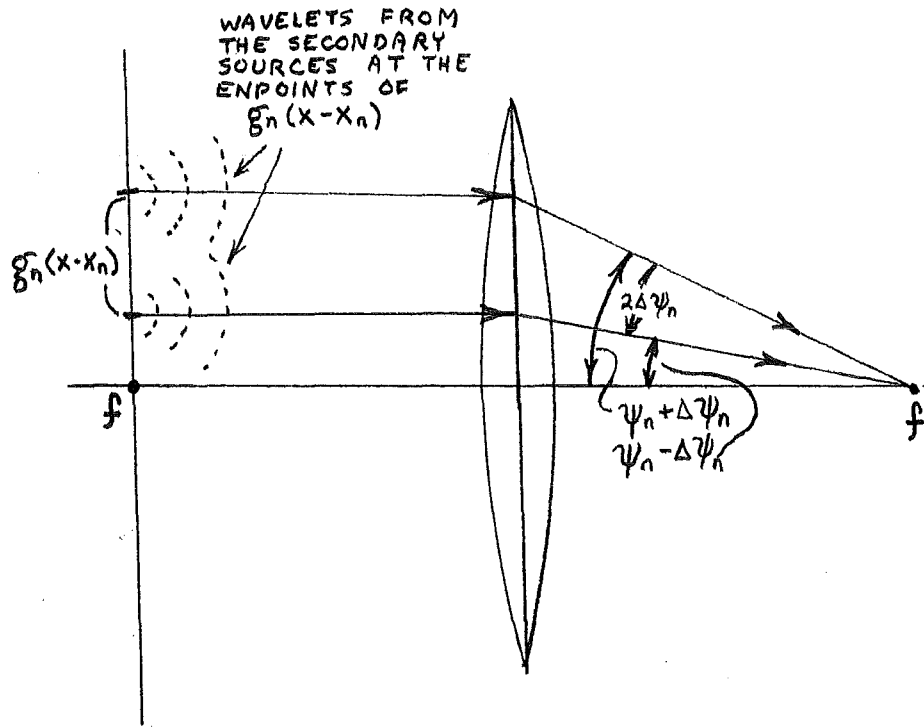


Fig. 33 : The maximum angular interval from an isoplanatic region is centered at ψ_n and has a width of $\Delta\psi_n$.

The concept of a function's angular interval is now employed in determining the diffraction efficiency in general volume hologram recordings.

2) The angular bandpass

Now consider the diffraction efficiency of a transfer function expression with a known angular interval when it is holographically recorded with a planar reference beam. One is not as much concerned with the physical diffraction efficiency function as with the angular interval over which the diffraction efficiency is non-zero.

Consider again Fig. 32a in which a transfer function expression is holographically recorded and assume that $H_n(f_x)$ has a finite angular interval $\psi_n \pm \Delta\psi_n$. The resulting recorded distribution may be thought of as a plane wave (the reference beam) beating with a number of rays lying within the transfer function expression's angular interval. For reconstruction, we are interested in the angular extent of diffraction efficiency from reconstruction with plane waves propagating in the angular regions about the reference beam, and the transfer function expression's angular intervals.

Consider first, the illumination of the developed hologram with plane waves about the region of the reference beam, noting the monotonic nature of the extinction angle function (Fig. 20), the maximum extinction angle formed by a constant reference beam and any variable ray direction in the transfer function expression's angular interval would result from $\psi_n - \Delta\psi_n$.

This extinction angle is denoted by $\Delta \theta_n'$. As such, the angular bandpass for reconstruction about the angle θ_n' (Fig. 34a) is given as

$$\theta_n' \pm \Delta \theta_n' \quad (4-35)$$

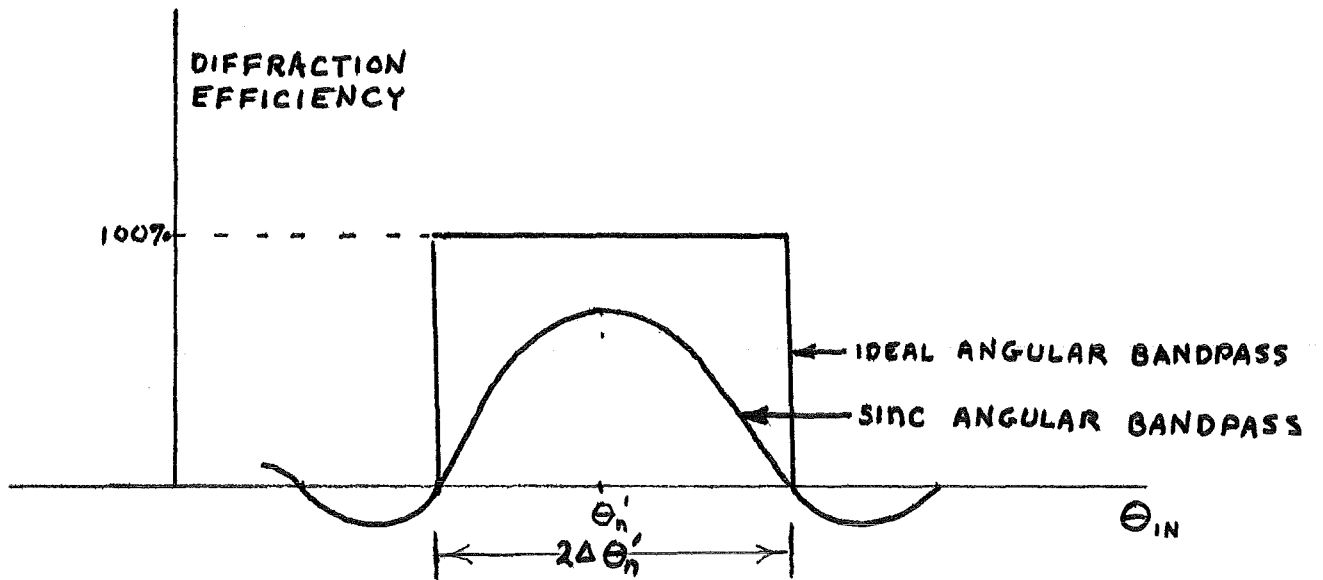
Next for examination is re-illumination with rays in the region of ψ_n . Here, roles are mathematically switched in that the rays within $\psi_n \pm \Delta \psi_n$ are now reference beams and θ_n' is the object beam. The extinction angles formed by $\psi_n + \Delta \psi_n$ and $\psi_n - \Delta \psi_n$ with θ_n will be denoted respectively by $\Delta \theta_{ne}$ and $\Delta \theta_{nu}$. Again from the extinction angle curve (Fig. 20)

$$\Delta \theta_{nu} \geq \Delta \theta_{ne} \quad (4-36)$$

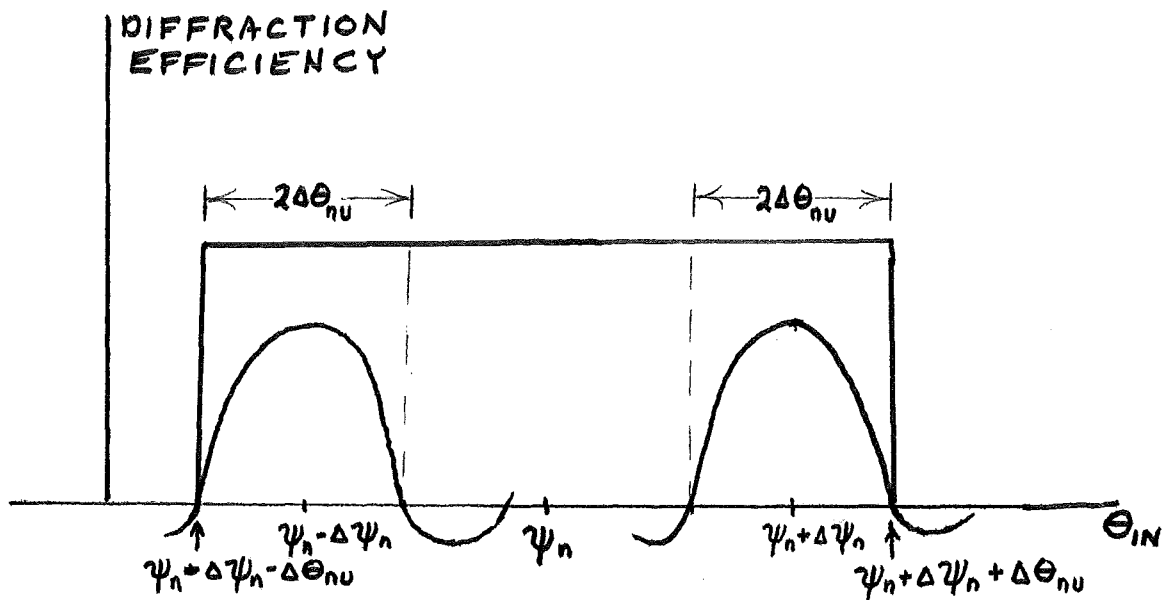
in fact, $\Delta \theta_{nu}$ is the maximum extinction angle formed from the interval $\psi_n \pm \Delta \psi_n$. As such, the angular bandpass about ψ_n (Fig. 34a) is safely defined as

$$\psi_n + \Delta \psi_n + \Delta \theta_{nu} \leq \theta_n \leq \psi_n - \Delta \psi_n - \Delta \theta_{nu} \quad (4-37)$$

The intervals given in (4-35) and (4-37) are the angular bandpasses encountered in reconstruction respectively in Figures 34b and 34c ideally yielding U_{θ_n} and U_{ψ_n} as given in (4-28) and (4-29). We wish to choose the best method of reconstruction. Obviously the narrower the passband, the more overall number of wavefronts one can store. This rules in favor of the reference beam direction reconstruction. The deciding vote is cast by the arbitrariness of the transfer function



a) Reconstruction with plane waves about the reference beam.



b) Reconstruction in $\psi_n \pm \Delta\psi_n$ region.

Fig. 34 : Angular bandpass resulting from reconstruction about (a) the reference beam, and (b) the object beam.

waveform which might possibly contain a null wave component within its angular interval. For this reason, reference beam reconstruction is chosen.

3) Recording and reconstruction

We now derive a procedure by which a variant linear system may be recorded employing the extinction angle. The resulting hologram should then have similar input-output relationships to the recorded hologram as prescribed by the piecewise isoplanatic approximation.

In order to formulate a recording scheme, one must first specify a reconstruction geometry. The one most obvious is pictured in Fig. 35. The input transmittance $g(x)$ is Fourier transformed and selectively multiplied by the holographic transmittance of the Fourier plane. The desired output then appears displaced a distance a from the system axis (so as not to interfere with the zero order wave) where it is reimaged.

We now examine this reconstruction scheme to see what must happen and what we would like to have happen. Dividing the input $g(x)$ into isoplanatic regions [(3-70), (3-71)] the Fourier plane sees

$$G(f_x) = \mathcal{F}[g(x)] = \sum_n G_n(f_x) e^{-j2\pi f_x x_n} \quad (4-37)$$

The frequency domain expression for the piecewise isoplanatic approximation, shifted a distance a , is (from 3-80)):

$$\tilde{G}_0(f_x) e^{-j2\pi f_x a} = \sum_n H_n(f_x) G_n(f_x) e^{-j2\pi f_x (x_n + a)} \quad (4-38)$$

Comparing the above two expressions dictates that the hologram transmittance must be

$$\bar{H}(f_x) = \sum_n H_n(f_x) e^{-j2\pi f_x a} \quad (4-39)$$

Furthermore, recording should be done in such a manner that the cross-talk elimination criterion [(3-83)] is fulfilled upon reconstruction.

The angular interval of each transformed strip is given by (4-34). In order to align diffraction efficiencies, the propagation direction of the nth reference beam should be ψ_n . For small angles

$$\psi_n = \phi_n = a \tan(-x_n/f) \cong -x_n/f \quad (4-40)$$

The wave expression for such a wave is

$$U_r(f_x) = e^{-j2\pi f_x x_n} \quad (4-41)$$

where a unit amplitude has been chosen for the sake of simplicity. This expression will appear in conjugate form in the intensity distribution. Comparison with (4-41) then dictates

$$\bar{H}_n(f_x) = H(f_x) e^{-j2\pi f_x (x_n + a)} \quad (4-42)$$

Employing the transform expression generation ideas previously discussed, this expression may be realized as in Fig. 36. The impulse input appears as the displaced line spread function $h_n(x-x_n)$ on the output. The transforming lens is placed a distance a below the system axis, and thus sees the line spread function as $h_n(x-x_n-a)$. The corresponding transform

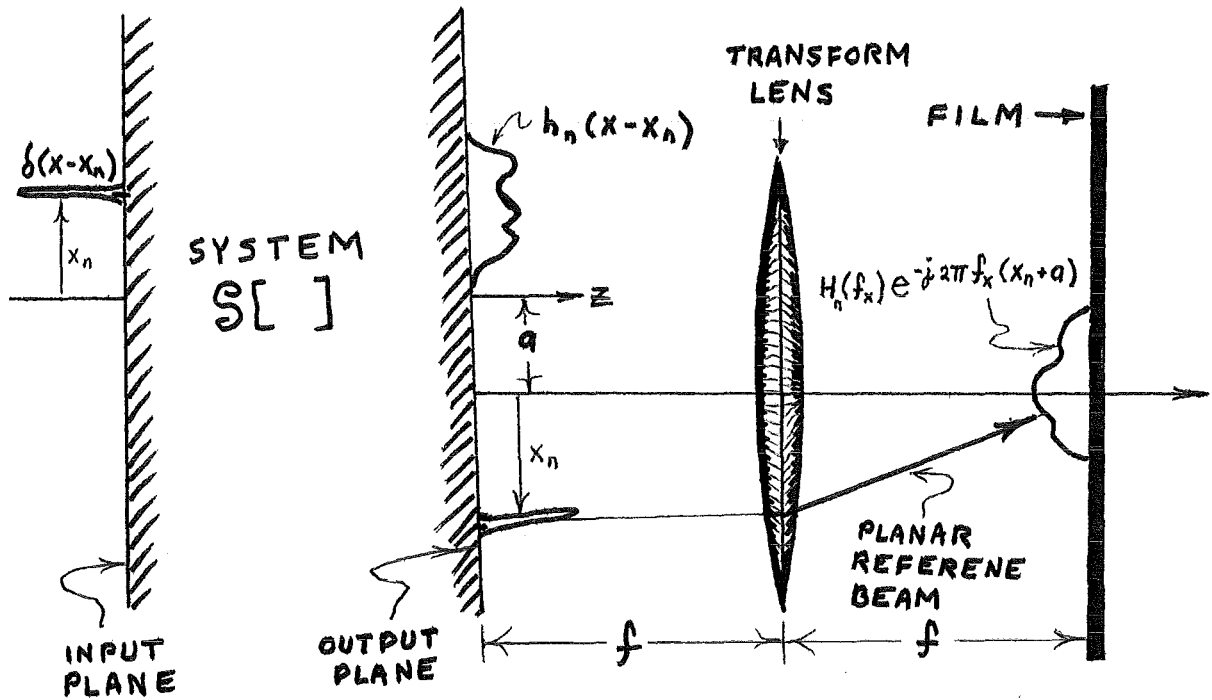


Fig. 36 : Holographic recording of the transfer function expression given by (4-42).

is accordingly that of (4-42).

Now to be examined is the fulfillment of the cross-talk elimination criterion via diffraction efficiency. The maximum extinction angle from a ray component within the angular interval of (4-42) and the n th reference beam will be denoted $\Delta\theta'_n$. The resulting angular bandpass is again given by (4-35). The angular interval of the transformed input region $[G_n(f_x)e^{-j2\pi f_x x_n}]$ must also lie in this band. As such, we must record each transfer function in such a manner as to have no overlap in adjacent bands. The spacing of these bands will be completely dictated by the angular interval of the transfer function expression [(4-42)]. This in turn will dictate the permissible isoplanatic patch density on the input plane.

As an example, we turn to the Fourier transformer, saving the magnifier for implementation purposes. As previously mentioned, attempting to conventionally record Dirac Delta is not advisable, but all will turn out well, assuming active film exists.

Consider Fig. 37 in which the recording scheme for the Fourier transformer is presented after the more general Fig. 35. Assume the plane wave focused to the input point source has a height d and focal length f . The point source thus has an angular interval of

$$0 \pm \Delta\psi_{ps} \quad \text{WHERE} \quad \Delta\psi_{ps} = a \tan(d/2f) \quad (4-43)$$

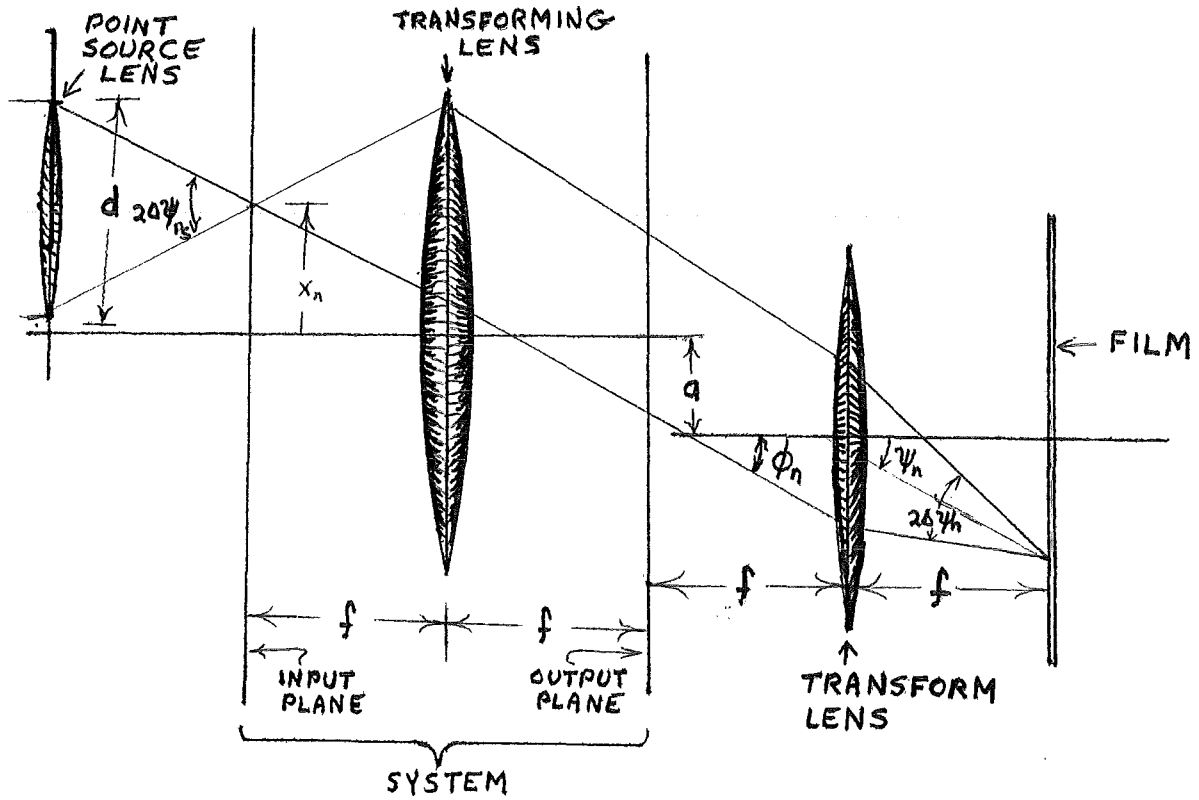


Fig. 37 : System recording of the Fourier Transformer after the more general Fig. 36.

The system transformer lens sees this point source in its front focal plane and collimates it into a plane wave propagating at an angle

$$\phi_n = a \tan(x_n/f) \quad (4-44)$$

and with a width d . (All lenses are conveniently assigned the same focal length f). This wave is essentially focused to a point source in the Fourier plane and is given by

$$\bar{H}_n(f_x) = \delta(f_x + f_n) e^{-j2\pi f_x a} e^{-j2\pi f_n x_n} \quad (4-45)$$

We are interested in the angular interval of this wave. From the geometry of Fig. 37, it can be shown that

$$\sin(2\Delta\psi_n) = \frac{d}{\sqrt{(a+x_n)^2 + f^2}} \quad (4-46)$$

and

$$\tan(\psi_n + \Delta\psi_n) = \frac{a+x_n}{f} \quad (4-47)$$

From these expressions one may easily extract the desired angular interval.

Suppose, for simplicity's sake, d may be varied to always yield $\Delta\psi_n = 15^\circ$. The film is assumed to be an active version of Kodak 649F plates, and illumination is accomplished with a helium neon laser. As such, we may employ the extinction angle curves in Fig. 20. The focal length of all lenses will be 10 cm. A value of 7 cm is assigned to a .

First, a point source is placed directly on the system axis yielding an angular interval of $\psi_0 \pm 15^\circ$

where, from (4-47), $\tan(\psi_0 + 15^\circ) = 0.7$

or

$$\psi_0 \approx 20^\circ$$

The planar reference beam for the zeroth patch from (4-37)

is incident at an angle of

$$\phi_0 = 0^\circ$$

The worst case condition for the extinction angle occurs with

$$\theta_r = \psi_0 - \Delta\psi_0 = 5^\circ, \text{ a point which lies off of the}$$

extinction angle plot. From (2-107), the resulting extinc-

tion angle turns out to be

$$\Delta\theta_0 \approx 27.5^\circ$$

From previous arguments, we must now find ψ_1 and ϕ_1 such that

$$\phi_1 - \Delta\theta_1 = \phi_0 + \Delta\theta_0 \quad (4-48)$$

or equivalently

$$\phi_1 - \Delta\theta_1 = 27.5^\circ$$

where $\Delta\theta_1$ is the extinction angle from ϕ_1 and $\psi_1 - \Delta\psi_1 = \psi_1 - 15^\circ$.

While innocent in appearance, this quest is quite complicated, involving combinations of four equations [(2-107), (4-40),

(4-47), and (4-48)]. If one does not assume a constant $\Delta\psi_n$,

(4-46) enters also. The operation is made much more palatable

by a trial and error procedure on the extinction angle curve.

Note the undesirable overlap of the object and reference

angular bandpasses that occur from only the first transfer

function. Note, also, that the extinction angles resulting

from further calibration attempts would also be on the order

of 30° , limiting the input plane to about three isoplanatic

patches.

Although impractical, the recording of the Fourier transformer exposes the limitations which must be placed on the angular interval of a linear system's transfer function when recorded on a "thin thick" hologram. An obvious solution to the large extinction angle problem is employment of a macroscopically thick emulsion which is discussed shortly.

We now focus attention on a system with the smallest of all angular intervals: the simple magnifier which can be recorded on Kodak 649-F plates employing extinction angle techniques.

4) Implementation of the holographic recording of a non-inverting magnifier

The transfer function of the magnifier is given in (4-31) and results from a plane wave propagating at an angle given by (4-32). The generalized recording procedure of Fig. 36 is again called upon and is pictured for the non-inverting magnifier case in Fig. 38. The first two lenses are placed in the system to invert the input function. The third system lens performs the magnification in the same manner as pictured in Fig. 7a. The magnification is governed by the system relationships in (1-19) and (1-20).

An input of $\delta(x-x_n)$ appears on the output as $\delta(x-Mx_n)$. The Fourier transform lens sees this impulse as $\delta(x-Mx_n-a)$ and collimates it to a plane wave propagating at an angle

$$\theta_n = a \tan \left(\frac{Mx_n + a}{f} \right) \quad (4-49)$$

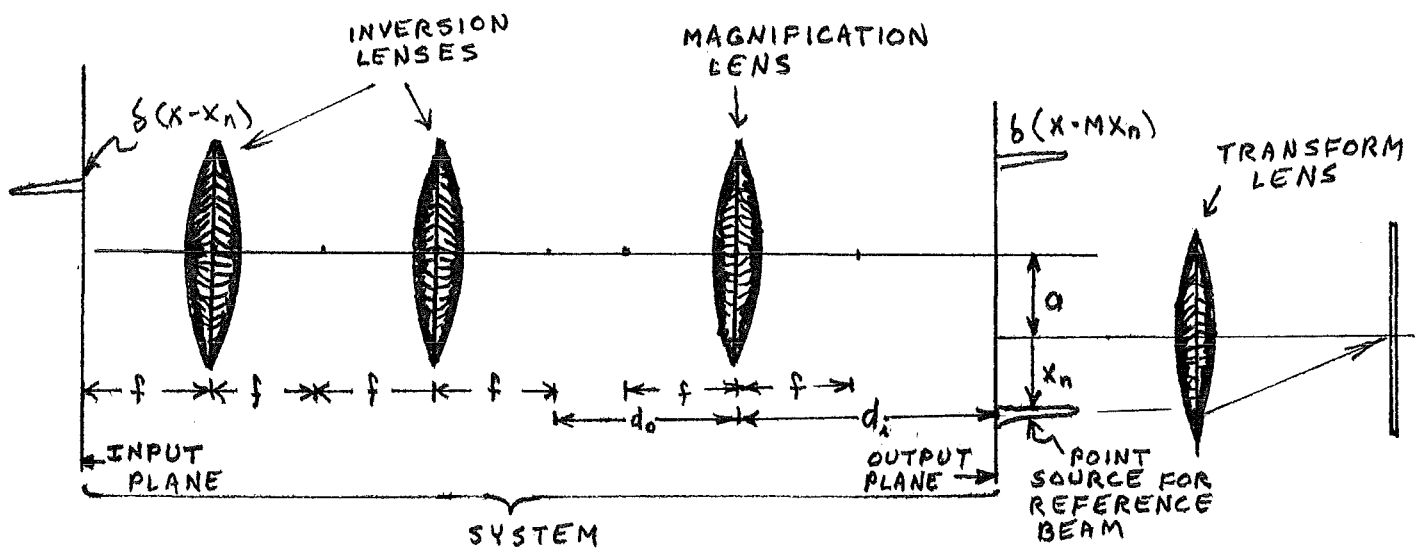


Fig. 38 : Extinction angle recording geometry for the non-inverting magnifier after the more general Fig, 36.

The corresponding propagation of the reference beam is given by (4-40) as

$$\phi_n = a \tan(-x_n/f) \quad (4-50)$$

As can be seen, the piecewise isoplanatic approximation of the simple magnifier results from beating plane waves. Consider then Figs. 39a and b in which two beating waves are recorded on a single thick emulsion. In the first exposure the parameters are

$$\begin{aligned} \theta_0 &= 30^\circ \\ X_0 &= 0 \\ \phi_0 &= 0 \end{aligned}$$

From Fig. 20, a rough interpolation of the corresponding extinction angle is $\Delta\theta_0 \approx 5^\circ$.

Also, we have from (4-49),

$$\tan \theta_0 = a/f$$

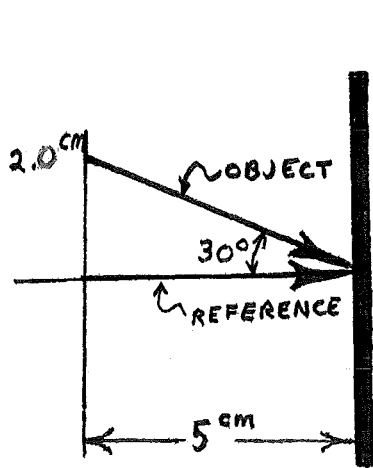
Let

$$a = 1.15 \text{ cm}$$

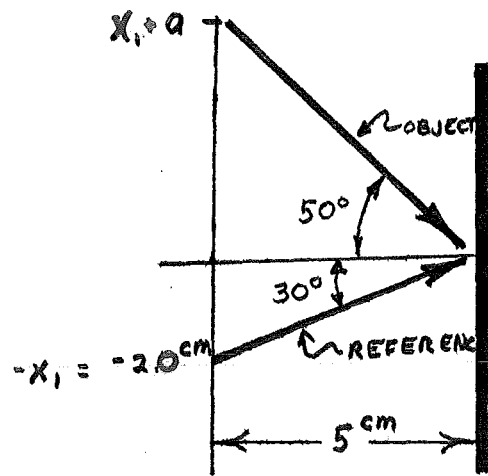
From the second exposure

$$\begin{aligned} X_1 &= 2.0 \text{ cm} \\ \theta_1 &= 50^\circ \\ \phi_1 &= 30^\circ \\ \Delta\theta_1 &\leq 2.5^\circ \\ M &\approx 1 \end{aligned}$$

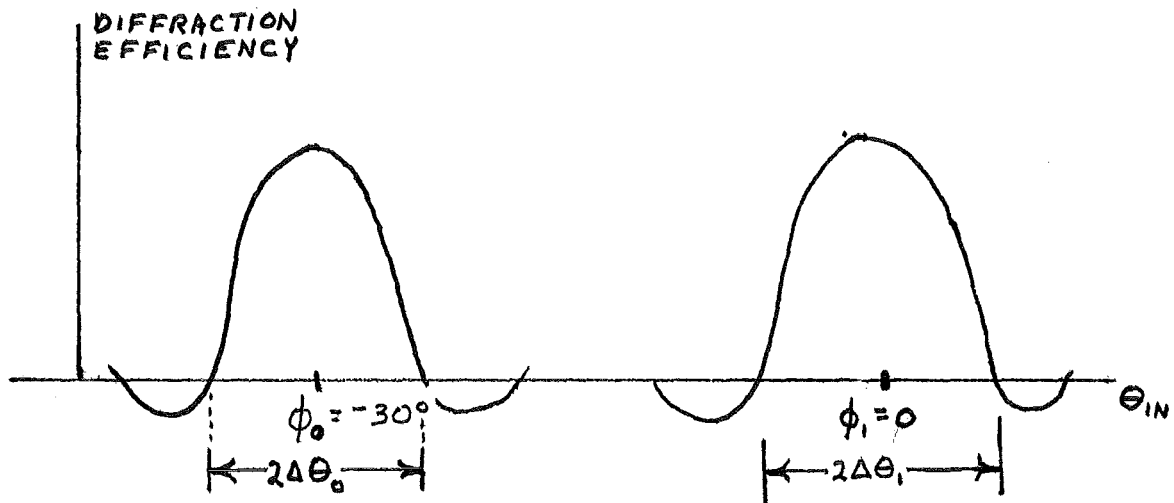
A rough sketch of the resulting diffraction efficiency (angular bandpasses) is offered in Fig. 39c. The optimal case for recording the adjacent transfer function would have the major lobes of these transfer functions meet at a common point.



a) First exposure.



b) Second exposure.



c) Resulting diffraction efficiency.

Fig. 39 : Recording two transfer functions of the non-inverting magnifier and the resulting diffraction efficiency.

(The recording geometry in (a) and (b) results directly from the transform lens in Fig. 38 for a point source placed in the magnifier's input plane.)

The recording method used, though not optimal, succeeds in illustrating the cross-talk elimination criteria of the piece-wise isoplanatic approximation via diffraction efficiency.

Consider now reconstruction. Two point sources are placed on the front focal plane of a 5 cm focal length lens at X_0 and X_1 . These give rise to plane waves propagating at angles ϕ_0 and ϕ_1 , respectively. These beams line up exactly with the corresponding angular bandpasses in Fig. 39c and are thus diffracted at angles θ_0 and θ_1 . This idea is verified by the reflection analogy.

The diffracted beams are now re-imaged by a 10 cm lens, and appear as point sources separated by 2.3 cm on the output. The reconstruction geometry is offered in Fig. 40a and a photograph of the output is in Fig. 40b.

Similar results from a variation of this scheme have been reported by Burton, Hagler and Krile⁽²⁵⁾.

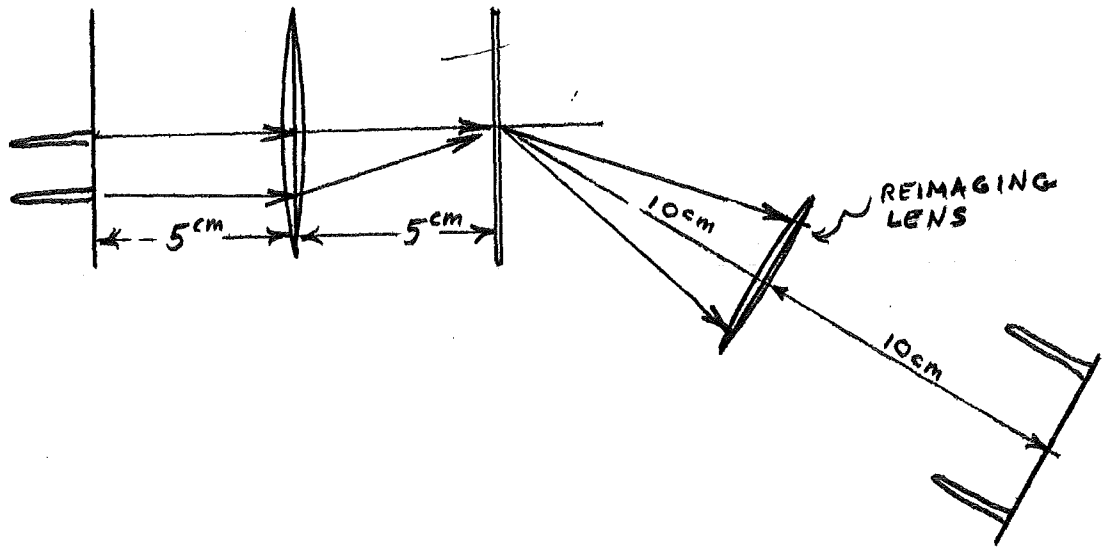
5) Macroscopically thick hologram system recording

Film having an emulsion thickness far greater than the illuminating light's wavelength will here be denoted as macroscopically thick. That is

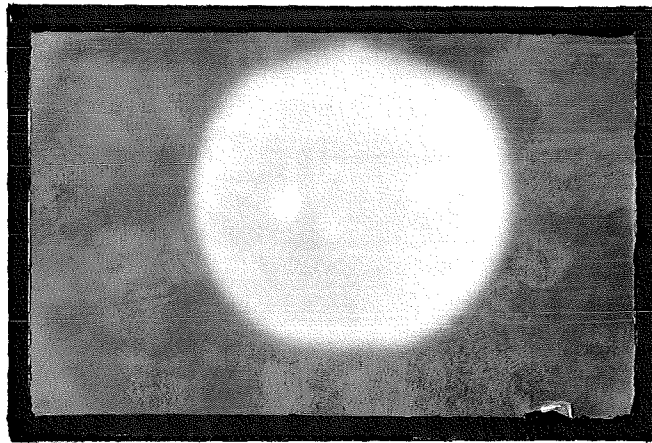
$$t \gg \lambda \quad (4-51)$$

We here attempt to theorize how such film might be employed in system recording.

For a macroscopically thick hologram, the extinction angle [(2-107)] is essentially zero. This rules out the pre-

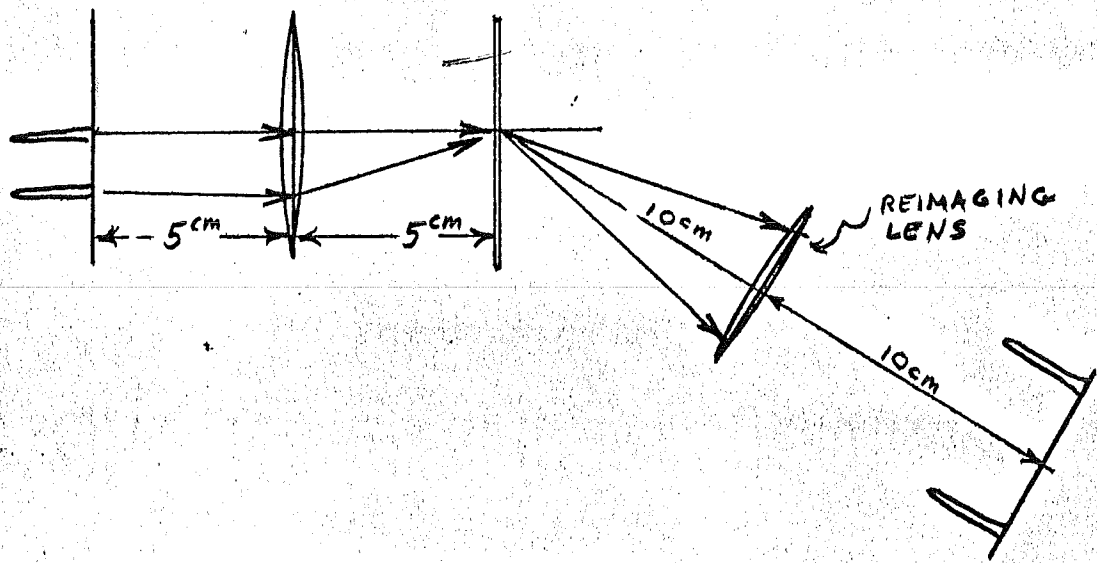


a) Reconstruction geometry.

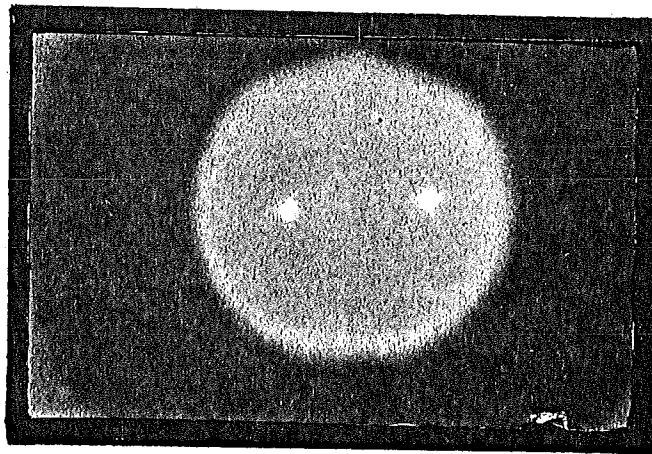


b) Resulting "magnified" point sources.

Fig. 40 : Reconstruction of the volume hologram made in Fig. 38 of two non-inverting magnifier transfer functions and the resulting image.

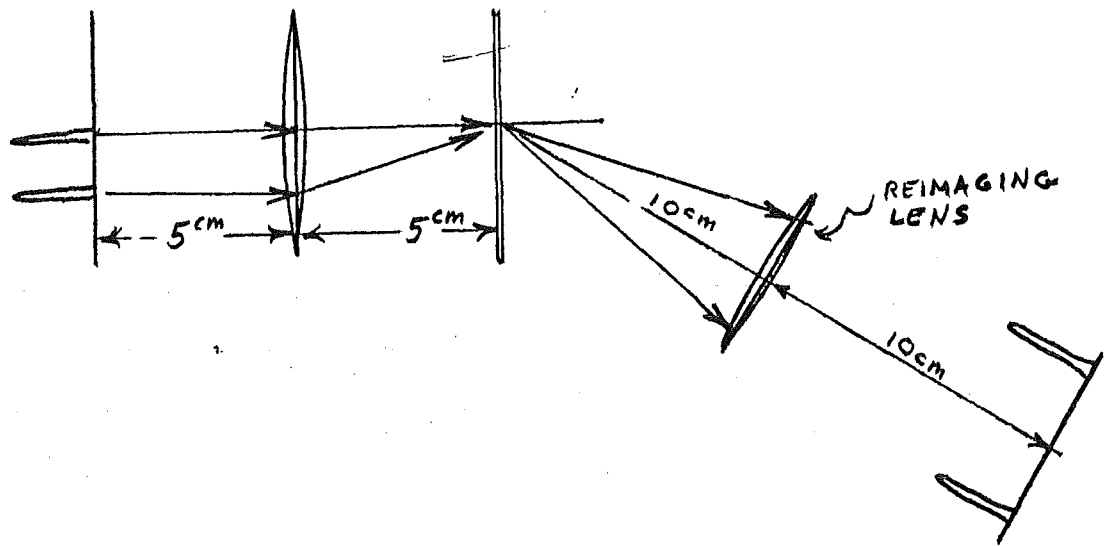


a) Reconstruction geometry.

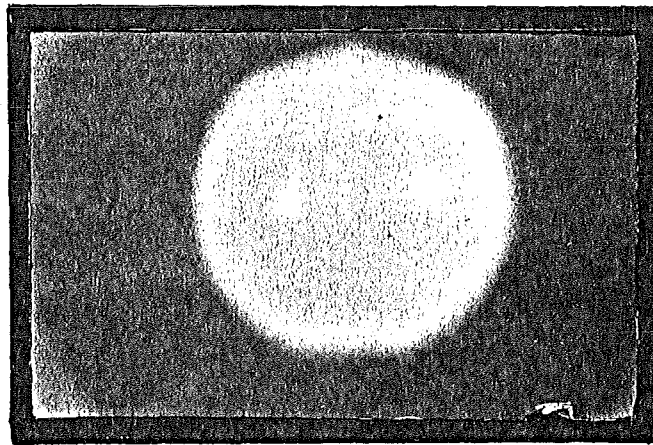


b) Resulting "magnified" point sources.

Fig. 40 : Reconstruction of the volume hologram made in Fig. 38 of two non-inverting magnifier transfer functions and the resulting image.



a) Reconstruction geometry.



b) Resulting "magnified" point sources.

Fig. 40 : Reconstruction of the volume hologram made in Fig. 38 of two non-inverting magnifier transfer functions and the resulting image.

viously presented recording scheme, since an extremely high isoplanatic patch density would result. The scheme's principles, however, remain valid. We hopefully need only to make appropriate revisions.

A necessary condition of reconstruction is alignment of angular bandpasses and corresponding patch transforms. As pictured in Fig. 41a this may be accomplished by using the transformed patch region as a reference beam. From the geometry, the back focal plane of the transform lens sees

$$U(f_x) = H_n(f_x) e^{-j2\pi f_x (x_n - a)} + 2\Delta x_n \text{sinc}(2\Delta x_n f_x) e^{-j2\pi f_x x_n} \quad (4-52)$$

The intensity term of interest resulting from expansion of this expression is

$$I_3(f_x) = 2\Delta x_n H_n(f_x) \text{sinc}(2\Delta x_n f_x) e^{-j2\pi f_x a} \quad (4-53)$$

Again, the form is not as important as the fact that the angular bandpass is aligned with the angular interval of the transformed isoplanatic region on reconstruction. This occurs because the angular intervals of the transformed patch reference beam and the transformed isoplanatic region are equivalent. (Compare Figs. 41a and 41b).

On reconstruction, the nth processed patch appears immediately to the right of the hologram as

$$G_{\text{OUT}}(f_x) = 2\Delta x_n H_n(f_x) G_n(f_x) \times \text{sinc}(2\Delta x_n f_x) e^{-j2\pi f_x (x_n - a)} \quad (4-53)$$

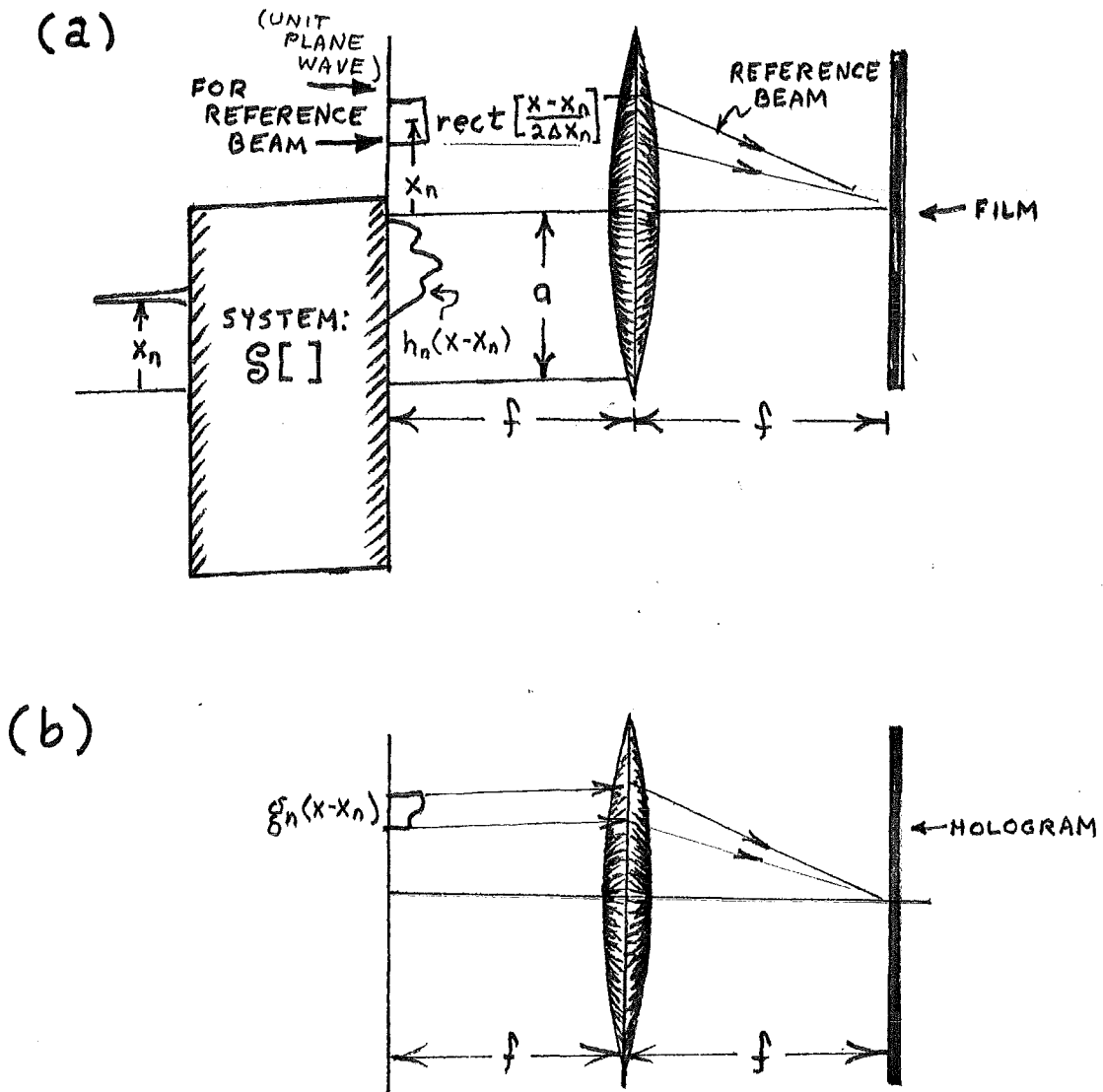


Fig. 41 : (a) Recording and (b) reconstruction with a macroscopically thick hologram. Note the equivalent angular interval of the transformed "rect" reference beam in (a) and the transformed isoplanatic region in (b). This assures alignment of the angular bandpass.

Inverse transforming gives

$$g_{OUT}(x) = h_n(x) * g_n(x-x_n) * \text{rect} \left[\frac{x}{2\Delta x_n} \right] \quad (4-54)$$

where the convolving shift term $\delta(x+a)$ has been dropped for clarity of analysis. Note that in the previous scheme, $\delta(x)$ appeared instead of $\text{rect} [x/2\Delta x_n]$ in the above output, and we had generated the nth term of the piecewise isoplanatic approximation. The substitution of the above expression into the convolution integral yields a means by which the consequences of this convolving rect affects the output. Specifically

$$g_{OUT}(x) = \int_{x_n - \Delta x_n}^{x_n + \Delta x_n} g(\eta) h_n(\eta - \xi) d\eta d\xi \quad (4-55)$$

As will be seen via an example, outputs tend to be "smoothed". This seemingly results from the sinc function in (4-53) acting as a low pass filter.

In the three examples to follow, a single isoplanatic patch input will be used

$$g_n(x) = \text{rect} \left[\frac{x}{2\Delta x_n} \right] \quad (4-56)$$

This reduces (4-54) to

$$g_{OUT}(x) = h_n(x) * \Lambda \left[\frac{x-x_n}{2\Delta x_n} \right] \quad (4-57)$$

where the triangle function $\Lambda(x)$ is defined as

$$\Lambda(x) = \begin{cases} 1 - |x| & ; |x| \leq 1 \\ 0 & ; \text{OTHERWISE} \end{cases} \quad (4-58)$$

Consider first the magnifier. Substituting its line spread function [(3-90)] into (4-57) gives

$$g_{out}(x) = \Lambda \left(\frac{x - Mx_n}{2\Delta x_n} \right) \quad (4-59)$$

The piecewise isoplanatic approximation, on the other hand, yields (Fig. 42a):

$$\tilde{g}_n(x) = \text{rect} \left[\frac{x - Mx_n}{2\Delta x_n} \right] \quad (4-60)$$

The integrator line spread function [(3-120)] substituted into (4-57) gives a piecewise quadratic output instead of the desired ramp. (Fig. 42b)

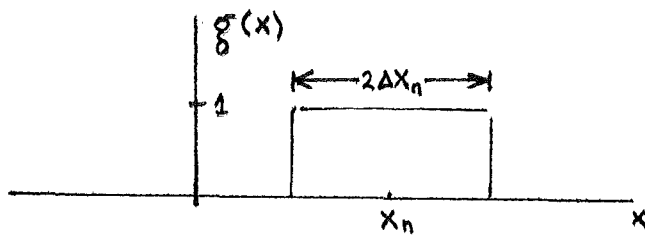
Lastly, the line spread function of the differentiator, [(3-122)], when substituted into (4-57), gives two rect functions instead of the two desired impulses (Fig. 42c).

The generalized output resulting from bandpass alignment in a macroscopically thick hologram is purely speculative and is subject to experimental verification. It was here presented as a possible foundation for future work.

c) Generalizations of system recording criteria

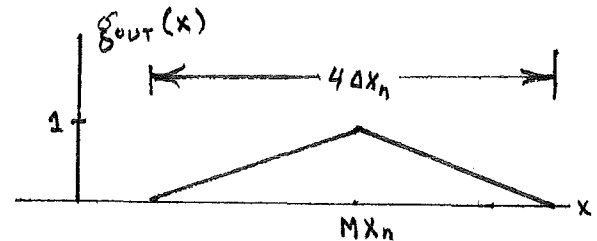
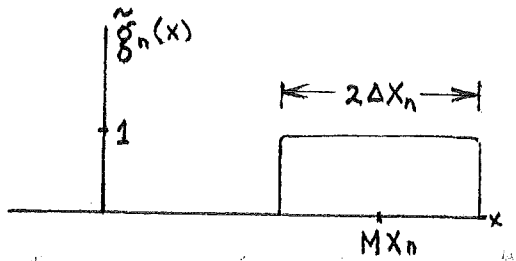
We venture here to illustrate how the piecewise isoplanatic statement of a space variant system might be holographically implemented by methods other than employment of the extinction angle. First, a detailed understanding of the diffraction efficiency method is needed.

Consider Fig. 43 in which the extinction angle recording reconstruction operation is presented in block form. The input is transformed and is separated by the angular bandpasses to

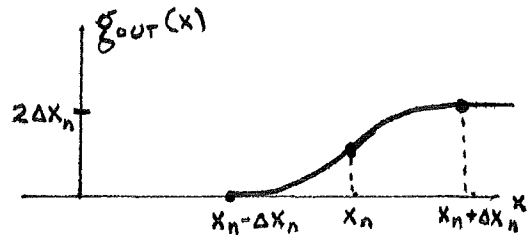
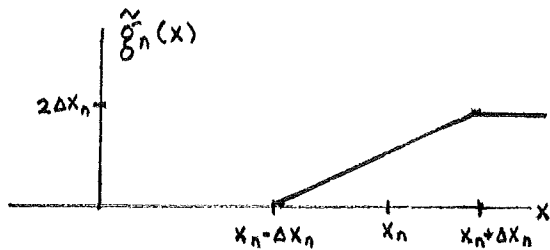


Isoplanatic Patch Input

a) Magnifier



b) Integrator



c) Differentiator

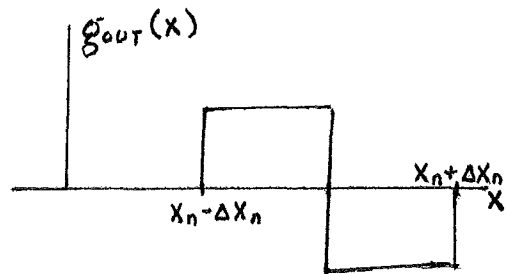
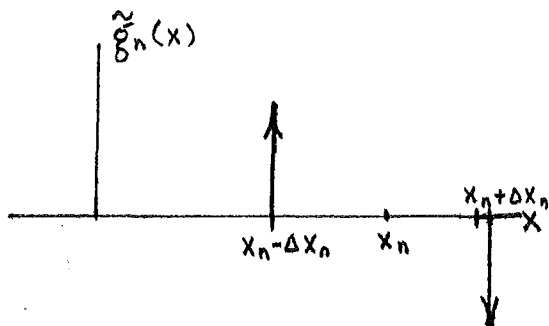


Fig. 42 : Comparison of outputs of left; piecewise isoplanatic approximation and right; theoretical output of a macroscopically thick system recording.

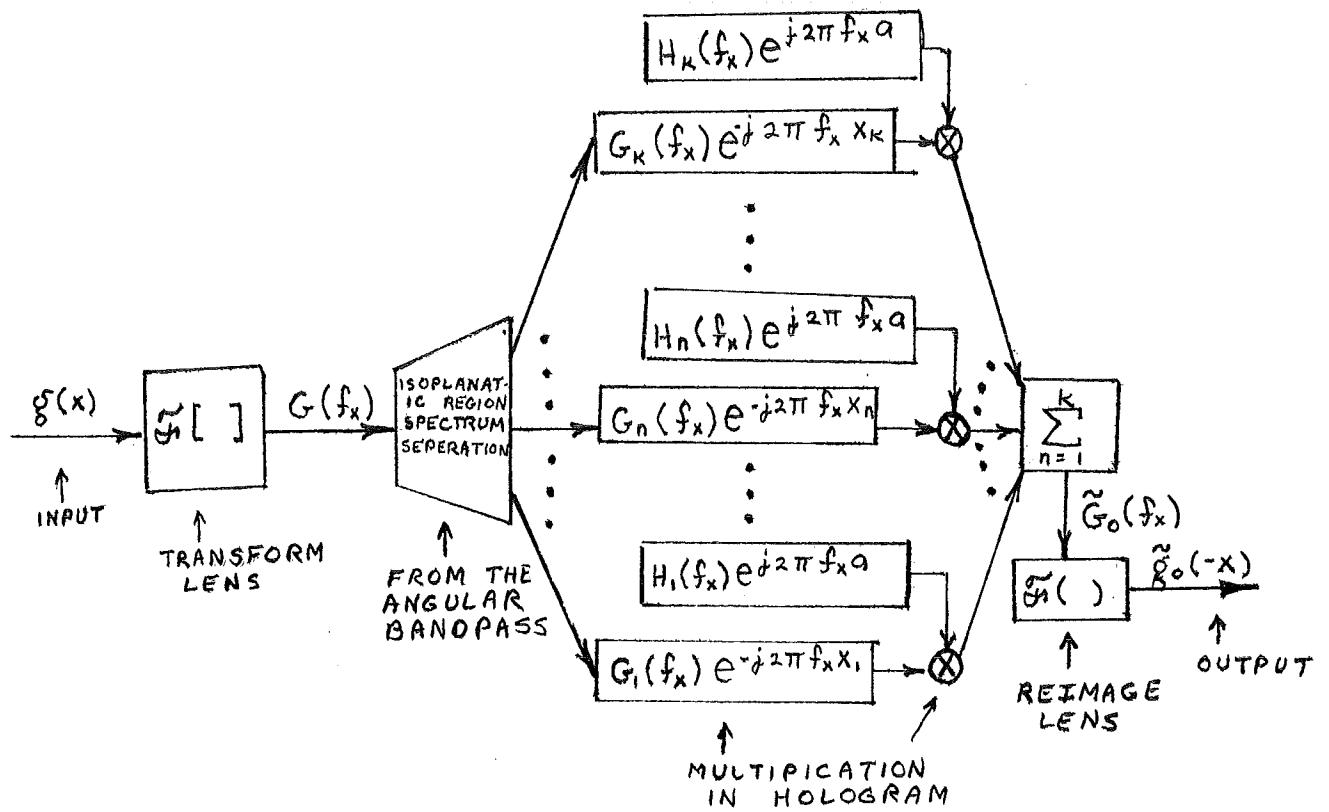


Fig. 43 : Block diagram of the extinction angle recording method fullfilling the piecewise isoplanatic approximation.

multiply corresponding transfer functions. The result is summed and Fourier transformed to give an inverted version of the piecewise isoplanatic approximation on the output.

In original piecewise isoplanatic approximation considerations, the input plane was divided into isoplanatic patches of non-overlapping unit height rectangular pulses. These patches may be thought of as constituting a block orthogonal basis set.

That is

$$\phi_n(x) \phi_m(x) = \begin{cases} 0 & ; m \neq n \\ 2\Delta x_n & ; m = n \end{cases} \quad (4-61)$$

where $\phi_i(x)$; $i = n, m$ refers to the region covered by the *i*th isoplanatic patch.

$$\phi_n(x) = \text{rect} \left[\frac{x - x_n}{2\Delta x_n} \right] \quad (4-62)$$

The input function was then expressed in terms of the rect functions [(3-71)]. Each resulting block orthogonal function was convolved with its corresponding line spread function and then all resulting functions were added together to yield the piecewise isoplanatic approximation to the recorded system's output.

A re-examination of Fig. 43 will show that this is not the case in the extinction angle implementation. The operation of separating the isoplanatic regions is done in the Fourier plane. This is valid due to the mapping of the block orthogonal input regions into block orthogonal angular intervals upon Fourier transformation. This process is illustrated in Fig. 44 and was essentially discussed previously under angular intervals. Each patch transform is selectively multiplied by the corresponding

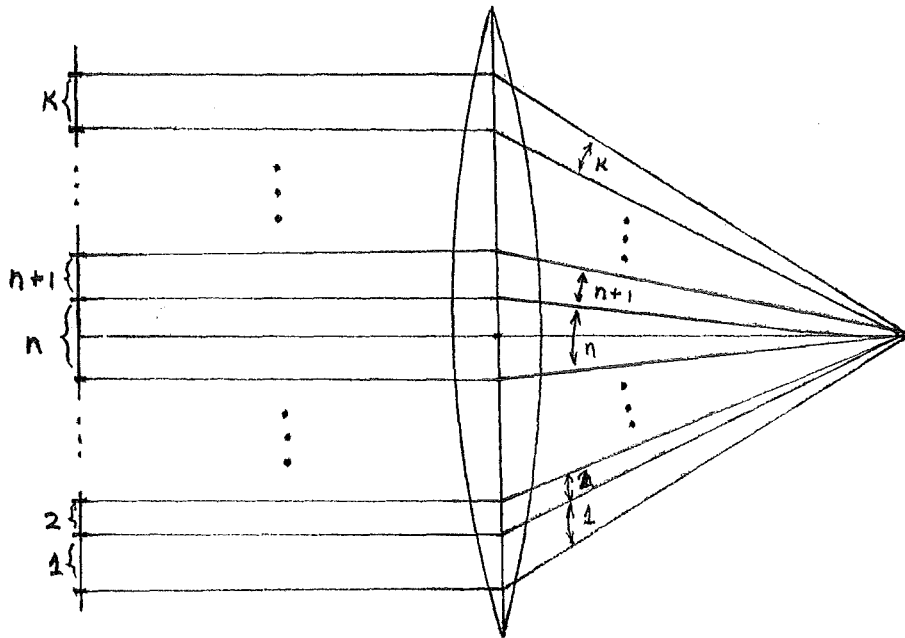


Fig. 44 : Mapping of block orthogonal isoplanatic regions to block orthogonal intervals.

transform function in the aligned angular bandpass. All processed patches are then summed and re-imaged.

The most probable alternative to the angular bandpass is individual processing of each isoplanatic patch. A general block diagram of such a process is offered in Fig. 45. The input function is divided into isoplanatic regions, Fourier transformed in some manner, multiplied by a corresponding transfer function expression, summed, and inverse transformed. The inverse transformation may possibly be done in each channel before final summation, depending upon the model. One can visualize a complicated optical apparatus by which the patches might be separated to be individually processed.

1) Fly's eye lens system recording

A matrix of identical lenslets is appropriately called the fly's eye lens and has found use primarily in three dimensional image synthesis and optical computing.

Consider Fig. 46a in which a transmittance $g(x)$ is placed in the front focal plane of a fly's eye lens and assume the n th isoplanatic patch is aligned with the n th lenslet. The back focal plane essentially sees

$$\sum_n G_n(f_x - f_n) \quad (4-63)$$

The further assumption is made that each transfer function is "essentially band limited" to the interval

$$f_x \pm \frac{\Delta x_n}{\lambda f} \quad (4-64)$$

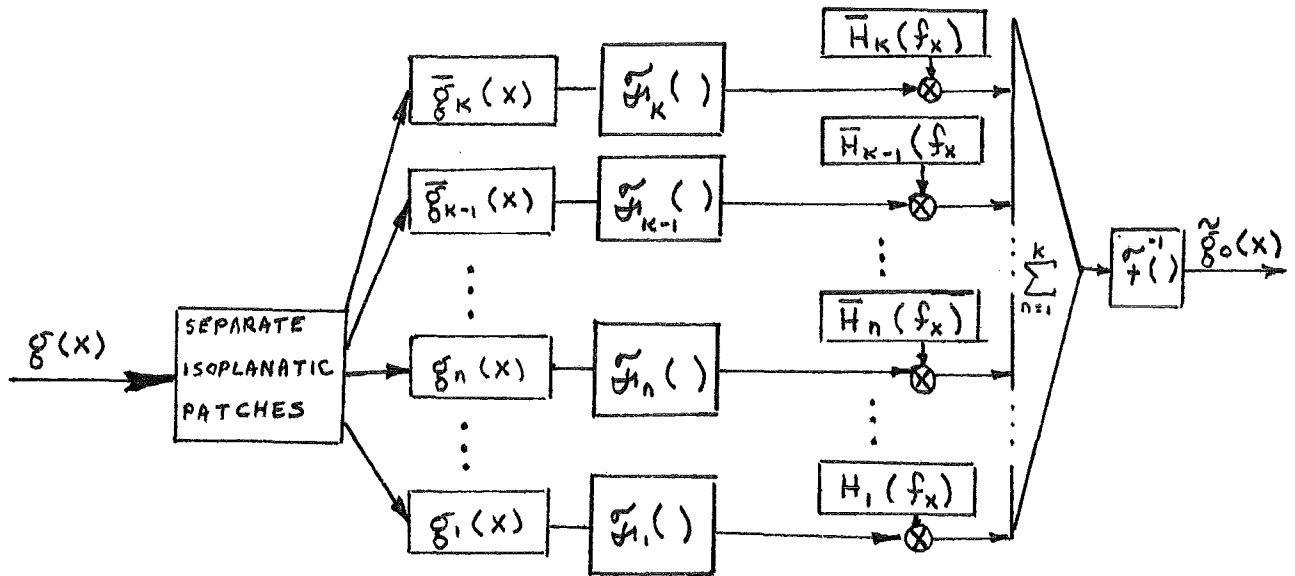
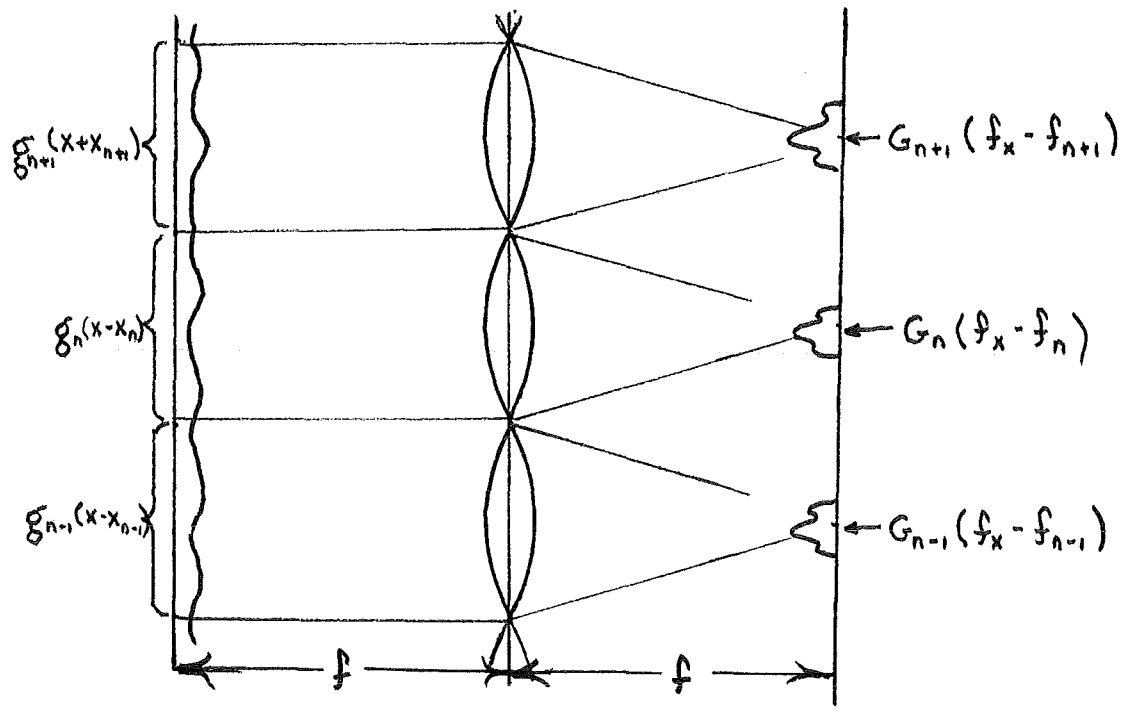
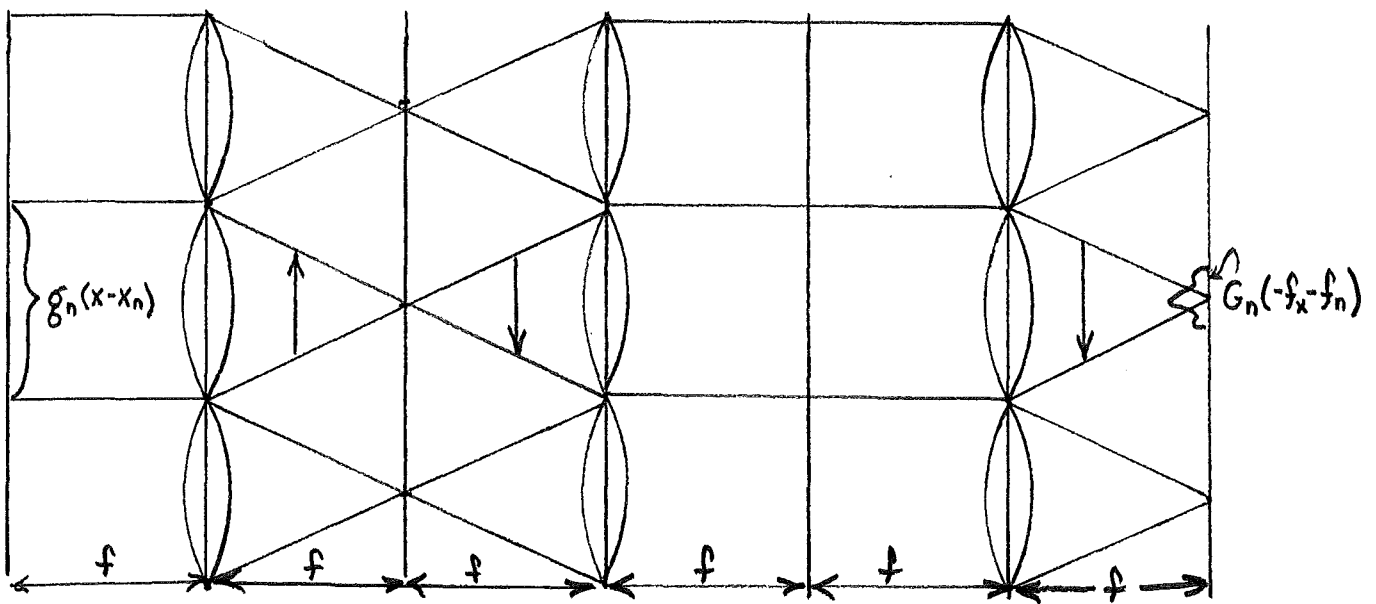


Fig. 45 : Alternate system synthesis scheme for implementing the piecewise isoplanatic approximation. All isoplanatic regions are Fourier Transformed in some manner and are multiplied by a corresponding transfer function. All processed patches are summed and transformed to give the system's approximated output.



a) Fly's eye lens employed as a Fourier Transformer.



b) Transforming with three fly's eye lenses to invert the resulting Fourier Transform of the input $g_n(x-x_n)$.

Fig. 46 : Fly's eye transformation.

A problem arises immediately. Each patch will be inverted on re-imaging. This might be overcome by the configuration in Fig. 46b where three identical fly' eye lenses are cascaded. The back focal plane now sees

$$\sum_n G_n(-f_x - f_n) \quad (4-65)$$

For any reconstruction scheme, one would expect the nth isoplanatic spectrum to multiply a transfer function expression containing $H_n(-f_x - f_n)$ giving something akin to

$$\sum_n H_n(-f_x - f_n) G_n(-f_x - f_n) \quad (4-66)$$

A problem now arises which is presently unsolved by the author for the general case. That problem is re-imaging.

Note first that re-imaging by a fly's eye lens for the general case would not be permissible, in that one is not assured of adequate separation of each processed patch. For example, consider the Fourier transformer's piecewise isoplanatic approximation [(3-111)]. Each patch essentially maps into a weighted plane wave which completely covers any pre-imaging fly's eye element.

This, then, suggests employment of a conventional lens for re-imaging. Note, however, that the Fourier transform of (4-66) gives

$$\begin{aligned} \sum_n [h_n(x) e^{j2\pi f_n x}] * [g_n(x) e^{j2\pi f_n x}] \\ = \sum_n [h_n(x) * g_n(x)] e^{j2\pi f_n x} \end{aligned} \quad (4-67)$$

To introduce the shift contained in the piecewise isoplanatic approximation [(3-77)] we need to convolve with $\delta(x-x_n)$ to give

$$\begin{aligned} & \sum_n [h_n(x) * g_n(x)] e^{j2\pi f_n x} * \delta(x-x_n) \\ & = \sum_n [h_n(x) * g_n(x-x_n)] e^{j2\pi f_n x} e^{-j2\pi f_n x_n} \quad (4-68) \end{aligned}$$

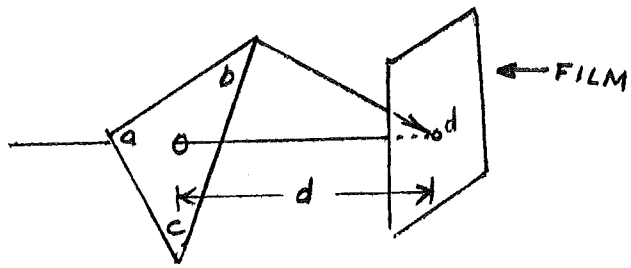
The re-imaging problem lies in elimination of the phase terms. This might be accomplished by an optical configuration which would have the re-imaging lens see all the waveforms shifted to the origin in its front focal plane. Note, interestingly, the unwanted phase term is equivalent to the conjugate line spread function of the Fourier transformer [(3-58)].

2) Fly's eye implementation of the magnifier

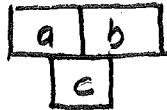
Although no descriptive theory has been derived by the author for general system recording the fly's eye lens, success in producing the piecewise isoplanatic approximation for the simple magnifier was accomplished employing fly's eye techniques. The system recording, as pictured in Fig. 47a, arises directly from the reflection analogy.

With reference to Fig. 47a an equilateral triangle was placed at a distance d from a photographic plate. Three separate exposures were taken of a beam aligned with each of the vertices and the hologram's midpoint (point d). The planar reference beam was the same in each case.

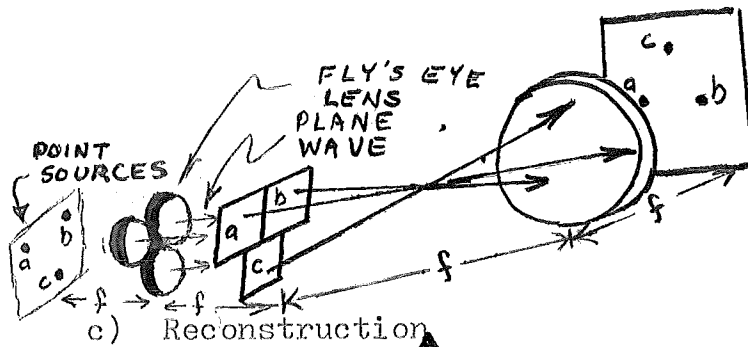
Once developed, the three holograms were cut and arranged as in Fig. 47b. The reconstruction geometry in Fig. 47c consists of plane wave illumination of each hologram with a normal plane wave, which is the equivalent of placing point sources in



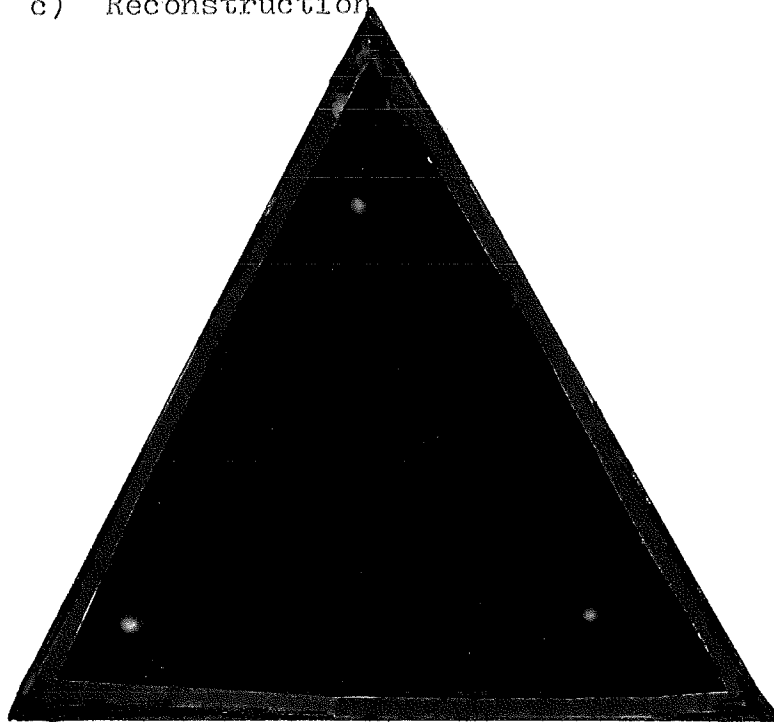
a) Recording geometry



b) Hologram Placement

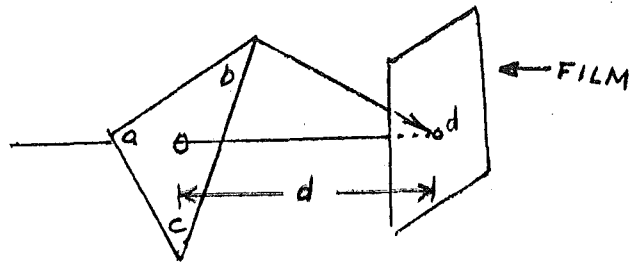


c) Reconstruction

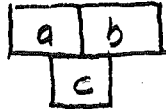


d) Photograph of output of "magnified" points

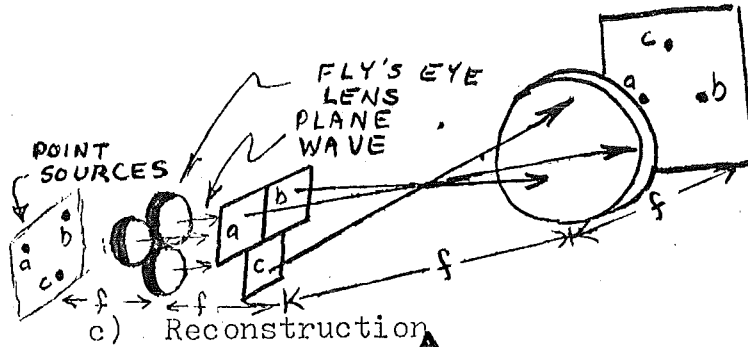
Fig. 47 : Magnifier system recording:fly's eye techniques.



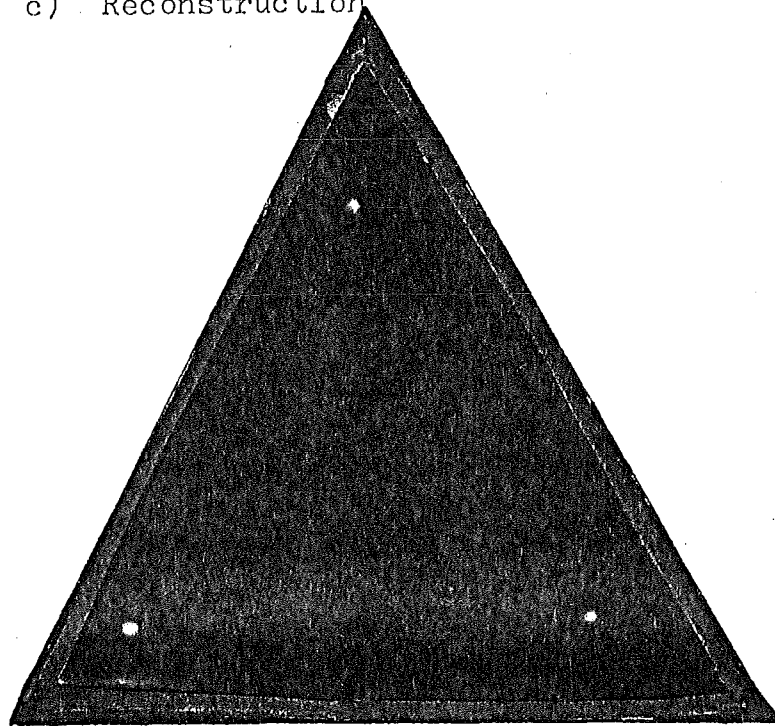
a) Recording geometry



b) Hologram Placement



c) Reconstruction



d) Photograph of output of "magnified" points

Fig. 47 : Magnifier system recording: fly's eye techniques.

the front focal plane aligned with each of the Fourier transforming fly's eye lenslets. The resulting diffracted waveforms were re-imaged by a single lens and photographed resulting in Fig. 47c.

Note that, in this particular scheme, no inversion problems were encountered due to the intersection of the three diffracted beams, as shown in 47b.

V. Conclusions

To this author's mind, employment of the extinction angle of the "microscopically" thick hologram for system recording leaves much to be desired due to the following reasons:

- 1) The sinc function's poor mimic of the ideal rectangular angular bandpass.
- 2) The undesired diffraction from this sinc functions minor lobes. This constitutes unwanted cross-talk.
- 3) The complete dictation of the emulsion thickness on the isoplanatic patch calibration on the input plane.
- 4) The limitations which must be made on the angular intervals of recorded transfer functions. (e.g. the Fourier transformer).
- 5) Distortion arising from reconstruction of a hologram when recorded with steep rays. (See appendix).

All but the last of these reasons have no proposed method of reconciliation. All but the last, however, may be avoided by employment of a macroscopically thick hologram, but a new problem arises from the low pass filter generated. As pre-

viously stated, this latter solution is in need of further experimental investigation.

On the more successful side, the proposition of recording a linear system has been thoroughly investigated. The formulated piecewise isoplanatic approximation may be employed to determine the consequences of division of a space variant system into a number of isoplanatic systems. Foundations for system recording schemes employing diffraction efficiency have been made. Sufficient and necessary criteria for piecewise isoplanatic system recording by any other method is also offered.

Future theoretical work might include a closer inspection of the relationship between a linear optical system's degree of space variance and asymptotic convergence of the piecewise isoplanatic approximation. Once formulated, the relationship might be applied to determine the optimal isoplanatic patch calibration for a given system.

Linear system notions herein are obviously not restricted to optics. They may be applied to any linear system with appropriate changes in terminology. Also, applications to invariant synthesis of variant systems are obvious.

V. Appendix

A) Distortion

A most worrisome encounter in attempts at implementation of system recording was distortion of diffracted waveforms. An investigation of the film's contribution to this distortion has been presented by McCauley, Simpson and Murbach⁽²⁶⁾ after the ray tracing predictions of Latta⁽²⁷⁾.

The distortion from a binary grating formed from plane waves propagating at 70° and $\pm 15^\circ$ were recorded. The diffracted waveforms are pictured in the figures below as a function of reconstruction angle. These images diffracted at nearly a right angle from the hologram normal and fell in the same x-z plane as that defined by the recording beams. Note the elongation of the circular input to the left of the 70° "bias" and the constriction to the right.

A rather amusing, yet effective proposal to eliminate this type of distortion is application of an inversely distorted input. For example, an elongated ellipsoid output would obtain the desired circular nature if one chose an appropriately constricted ellipsoid for an input.

The distortions from the sinusoidal grating seemingly become more pronounced as steeper recording plane waves are employed.

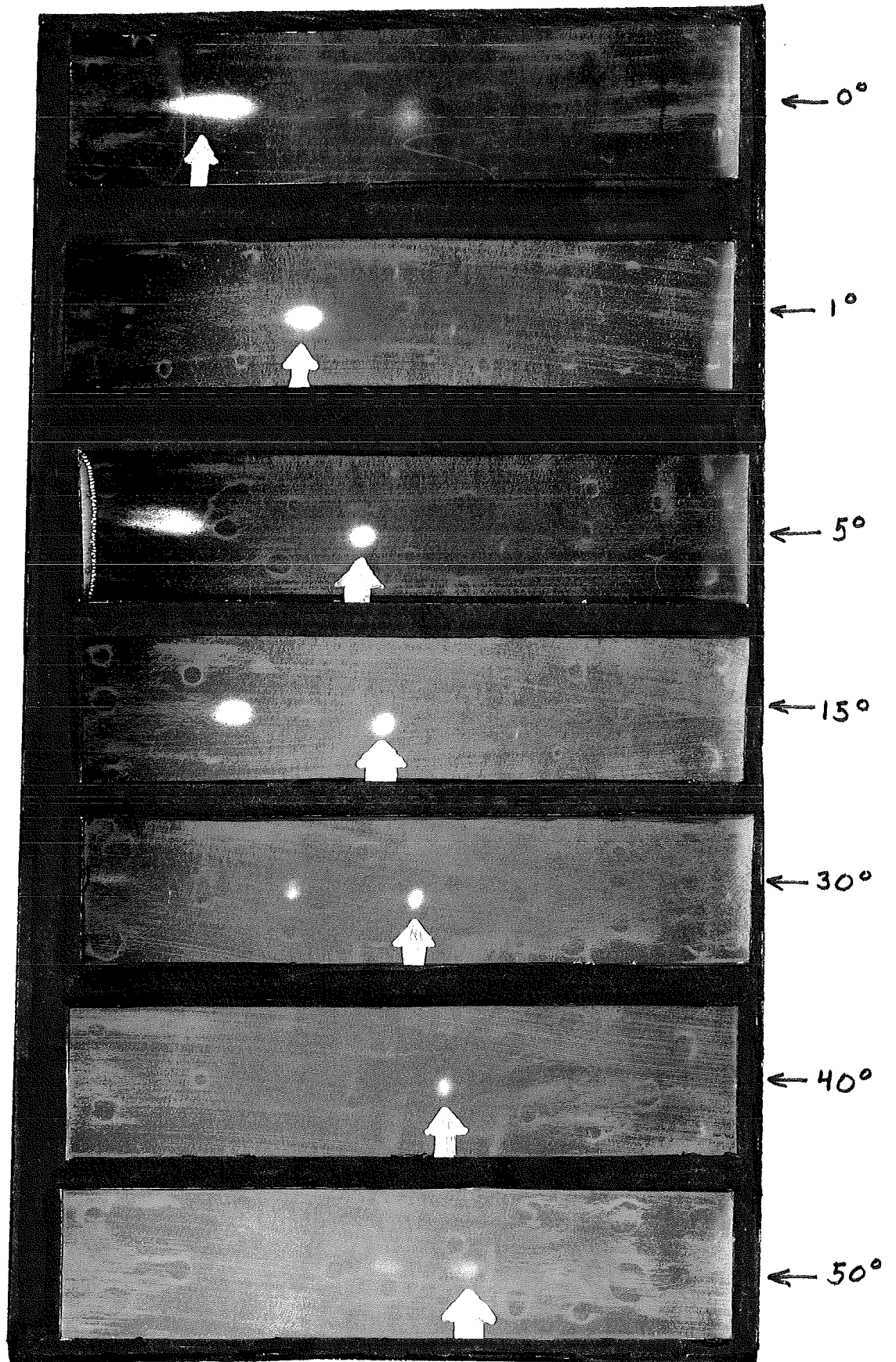


Fig. 48 : Distortion from diffracted waveforms from a binary grating as a function of reconstruction angle.

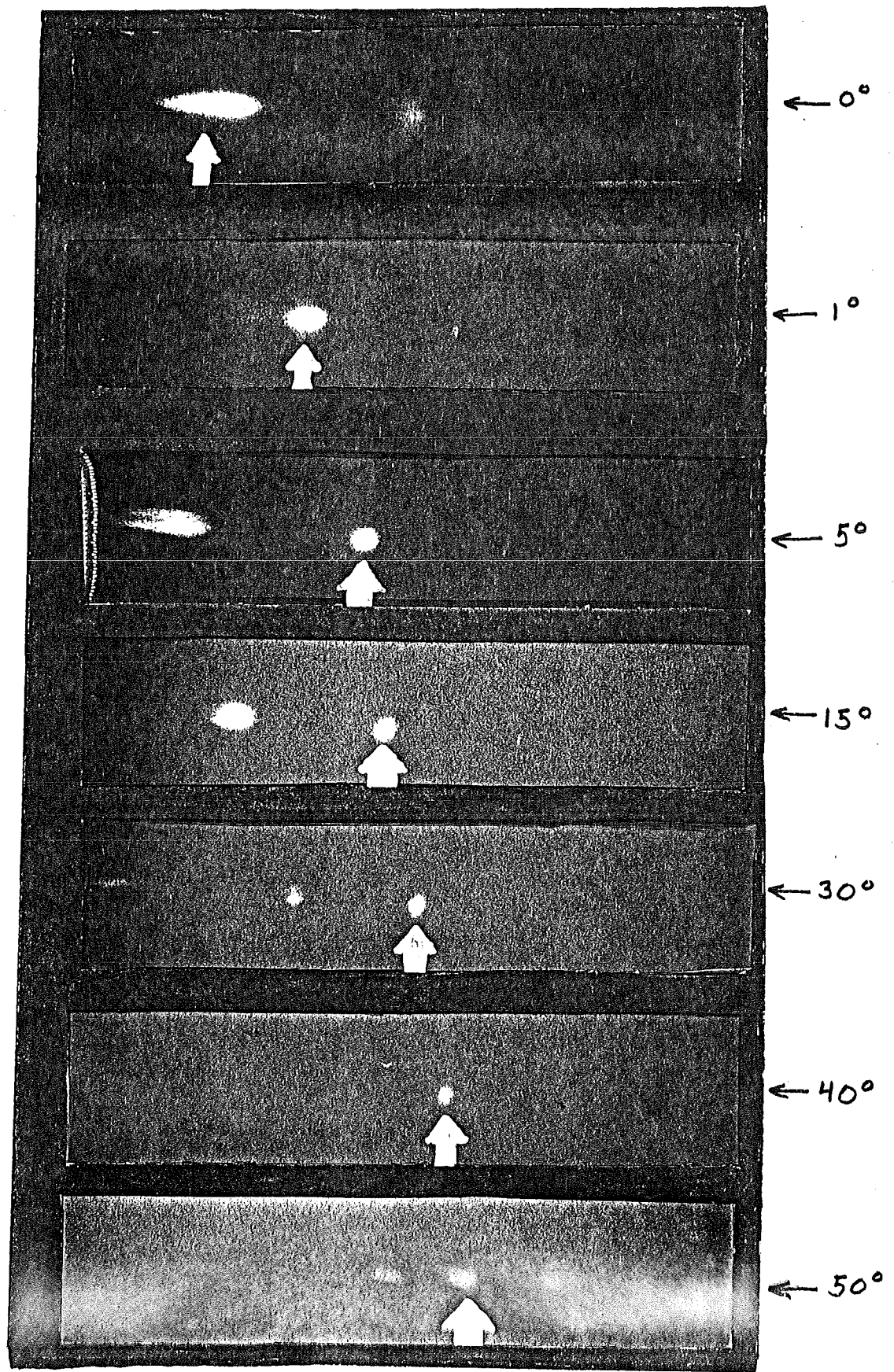


Fig. 48 : Distortion from diffracted waveforms from a binary grating as a function of reconstruction angle.

B) Fortran generation of extinction angle data

Offered here is the computer program by which the extinction angle curves of Fig. 20 from (2-107) were generated. Care has been taken to allow data to be generated from any set of system parameters (λ_a , t , n) and over any angular interval desired. The comments are hoped to suffice for explanation of the program's workings. (λ_a is read in angstroms, and t in micrometers.)

C) Fortran generation of the piecewise isoplanatic approximation to the Fourier transform of a pulse

This program was used to generate data for Fig. 23 from (3-108).

D) Photographic development of holograms

All holograms made in this report were exposed on Kodak 649F emulsion employing a helium neon laser ($\lambda_a = 6328\text{\AA}$).

Film developing was done as follows:

- 1) 6 minutes in Kodak D-19 developer.
- 2) $\frac{1}{2}$ minute in Kodak indicator stop bath.
- 3) 2 minutes in Kodak fixer.
- 4) 10 minute rinse in tap water.

When necessary, the hologram was bleached to decrease attenuation of the diffracted wave.

B) EXTINCTION ANGLE

PROGRAM XTNK(INPUT,OUTPUT,TAPE2=INPUT,TAPE5=OUTPUT)

REAL N,LAMA,LR,MR,LO,MO

C...EXTINCTION ANGLE CURVES FROM EXTERNAL PARAMATERS

C...INPUT

C SYSTEM PARAMATERS..N=REFRACTIVE INDEX..T=EMULSION THICKNESS

C IN MICROMETERS..LAMA=LASER WAVELENGTH IN AIR

READ(2,10)N,T,LAMA

C RECORDING AND ITERATION PARAMATERS (REF AND OBJ BEAMS)

C ALL ANGLES IN DEGREES

READ(2,11)THTAR,DELNR,NR

READ(2,11)THTAO,DELO,NO

C...DATA ECHOE

WRITE(5,12)N,T,LAMA

WRITE(5,13)NR,DELNR,THTAR,NO,DELO,THTAO

C...USEFUL CONSTANTS

PI=4.*ATAN(1.)

RTD=180./PI

DTR=PI/180.

FF=LAMA*0.0001/T

THTAI=THTAO

C...REFERENCE ANGLE LOOP

DO 9 NNR=1,NR

WRITE(5,14)NNR,THTAR

MR=SIN(THTAR*DTR)

LR=SQRT(N*N-MR*MR)

C...OBJECT ANGLE LOOP

DO 8 NNO=1,NO

MO=SIN(THTAO*DTR)

LO=SQRT(N*N-MO*MO)

IF(LU*MR-MO*LR)2,4,2

4 WRITE(5,17)

GO TO 3

2 EXT=(FF*LO/(LO*MR-MO*LR))*RTD

5 IF (EXT-360.)7,6,6

6 EXT=EXT-360.

GO TO 5

7 WRITE(5,15)THTAO,EXT

3 THTAO=THTAO+DELO

8 CONTINUE

THTAO=THTAI

THTAR=THTAR+DELNR

9 CONTINUE

STOP

10 FORMAT(3F10.5)

11 FORMAT(2F10.4,I3)

12 FORMAT('SYSTEM PARAMETERS',/, ' REFRACTIVE INDEX=',F10.4,/, ' EMU
ILSION THICKNESS=',F10.6, ' MICROMETERS',/, ' WAVELENGTH=',F10.4,
2 ' ANGSTROMS')

13 FORMAT(/,2X,I5, ' REFERENCE ANGLE ITERATIONS OF ',F10.6, ' DEGREES F
3ROM ',F10.6, ' DEGREES',/,2X,I5, ' OBJECT ANGLE ITERATIONS OF ',
4F10.6, ' DEGREES FROM ',F10.6, ' DEGREES',/)

14 FORMAT(///, ' CURVE ',I5, ' THTAR=',F10.6, ' DEGREES',/,7X, ' THTAO',
511X, ' XTNK')

15 FORMAT(2(5X,F10.6))

17 FORMAT(' *****0.0*****INFINITE*****')

END

LENGTH INCLUDING I/O BUFFERS

SAMPLE OUTPUT:

SYSTEM PARAMETERS

REFRACTIVE INDEX= 1.5000

EMULSION THICKNESS= 15.000000 MICROMETERS

WAVELENGTH= 6328.0000 ANGSTROMS

0 REFERENCE ANGLE ITERATIONS OF 10.000000 DEGREES FROM 40.000000 DEGR
 21 OBJECT ANGLE ITERATIONS OF 2.000000 DEGREES FROM -20.000000 DEGR

CURVE 1 THTAR= 40.000000 DEGREES

THTAO	XTNK
-20.000000	2.517376
-18.000000	2.604333
-16.000000	2.697229
-14.000000	2.796714
-12.000000	2.903539
-10.000000	3.018583
-8.000000	3.142872
-6.000000	3.277615
-4.000000	3.424248
-2.000000	3.584479
0.000000	3.760368
2.000000	3.954409
4.000000	4.169657
6.000000	4.409891
8.000000	4.679841
10.000000	4.985503
12.000000	5.334598
14.000000	5.737225
16.000000	6.206863
18.000000	6.761904
20.000000	7.428107

CURVE 2 THTAR= 50.000000 DEGREES

THTAO	XTNK
-20.000000	2.263101
-18.000000	2.329642
-16.000000	2.400001
-14.000000	2.474531
-12.000000	2.553632
-10.000000	2.637764
-8.000000	2.727452
-6.000000	2.823297
-4.000000	2.925998
-2.000000	3.036360
0.000000	3.155323
2.000000	3.283989
4.000000	3.423653
6.000000	3.575851
8.000000	3.742419
10.000000	3.925563
12.000000	4.127960
14.000000	4.352891
16.000000	4.604413

ETC.

C) P.I.A. SYNTHESIS OF $2A \text{ sinc}(2AX/\lambda f)$

```

// JCB T      384  31131      ROBERT J. MARKS II
*LIMITS T60,F4
// FORTRAN MAINLINE PROGRAM
*LIST SOURCE PROGRAM
*IOCS(1403 PRINTER,CARD)
      REAL LAMF,N
      PI=4.*ATAN(1.)
C  GENERATION OF THE PIECEWISE ISOPLANATIC APPROXIMATED OUTPUT OF A
C  FOURIER TRANSFORMER WITH AN INPUT OF RECT(X/2A).  THE TRUE OUTPUT
C  IS  $2A*\text{SINC}(2AX/\text{LAMF})$ .
C  SYSTEM CONSTANTS
C    A  =HALF WIDTH OF PULSE INPUT
C    LAMF=WAVELENGTH-FOCAL LENGTH PRODUCT
      READ(2,10)A,LAMF
C  PROGRAM PARAMETERS
C    NK =NUMBER OF FITS DESIRED
C    NIT=NUMBER OF ITERATIONS
C    DX =ITERATION LENGTH
      READ(2,11)DX,NIT,NK
C  PARAMETER ECHOE
      WRITE(5,12)A,LAMF,NK,NIT,DX
C  NK' TH APPROXIMATION LCOP
      DC 9 NN=1,NK
C  THERE ARE 2K+1 ISOPLANATIC PATCHES
      READ(2,13)K
      WRITE(5,14)NN,K
C  DELX=HALF WIDTH OF EACH ISOPLANATIC PATCH
      DELX=A/(2.*FLOAT(K)+1.)
      X=0.
C  COMPUTATION OF GCUT AT X
      DC 9 NNN=1,NIT
      SUM=1.
C  SUMMATION OF THE K TERMS OF GCUT AT X
      DC 8 NNNN=1,K
      N=FLOAT(NNNN)
      TERM=2.*SIN(4.*PI*N*DELX*DELX/LAMF)*COS(4.*PI*N*DELX*X/LAMF)/
      1(4.*PI*N*DELX*DELX/LAMF)
      SUM=SUM+TERM
      8 CONTINUE
      GCUT=2.*DELX*SUM
      WRITE(5,15)X,GCUT
      X=X+DX
      9 CONTINUE
      STOP
      10 FCRMAT(2F10.4)
      11 FCRMAT(F10.4,I5,5X,I5)
      12 FCRMAT('INPUT ECHOE'/' HALF PULSE WIDTH=',F5.3,/2X'FOCAL LENGTH-
      1WAVELENGTH PRODUCT=',E10.4,/2X,I5,' OUTPUT DATA GROUPS'/2X,I5,
      2' ITERATIONS OF ',F10.5,/)
      13 FORMAT(I3)
      14 FCRMAT('/' DATA GROUP ',I5,',', K=',I5,/8X'X'14X'GOUT')
      15 FCRMAT(2(5X,F10.6))
      END

```

SAMPLE OUTPUT:

INPUT ECHOE
 HALF PULSE WIDTH=1.000
 FOCAL LENGTH-WAVELENGTH PRODUCT=0.1000E 01
 6 OUTPUT DATA GRUPS
 31 ITERATIONS CF 0.10000

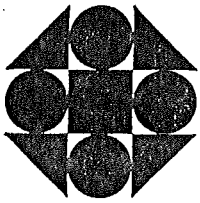
DATA GROUP	1, K=	1
X		GOUT
0.000000		1.607088
0.100000		1.525784
0.200000		1.295932
0.300000		0.957273
0.399999		0.568366
0.499999		0.196456
0.599999		-0.094149
0.699999		-0.253204
0.799999		-0.253205
0.899999		-0.094152
0.999999		0.196452
1.099999		0.568361
1.199999		0.957268
1.299999		1.295928
1.399999		1.525782
1.499999		1.607088
1.599998		1.525787
1.699998		1.295936
1.799998		0.957279
1.899998		0.568373
1.999998		0.196463
2.099998		-0.094145
2.199998		-0.253202
2.299998		-0.253206
2.399998		-0.094156
2.499998		0.196446
2.599998		0.568354
2.699997		0.957261
2.799997		1.295922
2.899997		1.525779
2.999997		1.607088

DATA GROUP	2, K=	2
X		GOUT
0.000000		1.838628
0.100000		1.731431
0.200000		1.431913
0.300000		1.001114
0.399999		0.524759
0.499999		0.093360
0.599999		-0.218451
0.699999		-0.368383
0.799999		-0.354741
0.899999		-0.214636
0.999999		-0.012675

ETC.

VI. References

1. Joseph W. Goodman, Introduction to Fourier Optics, McGraw-Hill, New York, 1968, pp. 77-80.
2. Robt. J. Collier, Christoph B. Burckhardt, and Lawrence H. Lin, Optical Holography, Academic Press, London, 1971, pp. 4-6.
3. Robt. Plonsey, and Robert E. Collin, Principles and Applications of Electromagnetic Fields, McGraw-Hill, New York, 1961, pp. 303-304.
4. Ibid. (2), p. 97
5. Samuel Silver, Microwave Antenna Theory and Design, Boston Technical Publishers Inc., 1964, pp. 110-111.
6. J. R. Meyer-Ardent, Introduction to Classical and Modern Optics, Prentice-Hall Inc., New Jersey, 1968, p. 56.
7. Ibid. (1), pp. 30-33.
8. Ibid. (1), pp. 275-276.
9. Ibid. (1), pp. 83-88.
10. Ibid. (2), pp. 97-101.
11. Ibid. (1), pp. 57-62.
12. Ibid. (1), pp. 198-205.
13. Ibid. (2), p. 461.
14. P. J. Van Heerden, "The Theory of Optical Information in Solids", Appl. Opt. Vol. 2, pp. 393-340. (1963).
15. Ibid. (2), pp. 288-291.
16. H. M. Smith, Principles of Holography, (Wiley, New York), pp. 58-73.
17. Ibid. (2), pp. 233-253.
18. Ibid. (1), pp. 17-21.
19. George Gamov, One Two Three...Infinity, (The Viking Press, New York), 1961, pp. 14-23.
20. G. R. Cooper, and C. D. McGillem, Methods of Signal and System Analysis, (Holt, Rinehart and Winston, Inc., New York), 1967, pp. 42-74.



ROSE POLYTECHNIC INSTITUTE

Graduate Council

APPOINTMENT OF FINAL EXAMINATION COMMITTEE

AND

FINAL EXAMINATION REPORT

Student Robert J. Marks II Degree M.S. E.E.

Department Electrical Engineering Date Aug 11, 1973

Thesis Title Holographic Recording of Optical Space Variant Systems.

Non-Thesis

I. EXAMINATION COMMITTEE

It is requested that the following committee be appointed to conduct the final examination of the student named above.

Table with 2 columns: Professor, Department. Rows include Thomas F. Krile (Chairman, EE), Michael J. Moloney (Physics), and Harold A. Sabbach (E.E.).

Requested by Dr. Krile Major Professor Approved by Dept. Chairman

II. FINAL EXAMINATION REPORT

Passed with recommendation for doctoral study

Passed

Failed

Date of Exam Aug 11, 1973 Committee Signatures

Handwritten signatures of Thomas F. Krile, Michael J. Moloney, and Harold A. Sabbach.

Note: When the report is complete, the Chairman of the Examining Committee should send this form to the Director of Graduate Studies. Copies will be returned to the Chairman of the Advisory Committee, Department Chairman, and student.

